NOAA Technical Memorandum ERL AOML-63

HEAT BUDGET AND CLIMATIC ATLAS OF THE TROPICAL WESTERN INDIAN OCEAN AND ARABIAN SEA DURING FGGE (1979)

Robert L. Molinari
John F. Festa
Eric Marmolejo

Atlantic Oceanographic and Meteorological Laboratory
Miami, Florida
April 1986

noaa NATIONAL OCEANIC AND ATMOSPHERIC ADMINISTRATION / Environmental Research Laboratories

NOAA Technical Memorandum ERL AOML-63

HEAT BUDGET AND CLIMATIC ATLAS OF THE TROPICAL WESTERN INDIAN OCEAN AND ARABIAN SEA DURING FGGE (1979)

Robert L. Molinari
John F. Festa
Eric Marmolejo

Atlantic Oceanographic and Meteorological Laboratory
Miami, Florida
April 1986

UNITED STATES DEPARTMENT OF COMMERCE

Malcolm Baldrige, Secretary

NATIONAL OCEANIC AND ATMOSPHERIC ADMINISTRATION

Anthony J. Calio, Administrator

Environmental Research Laboratories

Vernon E. Derr, Director

Contents

HEAT BUDGET AND CLIMATIC ATLAS OF THE TROPICAL WESTERN INDIAN OCEAN AND ARABIAN SEA DURING FGGE (1979)

Robert L. Molinari, John F. Festa, and Eric Marmolejo

ABSTRACT. Observations of surface oceanographic and meteorological fields collected during the first GARP Global Experiment (FGGE) in the tropical western Indian Ocean and Arabian Sea have been combined and averaged by month onto a 2° x 2° grid. Monthly distributions of sea-surface temperature, wind speed and direction, air temperature, specific humidity, and cloud cover have been generated for the period from December 1978 through November 1979. Net short-wave and long-wave radiation, and sensible and latent heat flux distributions have been generated from these surface data using the bulk aerodynamic formulas. Standard errors of the mean values have been computed along with monthly contoured plots of each oceanographic and meteorological variable.

1. INTRODUCTION

Equatorial oceans apparently play a large role in the global energy balance. Recent studies have shown that the Arabian Sea experiences a significant net annual heat gain through the sea surface (Hastenrath and Lamb, 1979a, for instance). Through advection this heat may serve to balance net heat deficits at poleward latitudes (Hastenrath, 1980). The historical studies have used data averaged over many years to derive the surface oceanic, meteorological, and energy exchange fields.

Molinari et al. (1986) considered the evolution of the sea-surface temperature (SST) field, meteorological variables, and surface energy in the equatorial Atlantic Ocean during the First GARP Global Experiment (FGGE), which was conducted in 1979. They compared the FGGE year with a climatological year given in Hastenrath and Lamb (1979b). This atlas is a byproduct of the Molinari et al. (1986) study in that all the mean monthly fields of SST, meteorological variables, and surface energy fluxes derived from the FGGE data are presented. Following Figs. 1-6, which show monthly distributions of surface observations, the fields are presented in a form similar to the one employed by Hastenrath and Lamb (1979a, 1979b) to permit a comparison of the two data sets. The following monthly smoothed and edited fields are presented: sea surface observations (Figs. 7-12); air temperatures (Figs. 13-18); wind speed and direction (Figs. 19-24); cloud cover (Figs. 25-30); and specific humidity (Figs. 31-36). Also included are the following fields computed from the above monthly smoothed and edited fields: latent heat flux (Figs. 37-42); sensible heat flux (Figs. 43-48); long-wave radiation (Figs. 49-54); short-wave radiation (Figs. 55-60); and total heat gain (Figs. 61-66). Five annual average fields are computed: latent heat flux and sensible heat flux (Fig. 67); long-wave radiation and short-wave radiation (Fig. 68); and total heat gain (Fig. 69).

2. DATA SOURCES AND ANALYSIS

Data were collected during the time period December 1978 through November 1979. Only data in the region 20°S-24°N and 40°E-50°E were considered in the analysis. The following steps were taken to edit, smooth, and fill in the SST and meteorological fields. Obvious outliers were removed by setting specified ranges for each of the parameters (Table 1). Daily averages of each parameter were computed on a 2° x 2° grid to reduce the influence of time-series stations (the grid size was a necessary compromise between data availability and desired spatial resolution). The daily averages were then averaged on the 2° x 2° grid to yield mean monthly distributions. Whenever sufficient data existed, a biased sample variance was computed for the grid point. A mean standard error for the entire domain was computed by averaging the resulting root mean square (rms) values.

The fields were further smoothed by first computing differences between mean daily, and mean monthly values at each grid point. When the difference exceeded two mean standard errors, the daily average was removed and new monthly averages and rms values were computed. Several regions outside the shipping lanes had few if any data points (Figs. 1-6). A nine-point Laplacian estimator was used to edit and fill in values at grid points within these regions. The functional form of the estimator, similar to a weighted average over a plane, is as follows:

$$\hat{A}_{KL} = \frac{\sum_{i=K-1}^{K+1} \sum_{j=L-1}^{L+1} w_{ij} A_{ij}}{\sum_{i=K-1}^{K+1} \sum_{j=L-1}^{L+1} w_{ij}}$$

such that when K = i and L = j, $\hat{A}_{KL} = \hat{A}_{ij} = 0$. The parameters are defined as follows:

A_{ij} = available monthly average at grid location i, j

$\hat{A}_{KL}$ = estimated value at location K, L

w_{ij} = weight values assigned as follows:

1	4	1
4	KL	4
1	4	1

To edit the data, the Laplacian operator was used as follows: if the number of observations making up the monthly average was less than 5, the data were removed if $|\hat{A}_{ij} - A_{ij}| > 2$ MSE.

To smooth the data, the following criteria were used:

(1) Data values based on 5 or more observations were left unchanged.

(2) Data values based on less than 5 days within a month were changed as follows:

$$A_{ij} = \hat{A}_{ij} \text{ if } |\hat{A}_{ij} - A_{ij}| > 2 \text{ MSE.}$$

$$A_{ij} = 1/2(\hat{A}_{ij} + A_{ij}) \text{ if } |\hat{A}_{ij} - A_{ij}| < 2 \text{ MSE.}$$

3. COMPUTATION OF HEAT BUDGET PARAMETERS

The latent heat flux (Q_e) and sensible heat flux (Q_s) were computed by using the bulk aerodynamic formulas following Hastenrath and Lamb (1978):

$$Q_s = \rho_a C_d \, C_p (T_s - T_a) w$$

$$Q_e = \rho_a C_d \, L(q_s - q_a) w$$

ρ_a = density of air, 1.175 kg/m^3

C_d = drag coefficient, 1.4×10^{-3}

C_p = specific heat of air, 1.012 (kj/kg)/°C

T_s, T_a = sea surface temperature and air temperature respectively (°C)

w = scalar wind speed (m/s)

L = latent heat of vaporization, $(2484 - 2.39 \times T_s)$ kj/kg

T_d = dew point temperature (K) = T_a - dew point depression

$$q_s = \frac{621.97 \times E_s}{p - .377 \times E_s} \text{ saturation specific humidity (g/kg) at } T_s$$

$$q_a = \frac{621.97 \times E_a}{p - .377 \times E_a} \text{ specific humidity (g/kg) at } T_d$$

$$E_s = 10^{(22.5578 - (2937.4)/T_s \; 4.92831 \times \log(T_s))}$$

$$E_a = 10^{(22.5578 - (2937.4)/T_s \; 4.92831 \times \log(T_d))}$$

p = atmospheric pressure (mb)

The shortwave radiation balance (SW) and the net longwave radiation balance (LW) are computed following Hastenrath and Lamb (1978) and Bunker (1976), respectively, as

$$LW = \epsilon T_s^4 \sigma \times (0.39 - .056\sqrt{q_a}) \times (1 - 0.53C^2) + 4\epsilon\sigma T_s^3 \times (T_s - T_a)$$

$$SW = Q_o \times (1 - aC - bC) \times (1 - \alpha)$$

ϵ = emissivity = 1

σ = Stefan Boltzmann's constant, 567 x 10 $(W/m^2)/K^4$

C = fraction of cloud cover in tenths

Q_o = shortwave radiation incident on Earth's surface on a cloudless day, from a table developed by Berliand (1960)

a=b = 0.38 from Bunker (1976)

α = albedo = .06

The net oceanic heat gain Q is computed as

$$Q = SW - LW - Q_s - Q_e \ (W/m^2).$$

The heat budget parameters were computed from the monthly mean Laplacian interpolated observed fields of T_s, T_a, w, etc.

4. ERROR ANALYSIS

Standard error of the mean (SEM) values have been computed for each variable at each grid point. Ensemble average values of SEM, computed from a biased sample variance, are given in Table 2 for observed values. The SEM is computed as follows:

$$S_x = \frac{\text{variance in } x}{\sqrt{n}}$$

where n = the number of values in the sample, and variance in x = the biased sample variance of the values. Typically larger errors are found outside the shipping lanes (where quadrangles typically have less than 10 data points). A propagation-of-error analysis was performed to determine errors in computed quantities. Considering a monthly average function $z = \overline{f(x,y,\ldots)}$ of two or more measured quantities x,y,..., the SEM of z can be written as

$$S_z = \sqrt{\left(\frac{\partial \overline{f(x,y)}}{dx}\right)^2 S_x^2 + \left(\frac{\partial \overline{f(x,y)}}{\partial y}\right)^2 S_y^2 + \ldots}$$

where S_y, S_x = SEM of measured quantity y and x, respectively, and

$\frac{\partial \overline{f(x,y)}}{\partial x}$ $\frac{d\overline{f(x,y)}}{dy}$ = partial derivatives of the monthly average function $z = \overline{f(x,y)}$ with respect to the measured quantity.

Table 3 lists the average SEM's of the computed quantities. As before, errors are considerably larger outside the shipping lanes.

5. REFERENCES

Berliand, T. C. (1960). Method of climatological estimation of global radiation. Meteor. Gidrol., 6, 9-12.

Bunker, A. F. (1976). Computations of surface energy flux and annual air-sea interaction cycles of the North Atlantic Ocean. Mon. Wea. Rev., 104, 112-114.

Hastenrath, S., and P. Lamb (1979a). Climatic atlas of the Indian Ocean, Part II: the oceanic heat budget. University of Wisconsin Press, Madison, WI, 93 pp.

Hastenrath, S., and P. Lamb (1979b). Climatic atlas of the Indian Ocean, Part I: surface climate and atmospheric circulation. University of Wisconsin Press, Madison, WI, 116 pp.

Hastenrath, S., and P. Lamb (1980). On the heat budget of hydrosphere and atmosphere in the Indian Ocean. J. Phys. Oceanogr., 10, 694-708.

Molinari, R. L., J. Swallow, and J. F. Festa (1986). Evolution of the near-surface thermal structure in the western Indian Ocean during FGGE, 1979. Submitted to J. Mar. Res.

Table 1. Ranges of Parameters.

Parameter	Acceptable Range
Sea surface temperature	
Coastal grid points	15°-31°C
Interior grid points	18°-31°C
Scalar wind speed	0-20 m/s
Air temperature	16°-38°C
Dew point depression	0°-15°C

Table 2. Ensemble average standard error of the mean values for quadrangles within the shipping lanes (10-15 values) and outside the shipping lanes (5-10 values).

	10-15 Values	5-10 Values
SST (°C)	.24	.29
Dew point temperature (°C)	.35	.42
Air temperature (°C)	.29	.35
Wind speed (m/s)	.59	.73
Cloud cover (tenths)	.6	.8

Table 3. Ensemble average standard error of the mean values for quadrangles within the shipping lanes (10-15 values) and outside the shipping lanes (5-10 values).

	Indian Ocean	
	10-15 Values	5-10 Values
Saturation specific humidity (g Kg^{-1})	0.33	0.40
Specific humidity (g Kg^{-1})	0.37	0.46
Sensible heat flux (W/m^{-2})	4.2	5.0
Latent heat flux (W/m^{-2})	17.9	21.9
Longwave radiation (W/m^{-2})	3.3	4.4
Shortwave radiation (W/m^{-2})	13.5	18.6

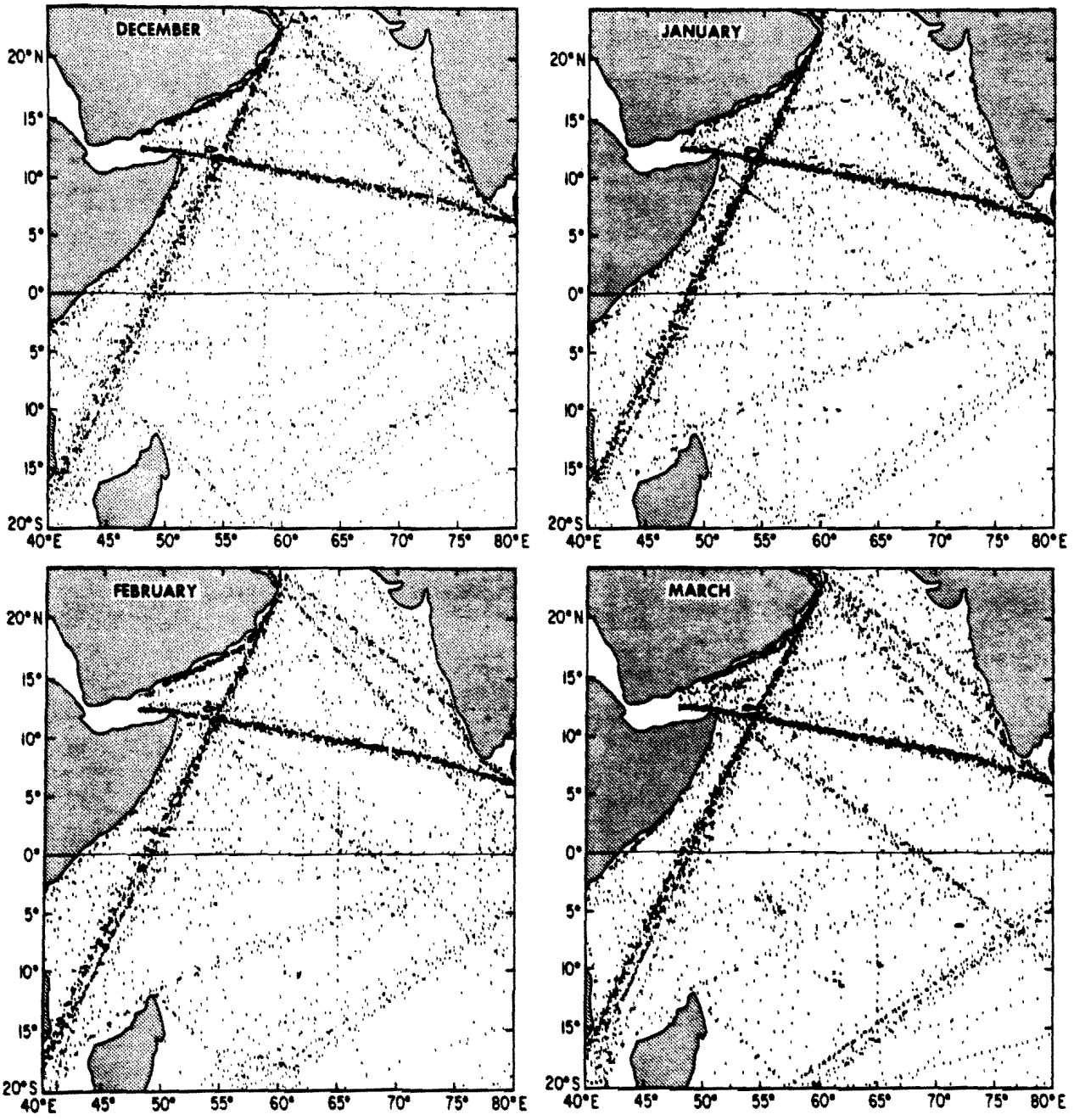

Figure 1. Monthly distribution of surface observations for December 1978, January 1979, February 1979 and March 1979.

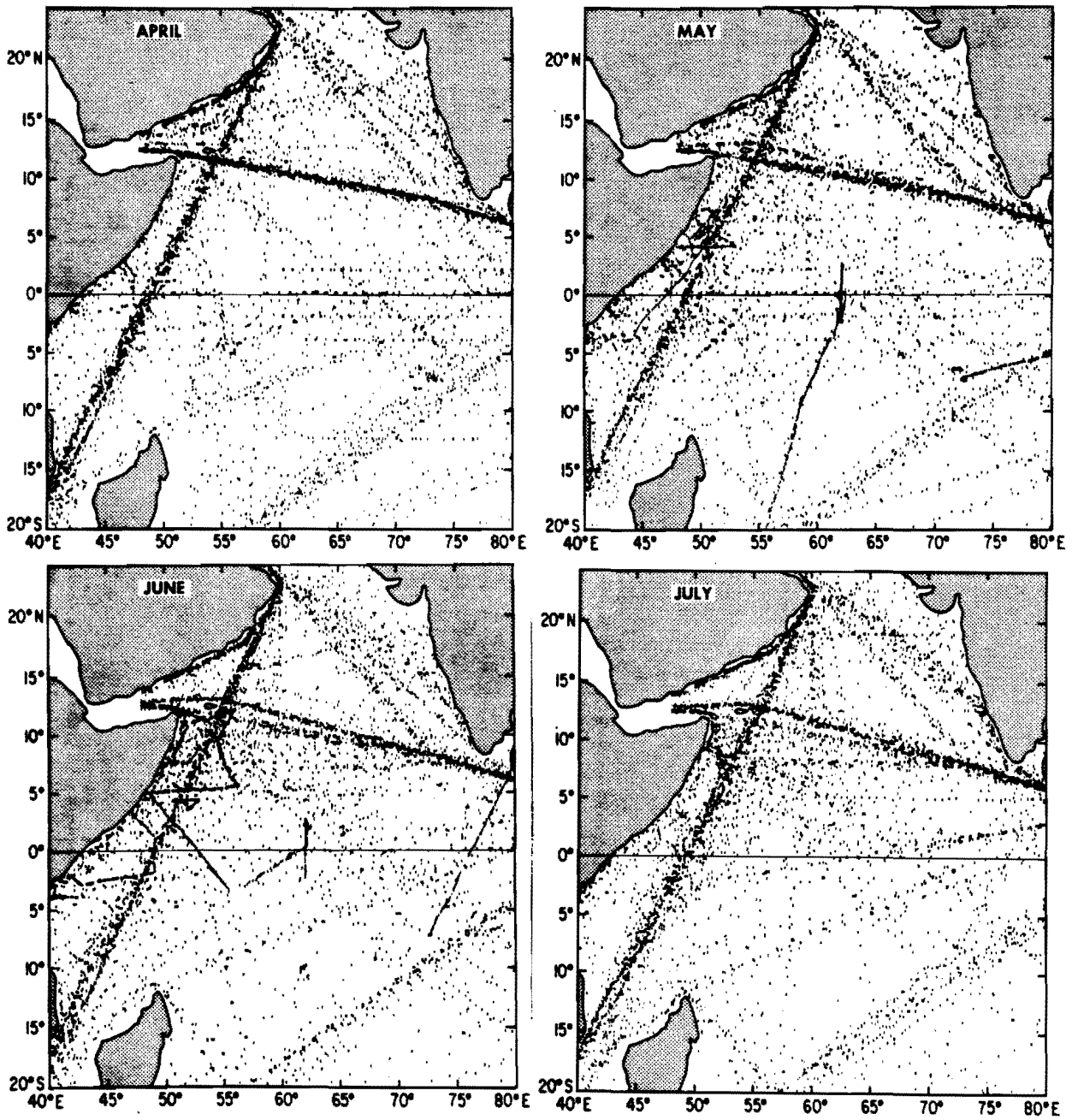

Figure 2. Monthly distribution of surface observations for April, May, June and July 1979.

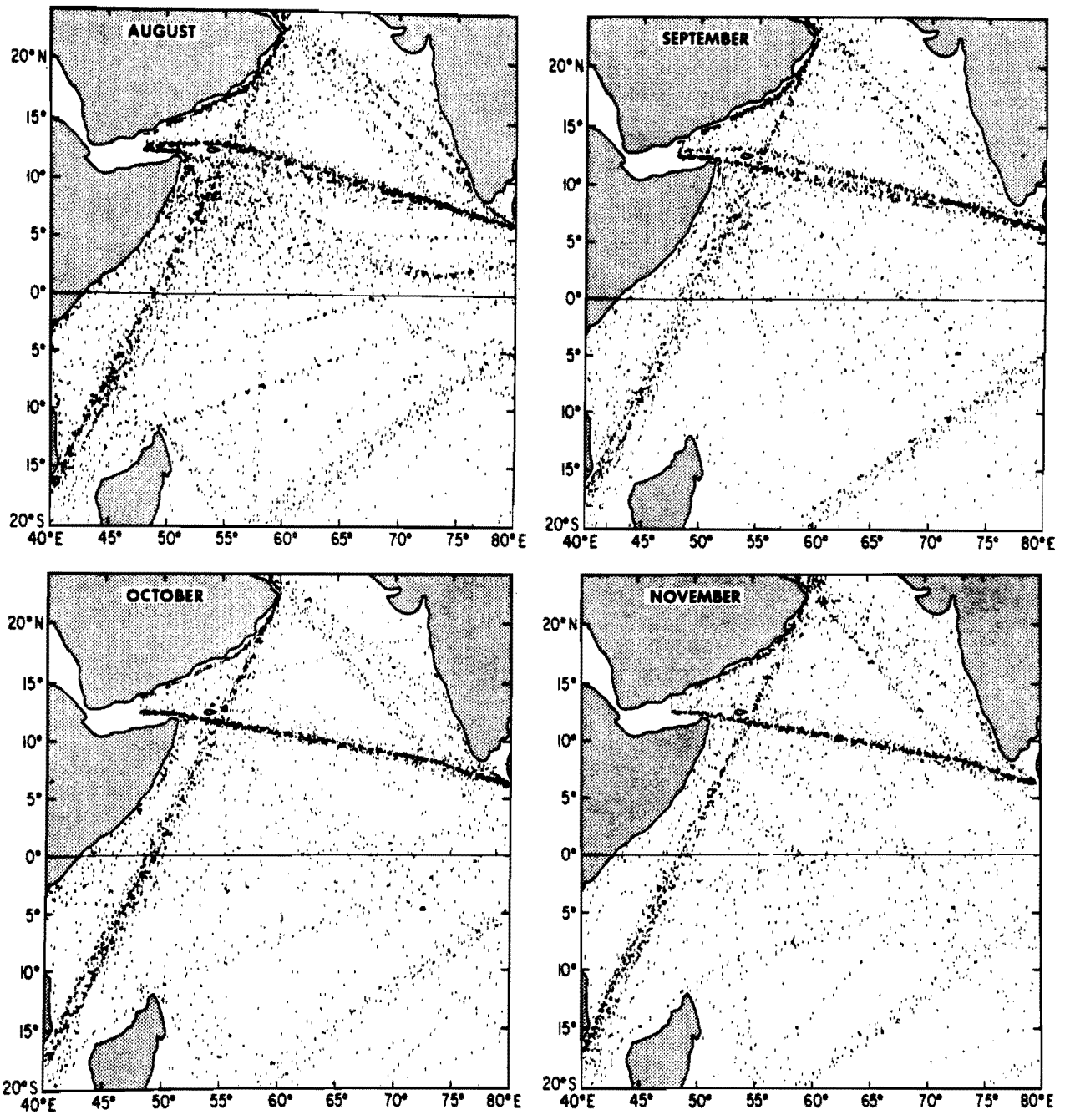

Figure 3. Monthly distribution of surface observations for August, September, October and November 1979.

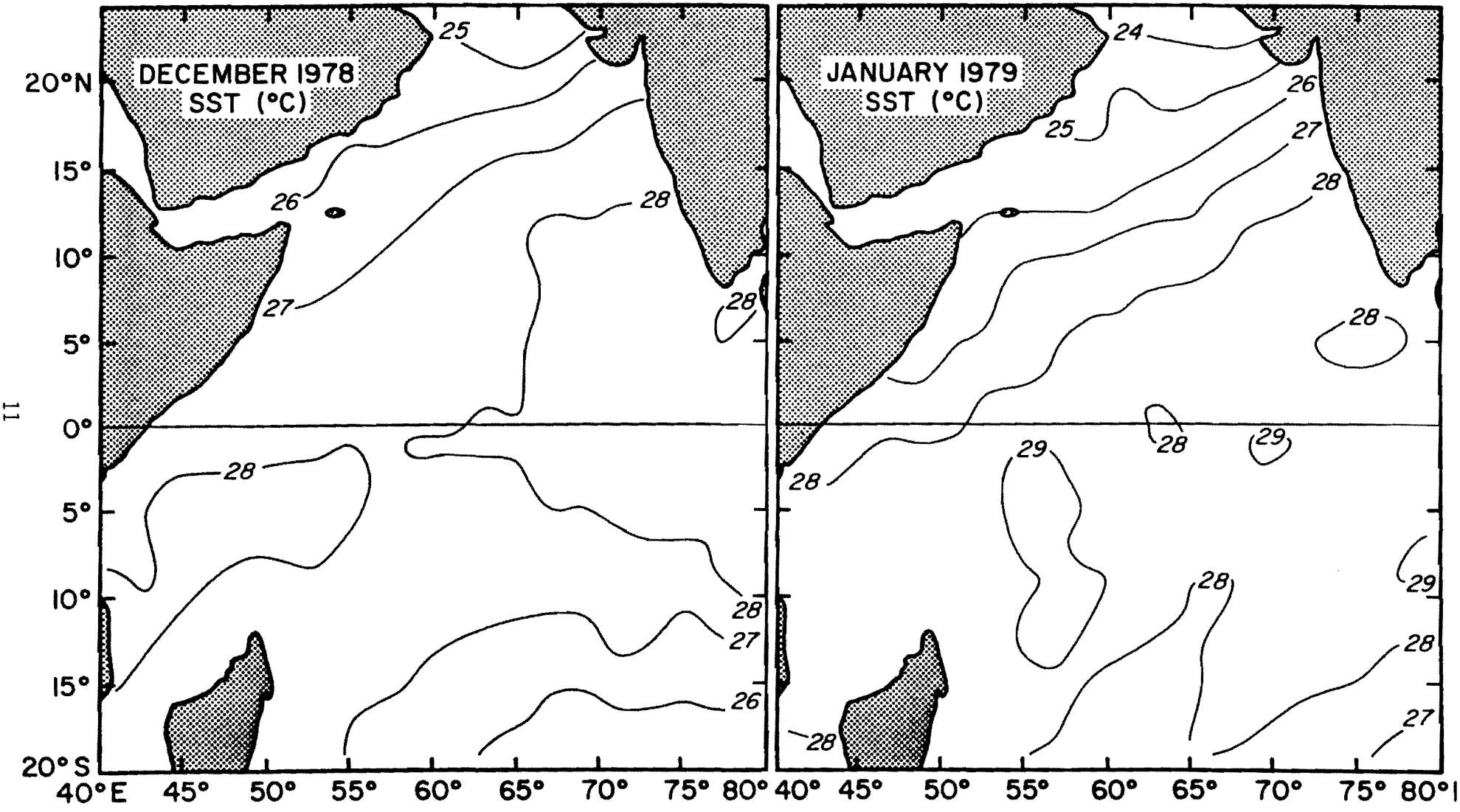

Figure 4. Monthly edited and smoothed sea surface temperatures for December 1978 and January 1979, contoured every 1°C.

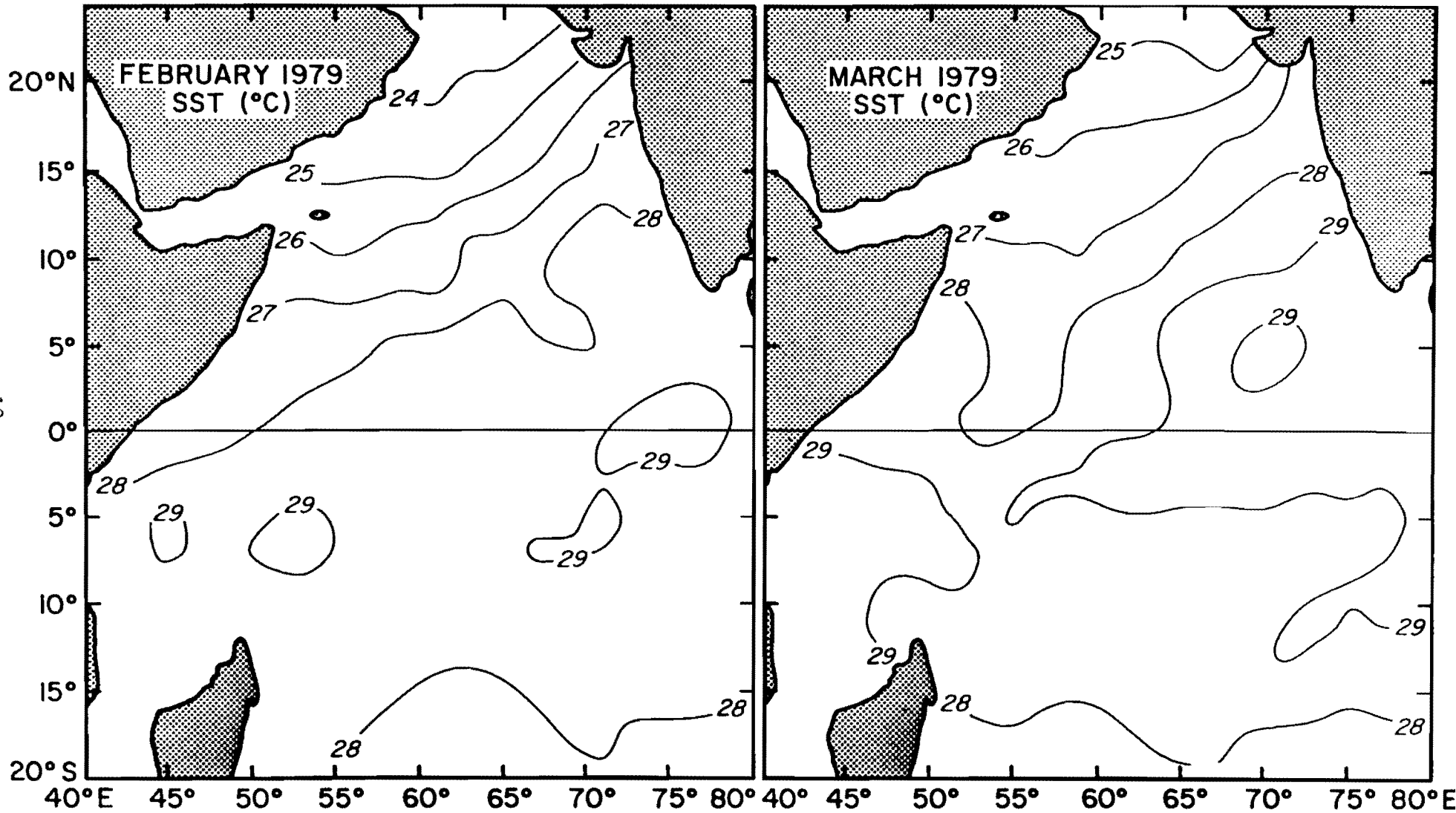

Figure 5. Sea surface temperatures for February and March 1979 (as in Figure 4).

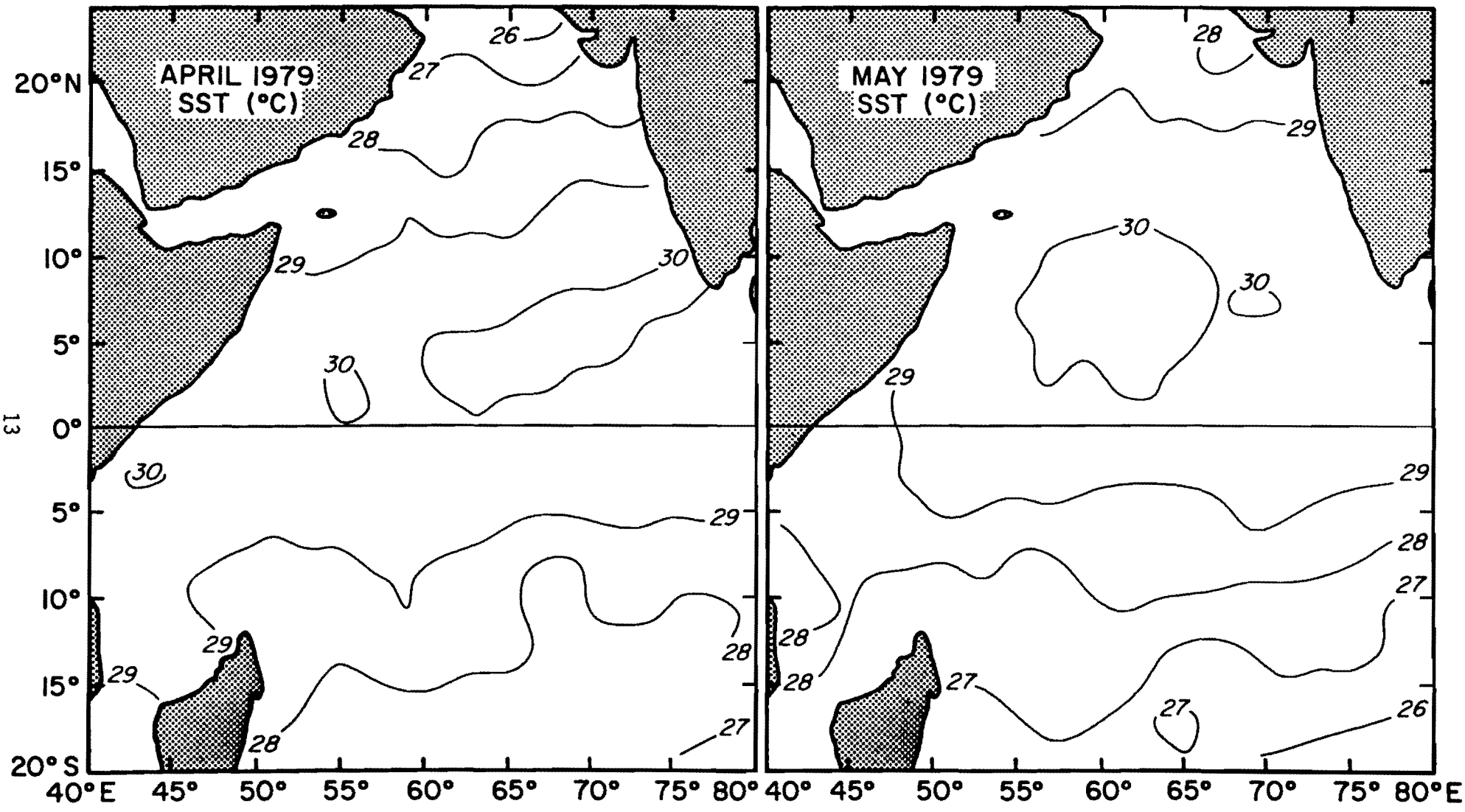

Figure 6. Sea surface temperatures for April and May 1979 (as in Figure 4).

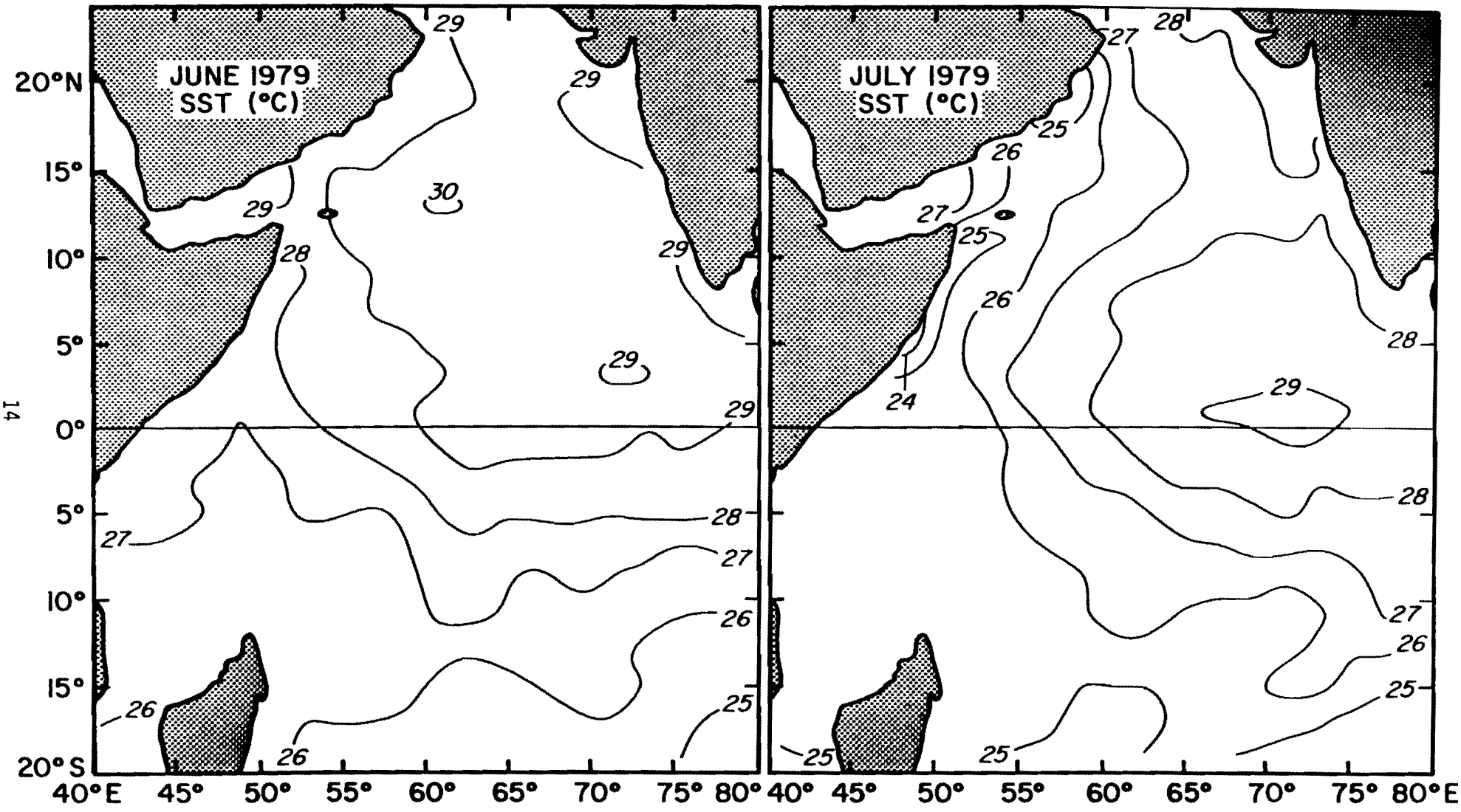

Figure 7. Sea surface temperatures for June and July 1979 (as in Figure 4).

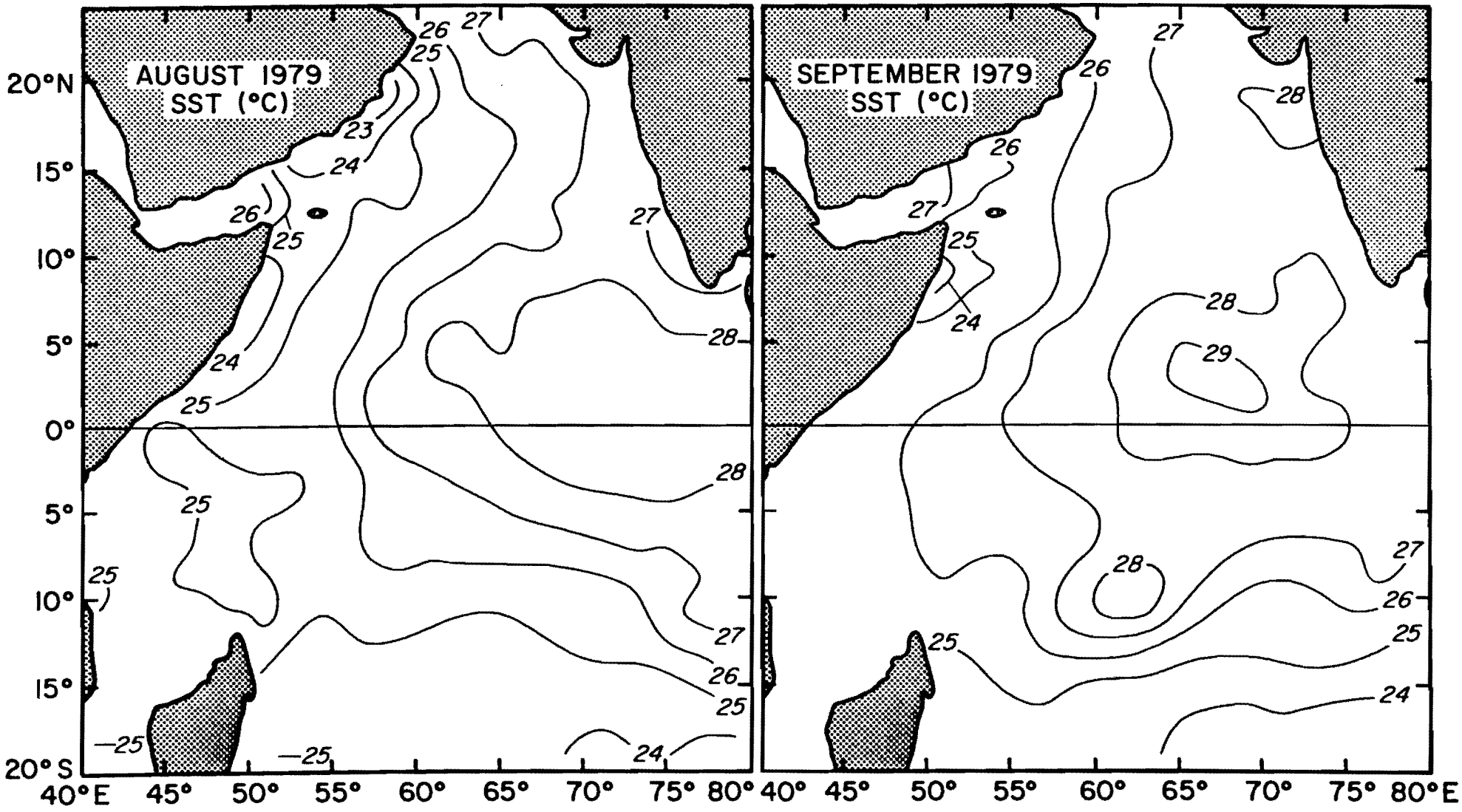

Figure 8. Sea surface temperatures for August and September 1979 (as in Figure 4).

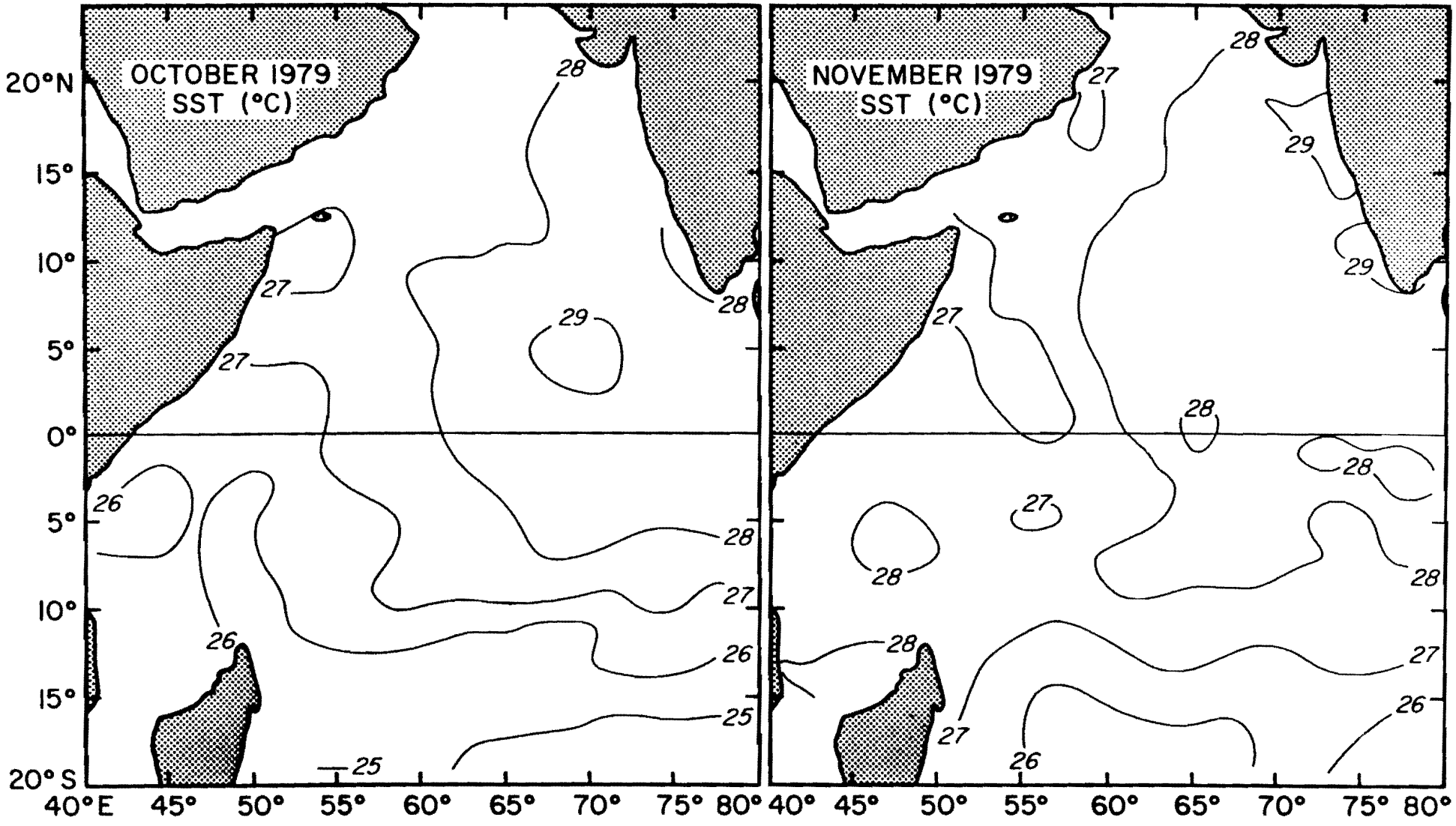

Figure 9. Sea surface temperatures for October and November 1979 (as in Figure 4).

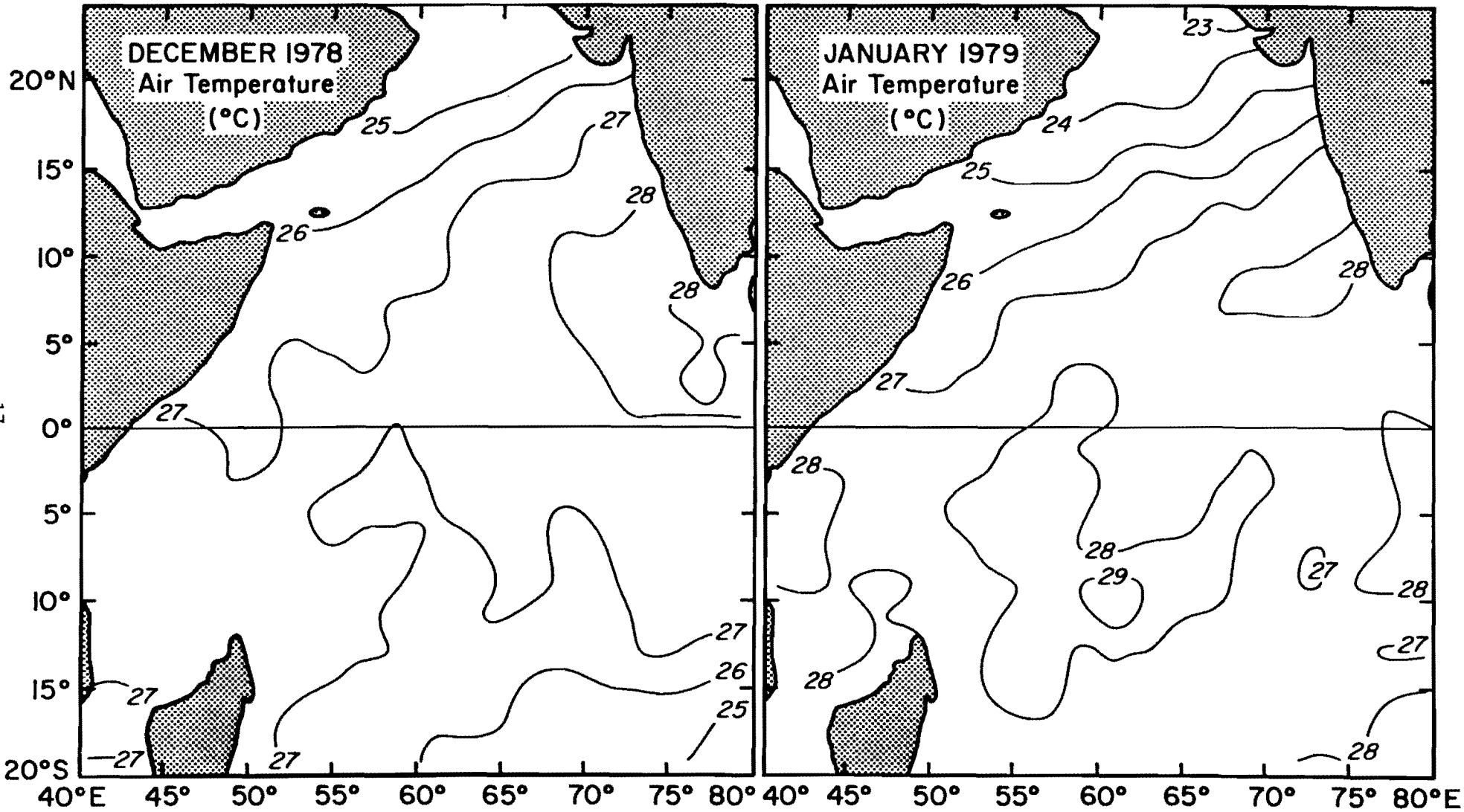

Figure 10. Monthly edited and smoothed air temperatures for December 1978 and January 1979, contoured every 1°C.

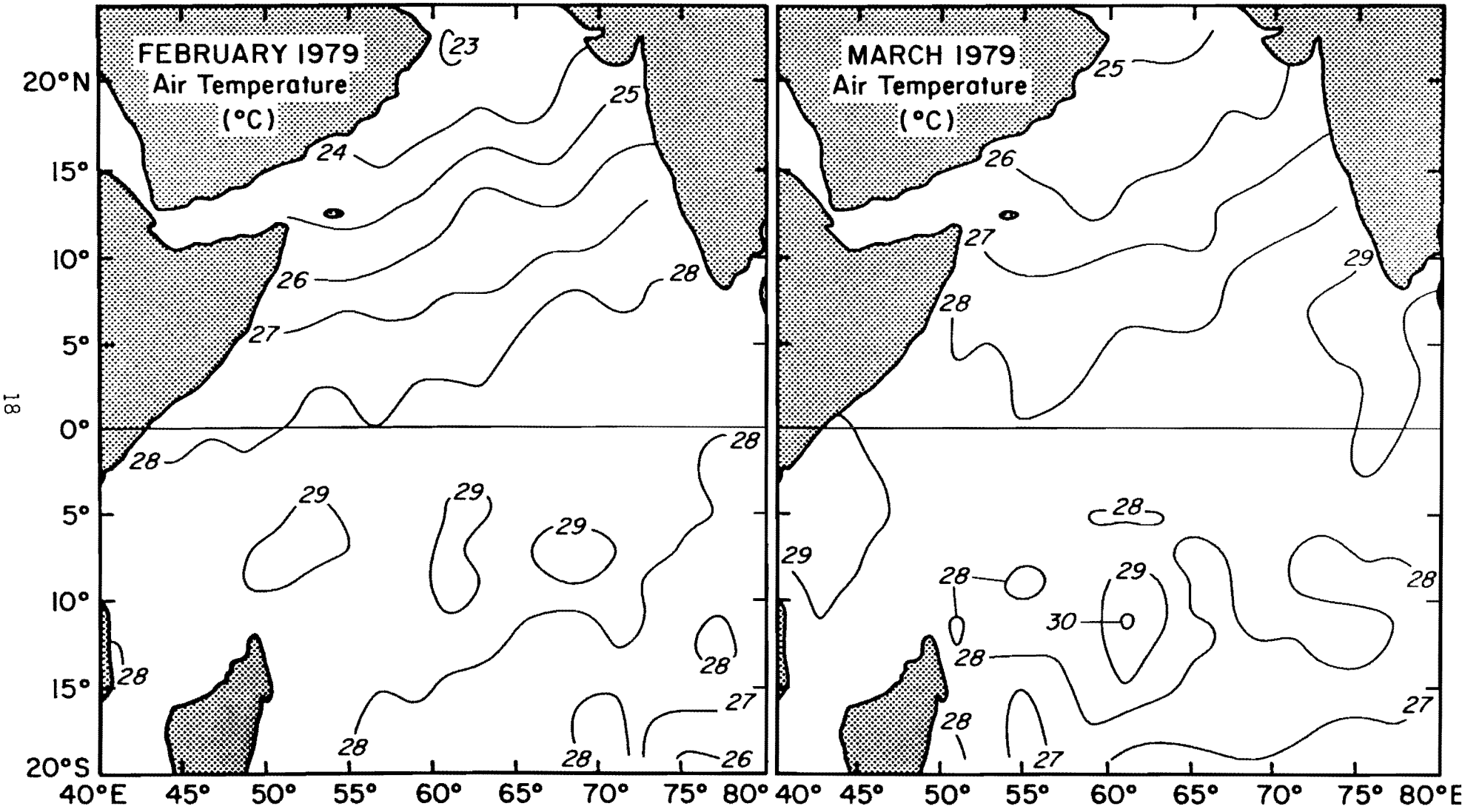

Figure 11. Air temperatures for February and March 1979 (as in Figure 10).

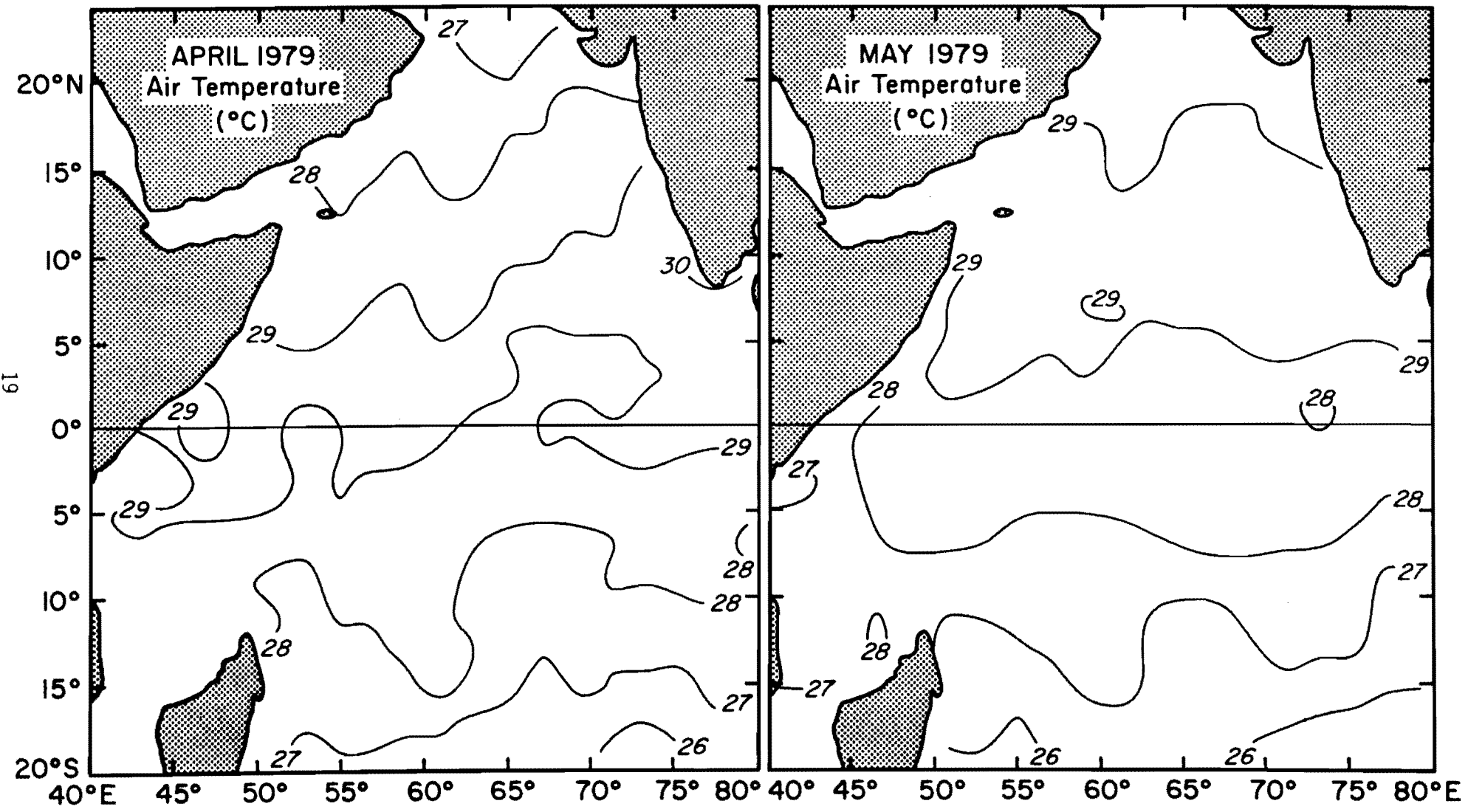

Figure 12. Air temperatures for April and May 1979 (as in Figure 10).

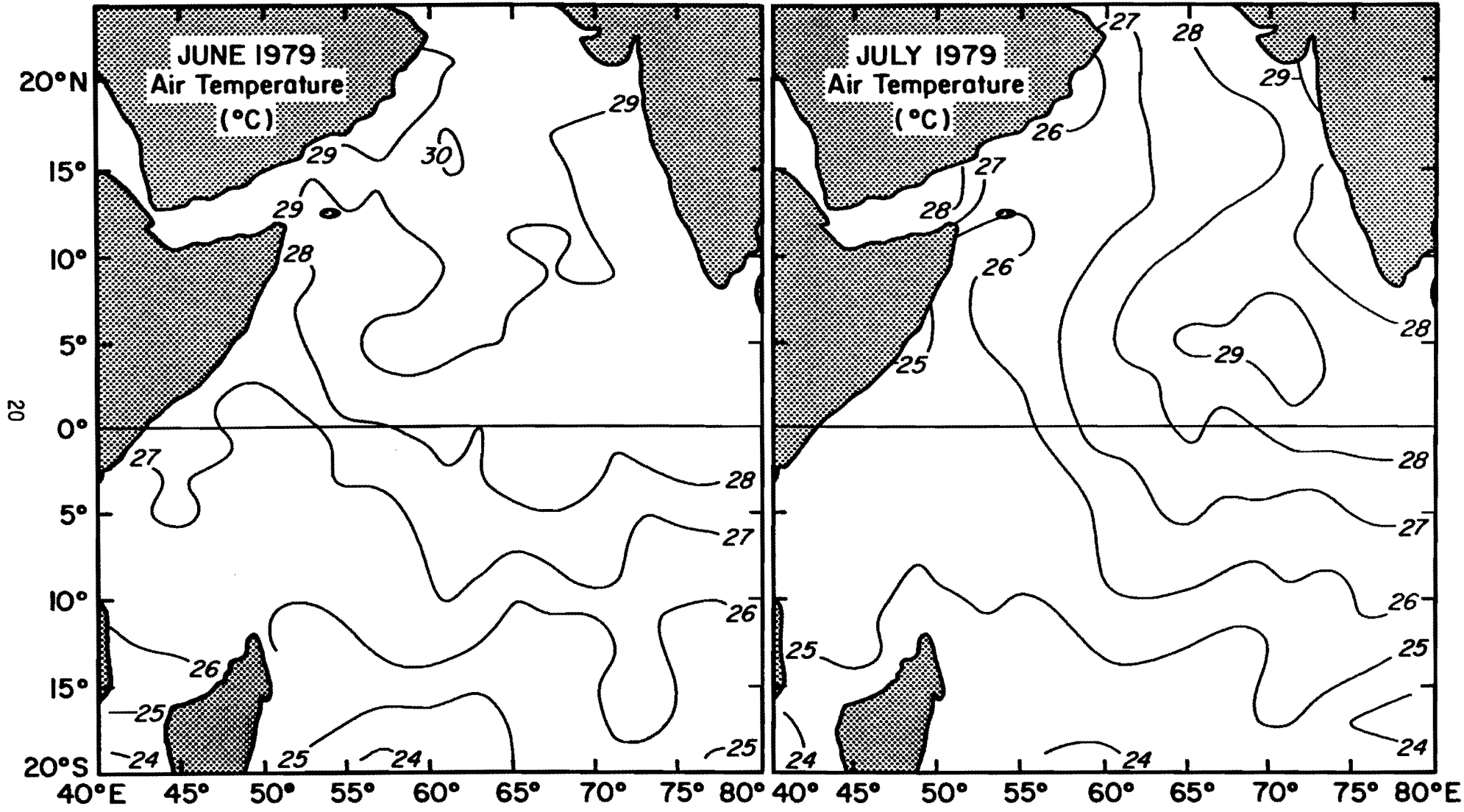

Figure 13. Air temperatures for June and July 1979 (as in Figure 10).

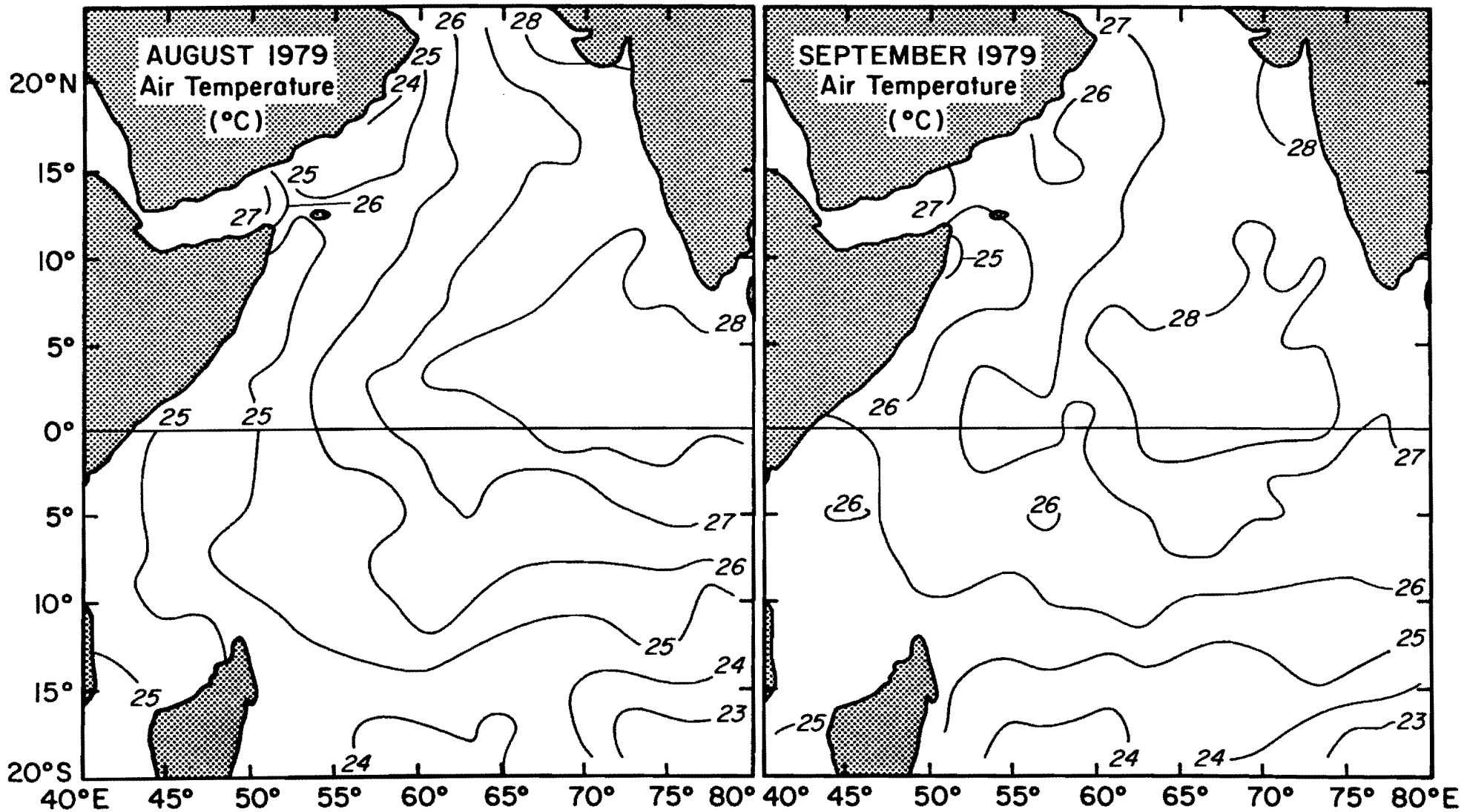

Figure 14. Air temperatures for August and September 1979 (as in Figure 10).

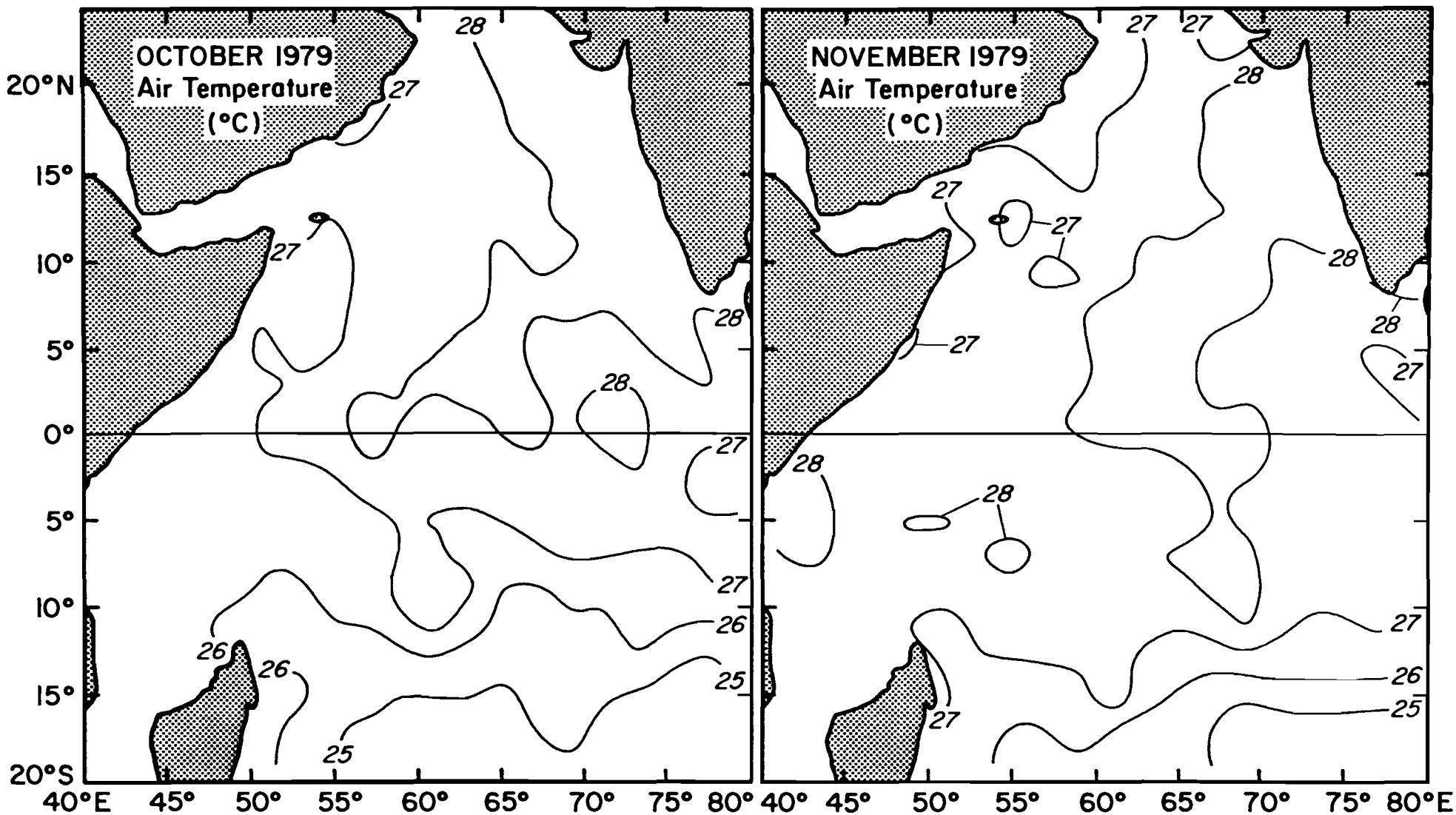

Figure 15. Air temperatures for October and November 1979 (as in Figure 10).

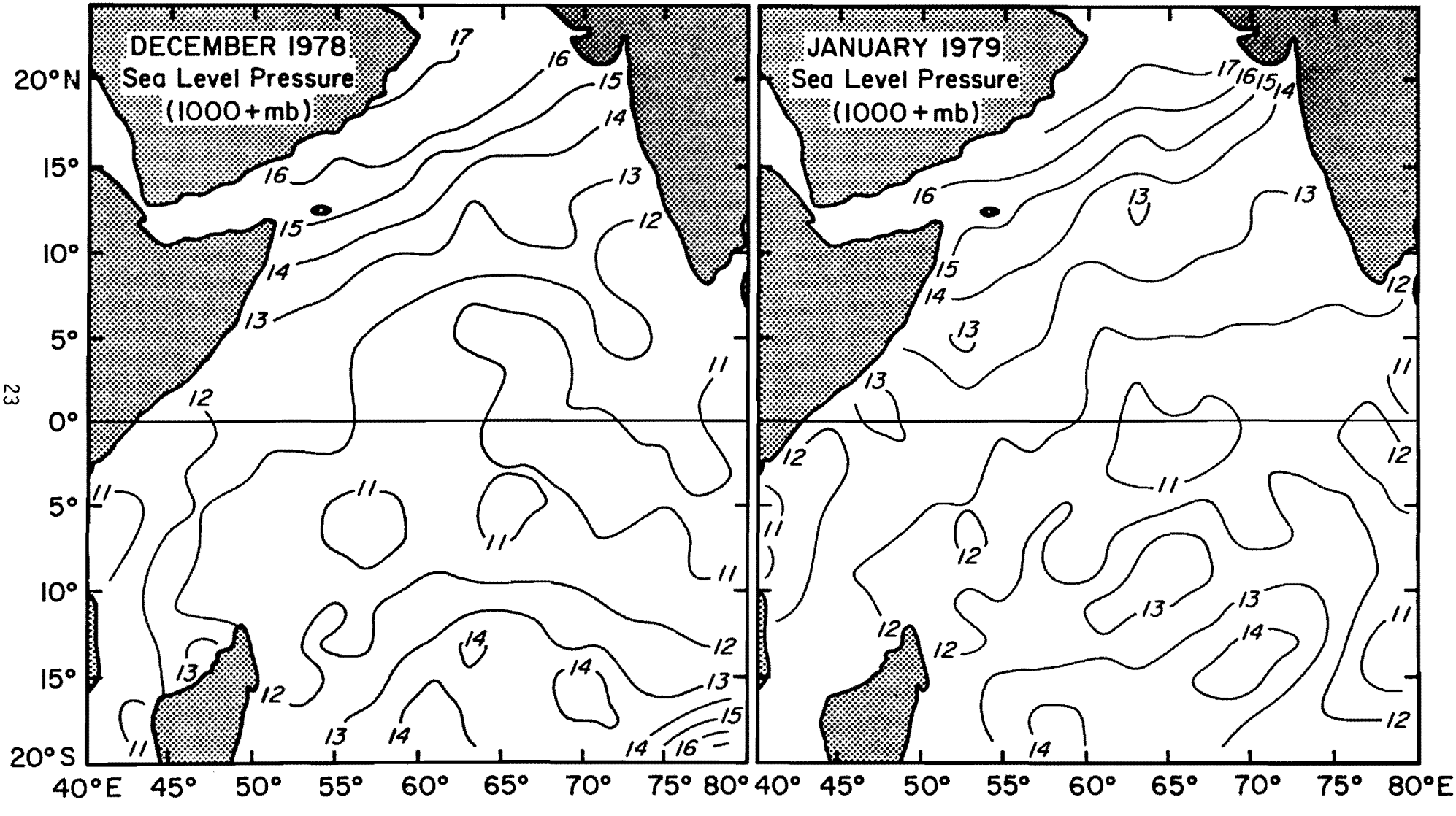

Figure 16. Monthly edited and smoothed sea-level pressures for December 1978 and January 1979, contoured every 1 mb.

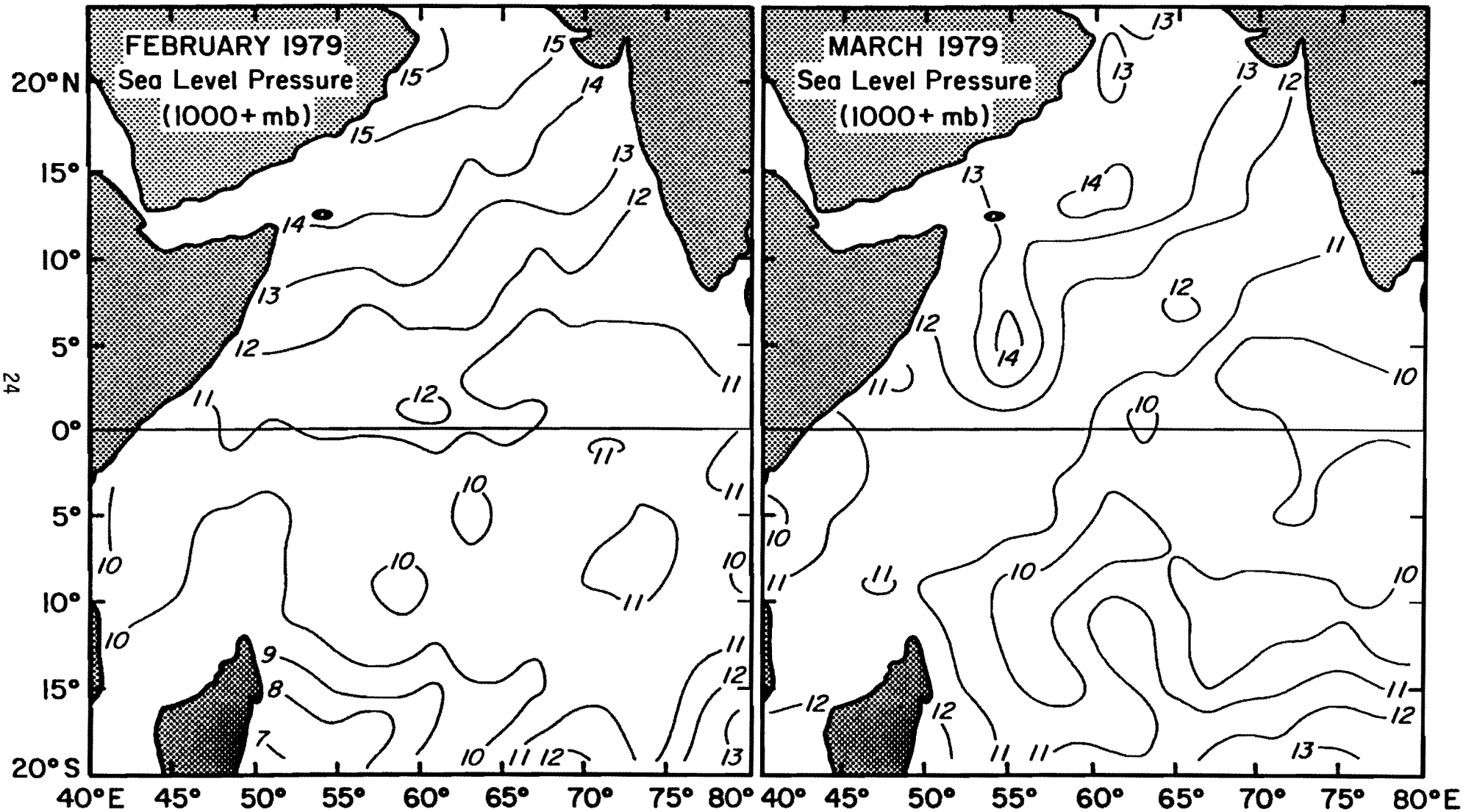

Figure 17. Sea-level pressures for February and March 1979 (as in Figure 16).

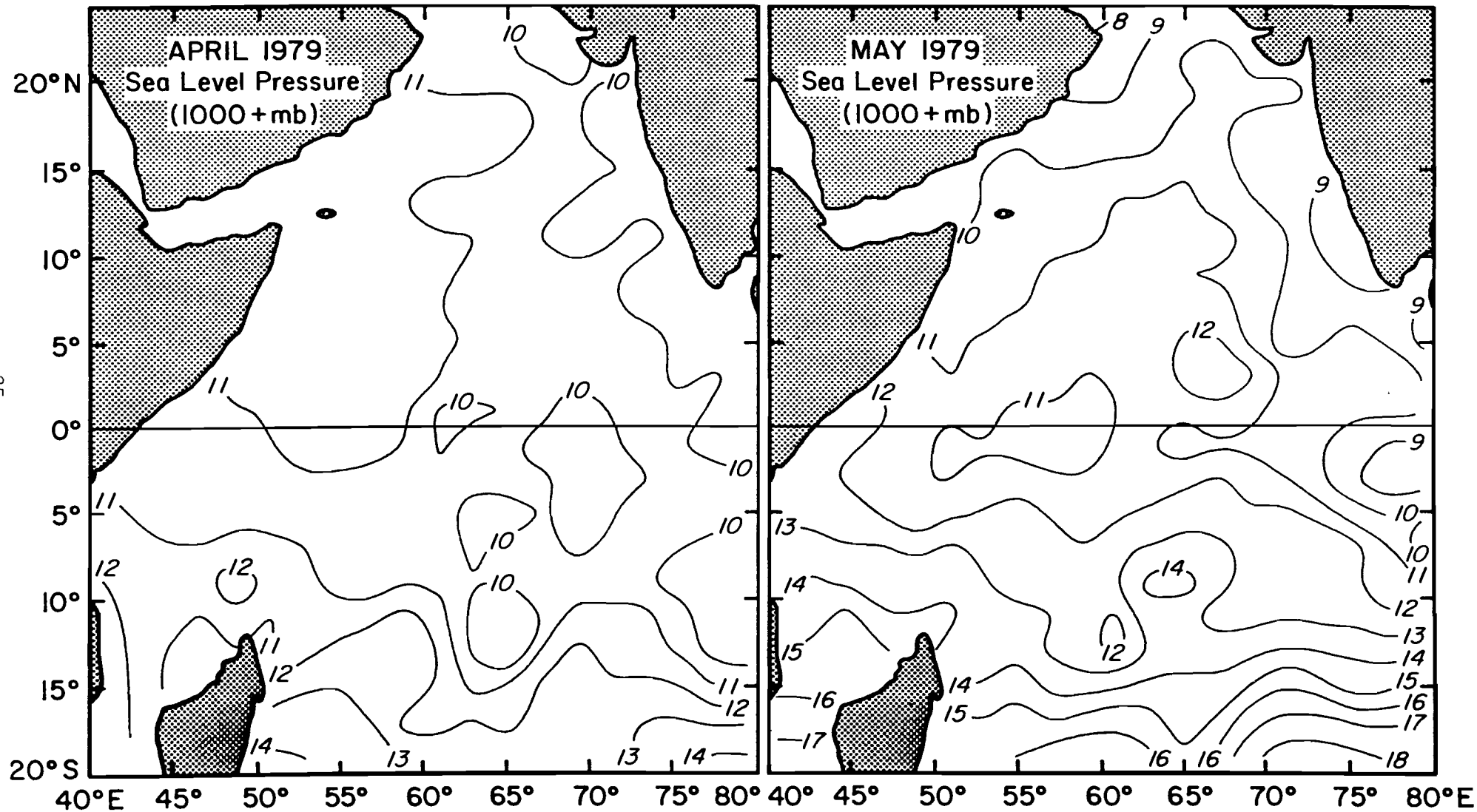

Figure 18. Sea-level pressures for April and May 1979 (as in Figure 16).

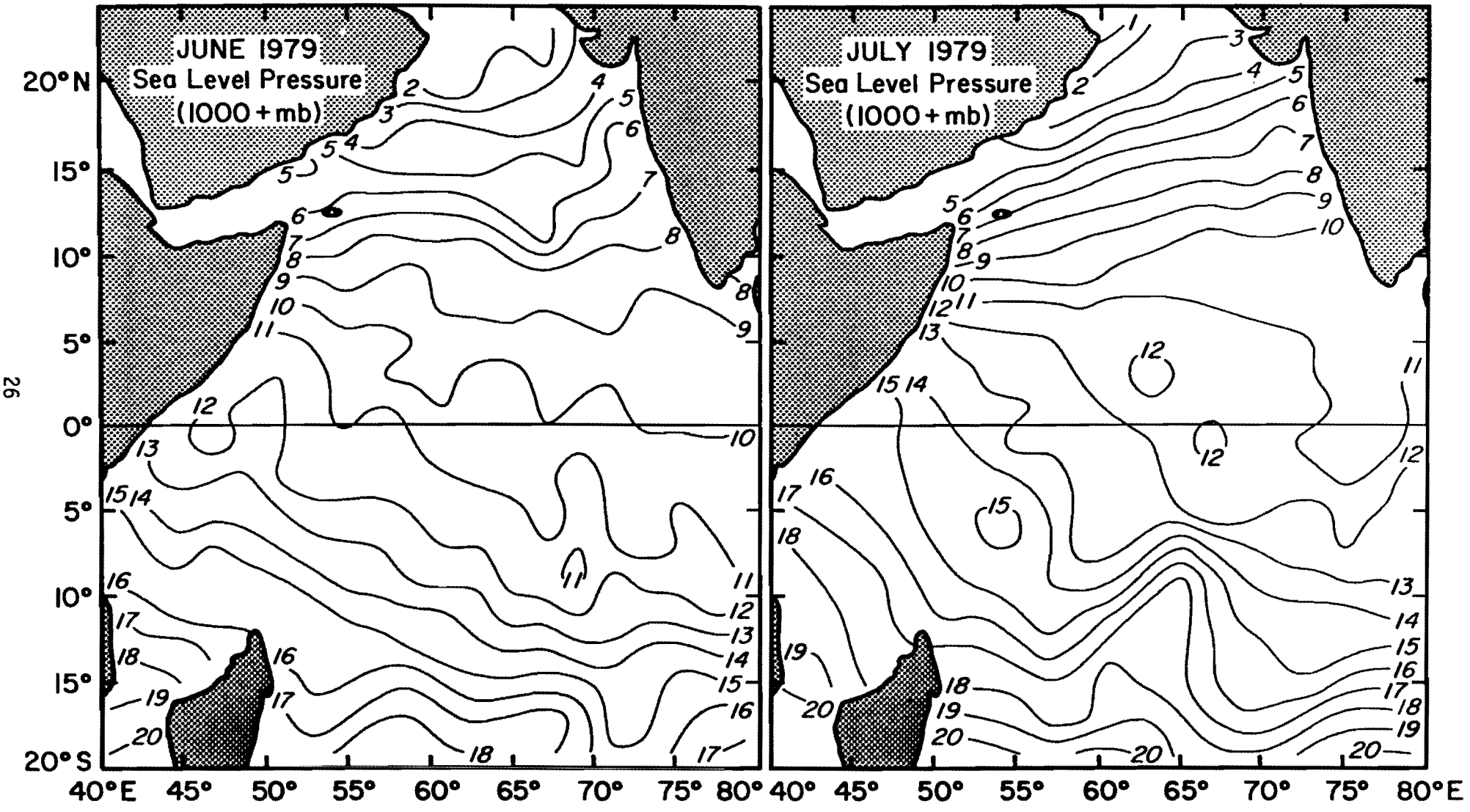

Figure 19. Sea-level pressures for June and July 1979 (as in Figure 16).

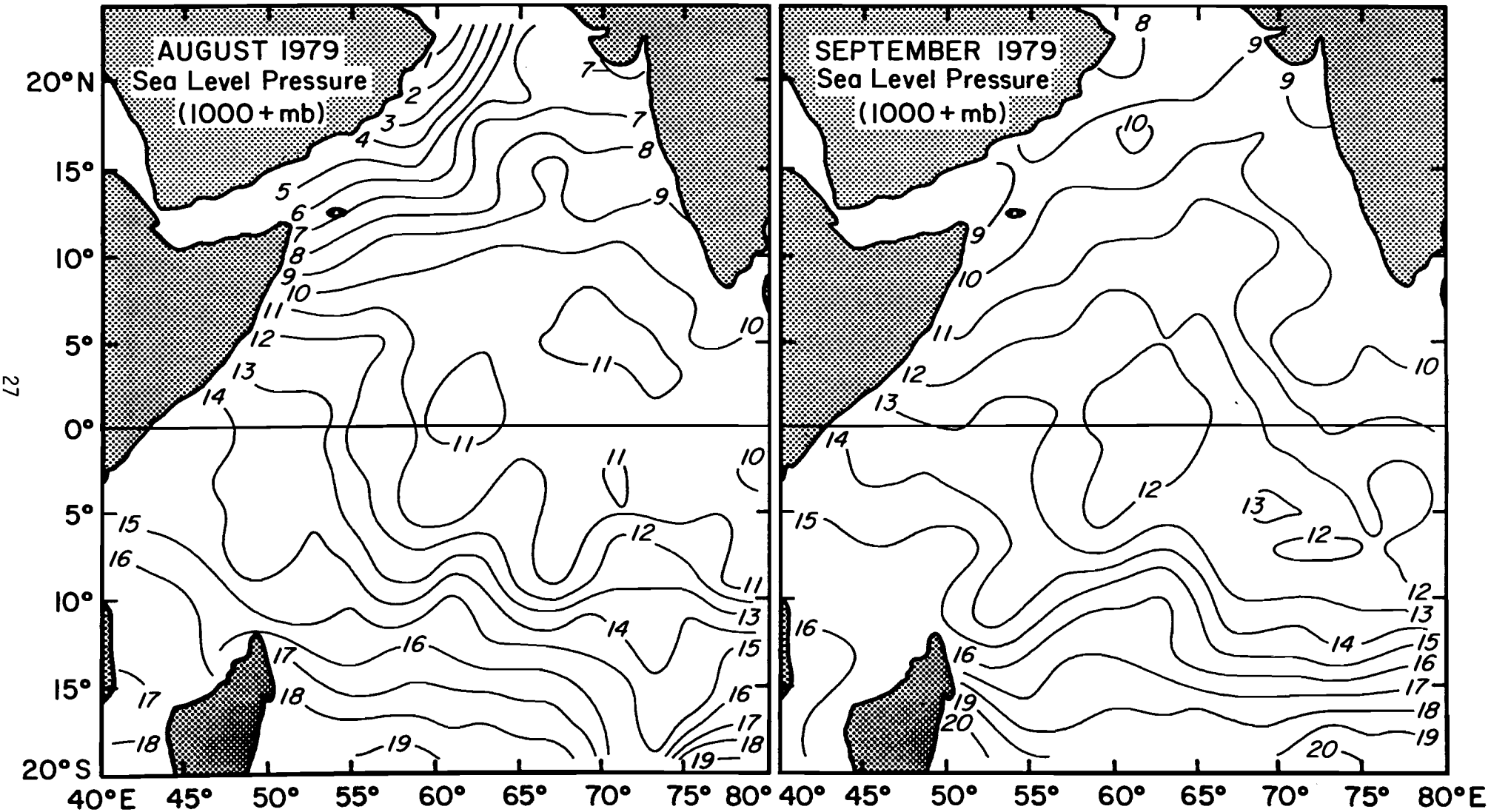

Figure 20. Sea-level pressures for August and September 1979 (as in Figure 16).

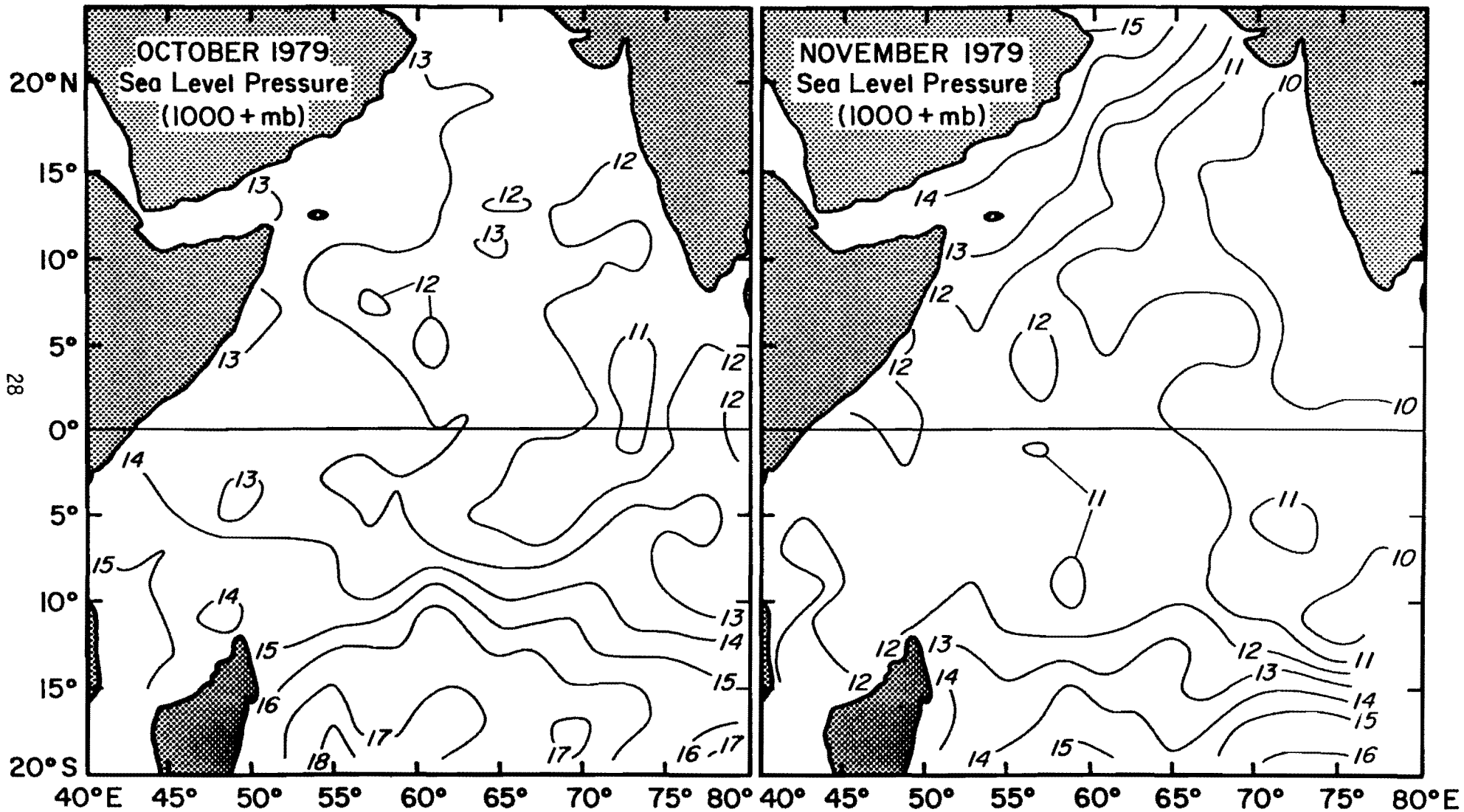

Figure 21. Sea-level pressures for October and November 1979 (as in Figure 16).

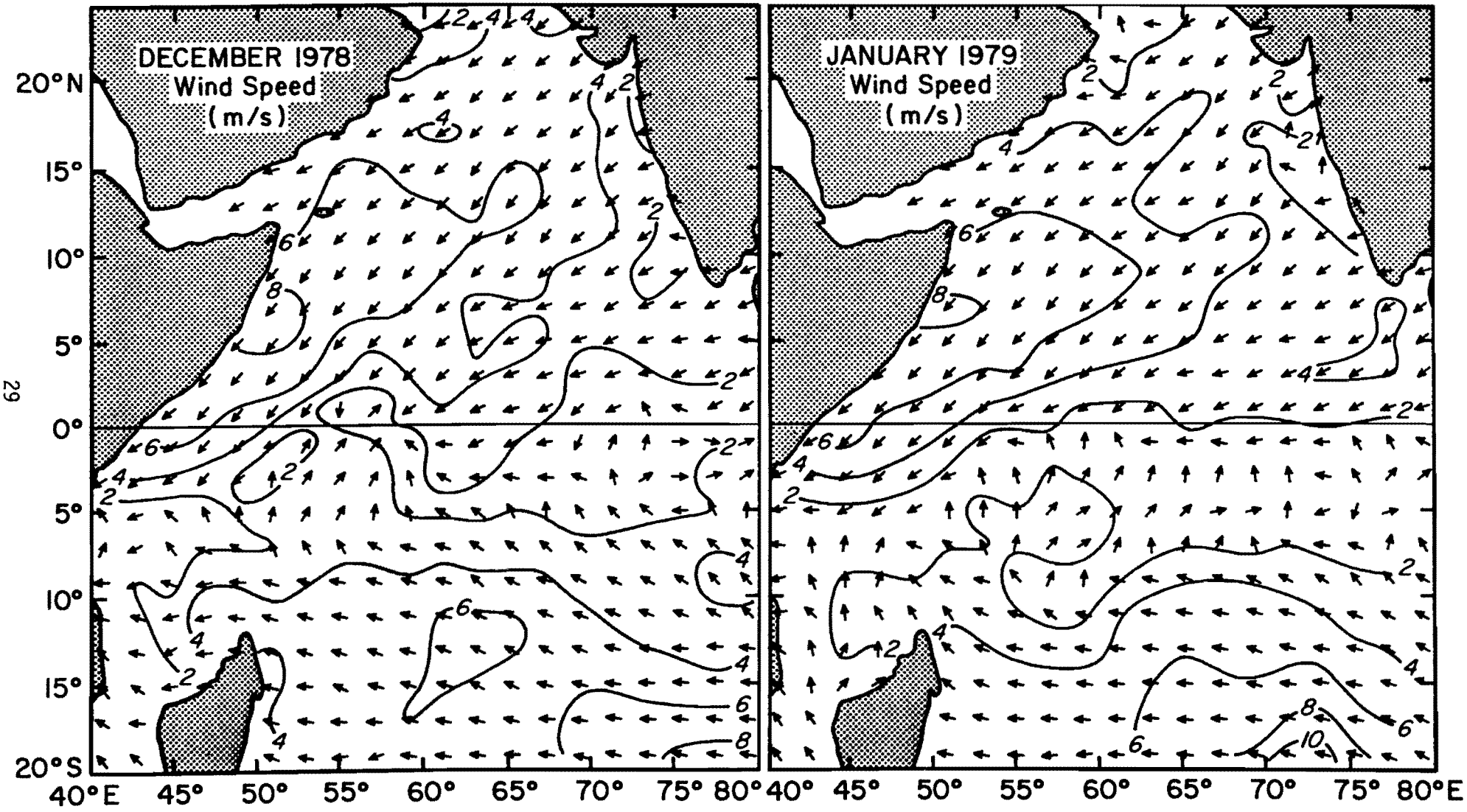

Figure 22. Monthly edited and smoothed wind speeds and directions for December 1978 and January 1979, contoured every 2 m/s.

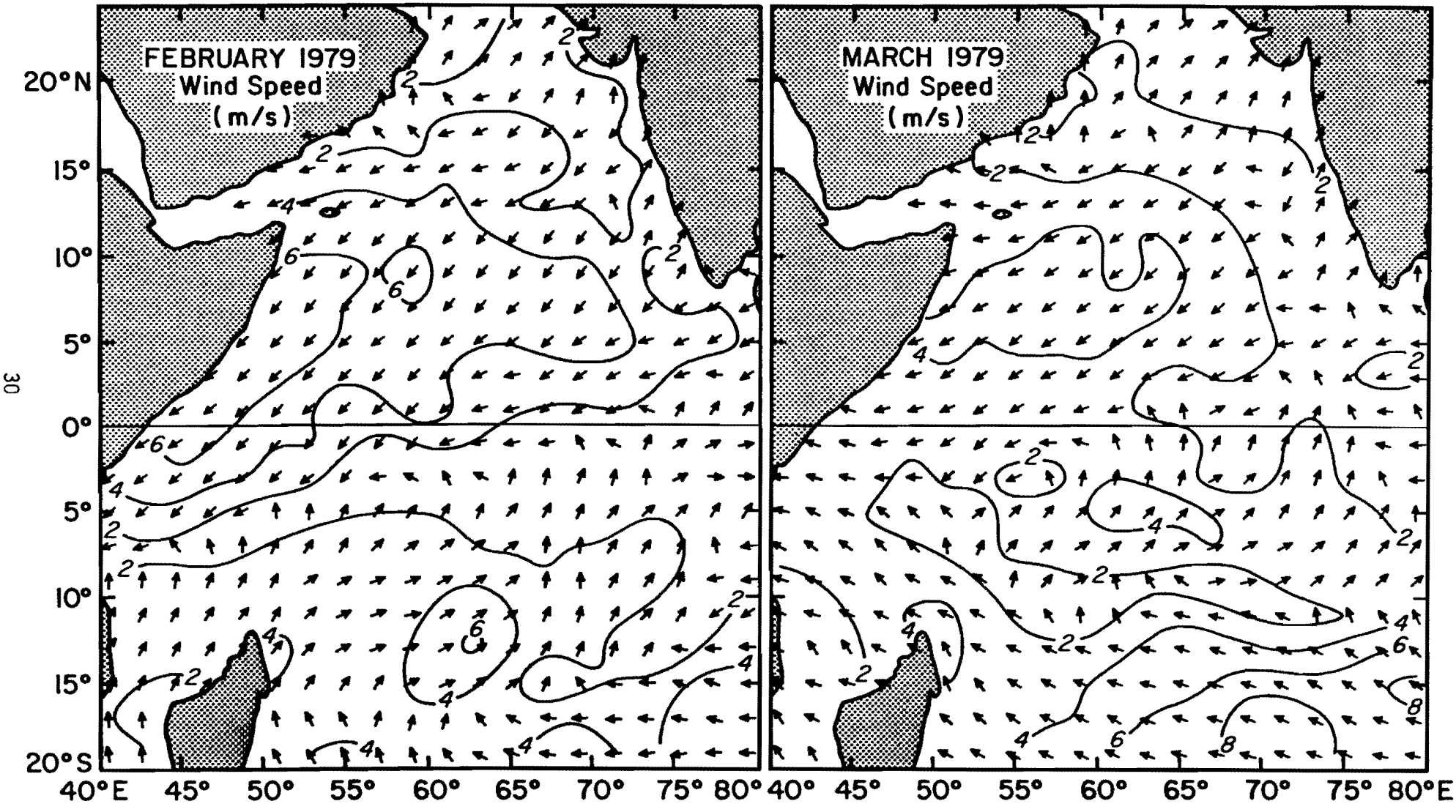

Figure 23. Wind field for February and March 1979 (as in Figure 22).

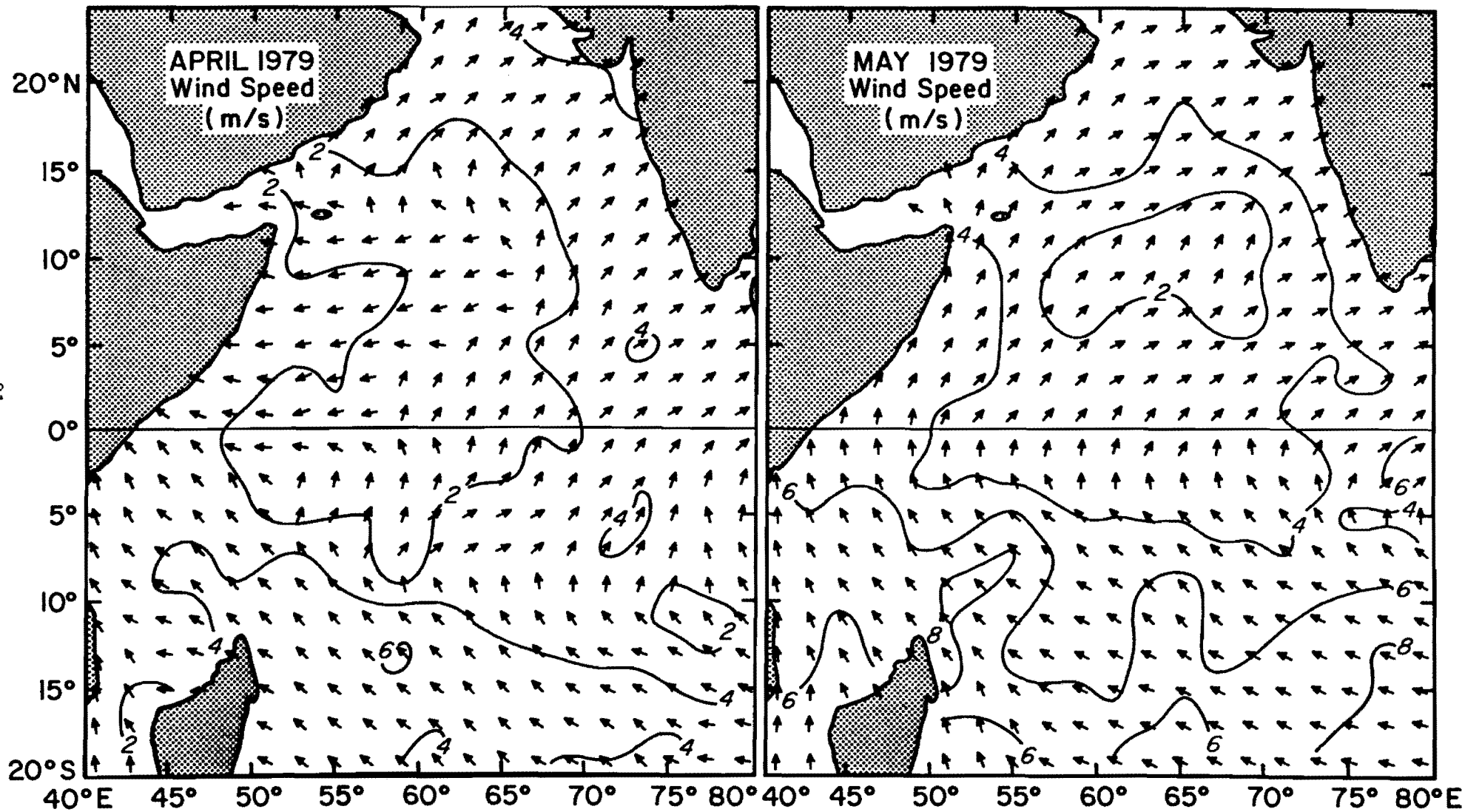

Figure 24. Wind field for April and May 1979 (as in Figure 22).

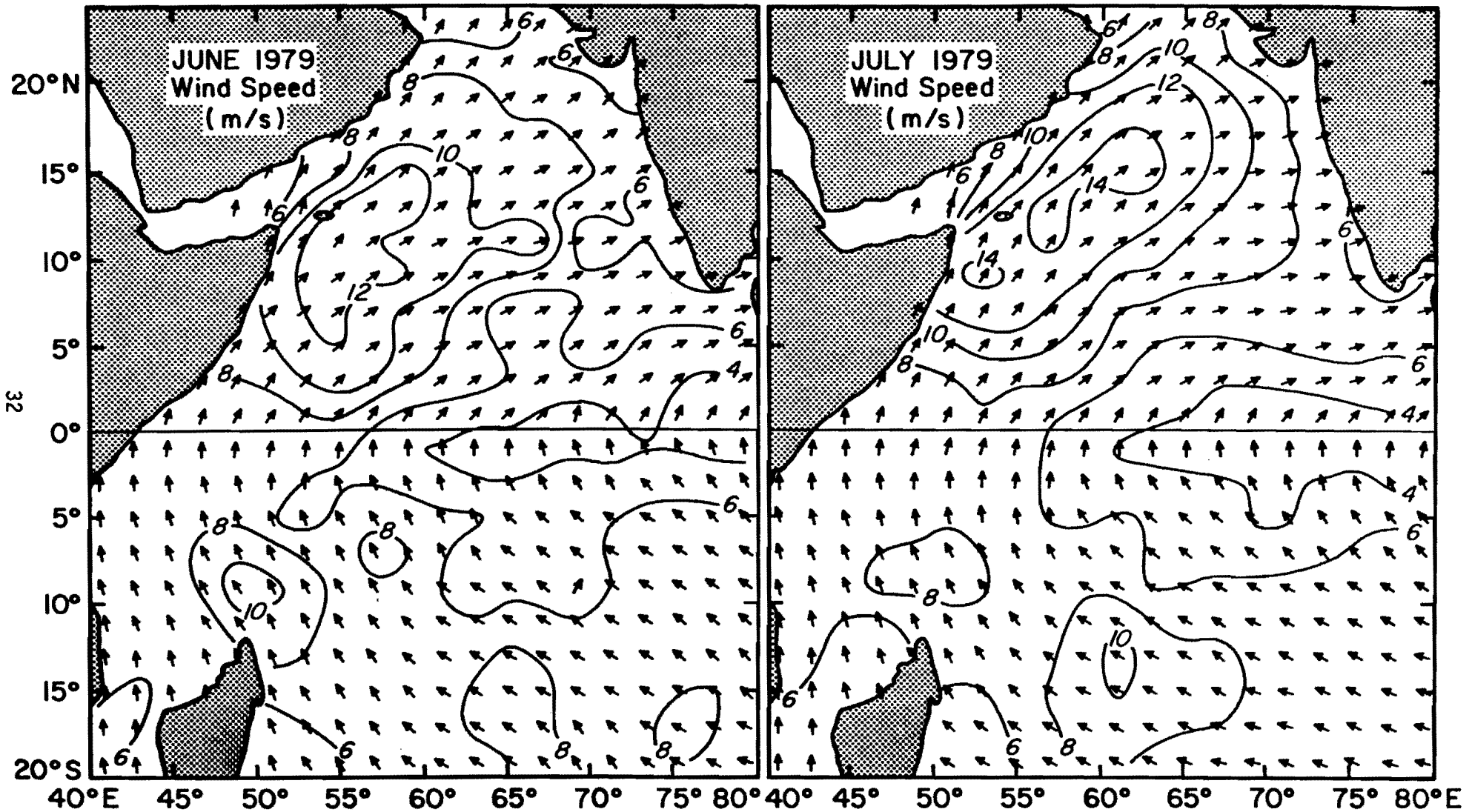

Figure 25. Wind field for June and July 1979 (as in Figure 22).

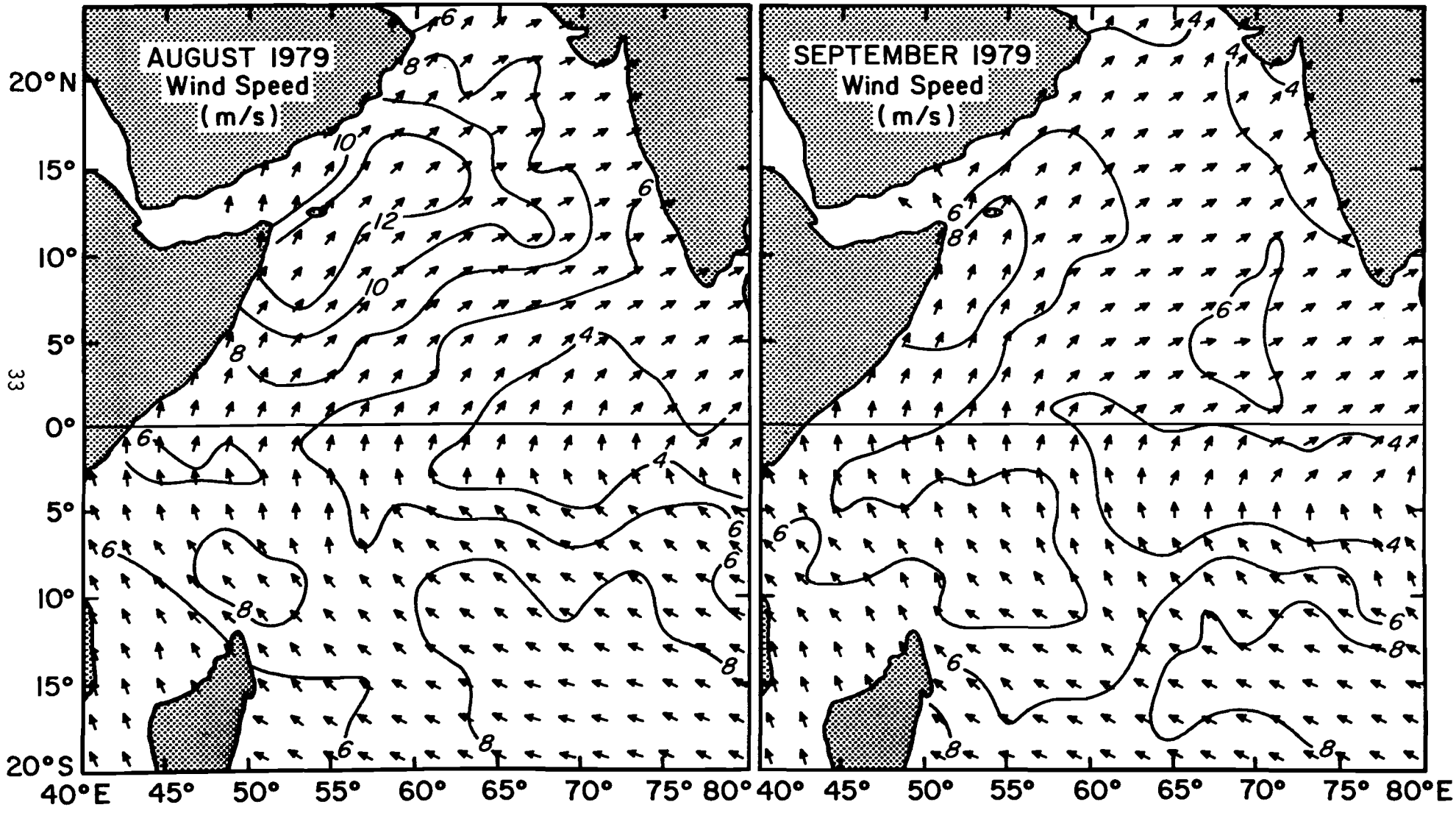

Figure 26. Wind field for August and September 1979 (as in Figure 22).

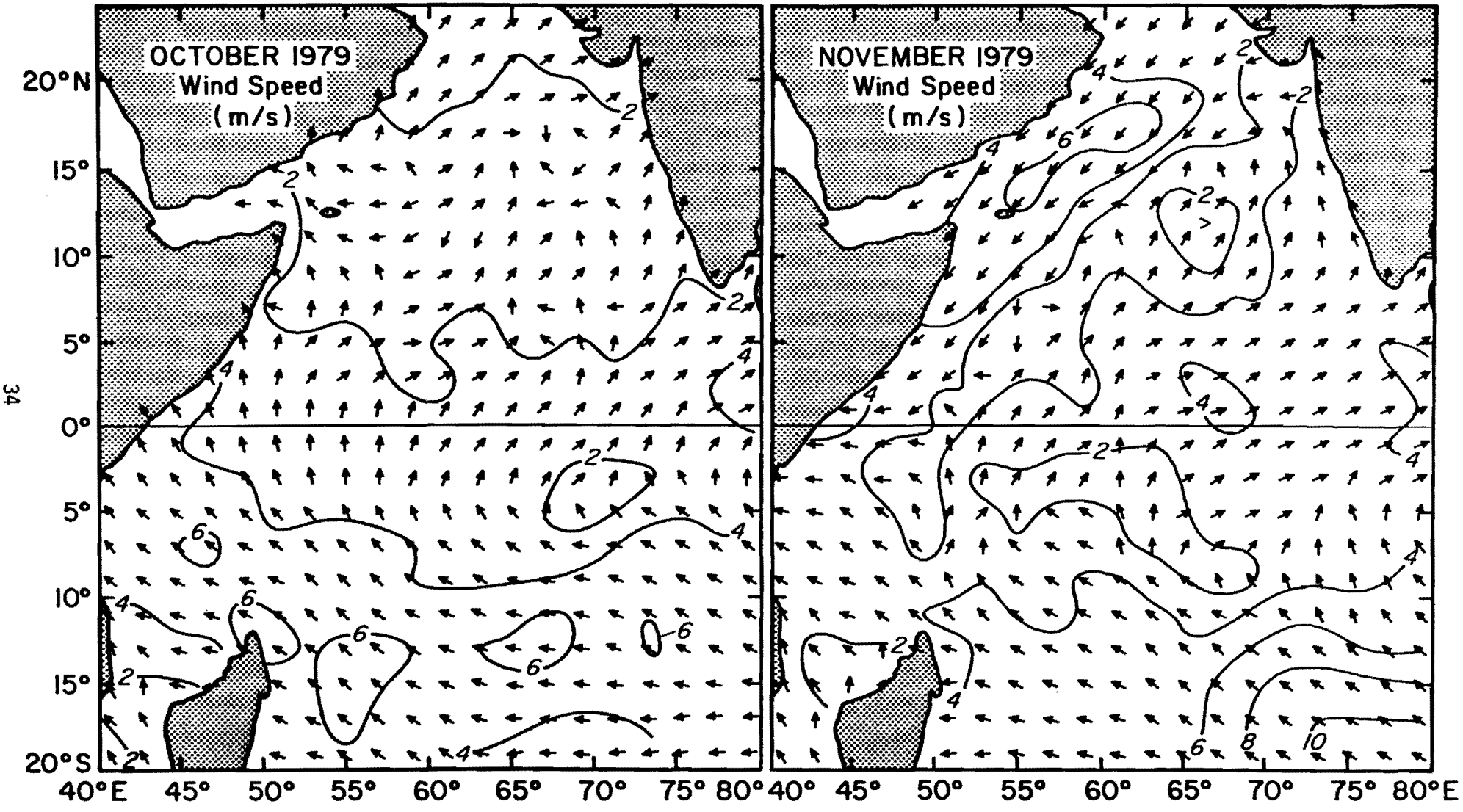

Figure 27. Wind field for October and November 1979 (as in Figure 22).

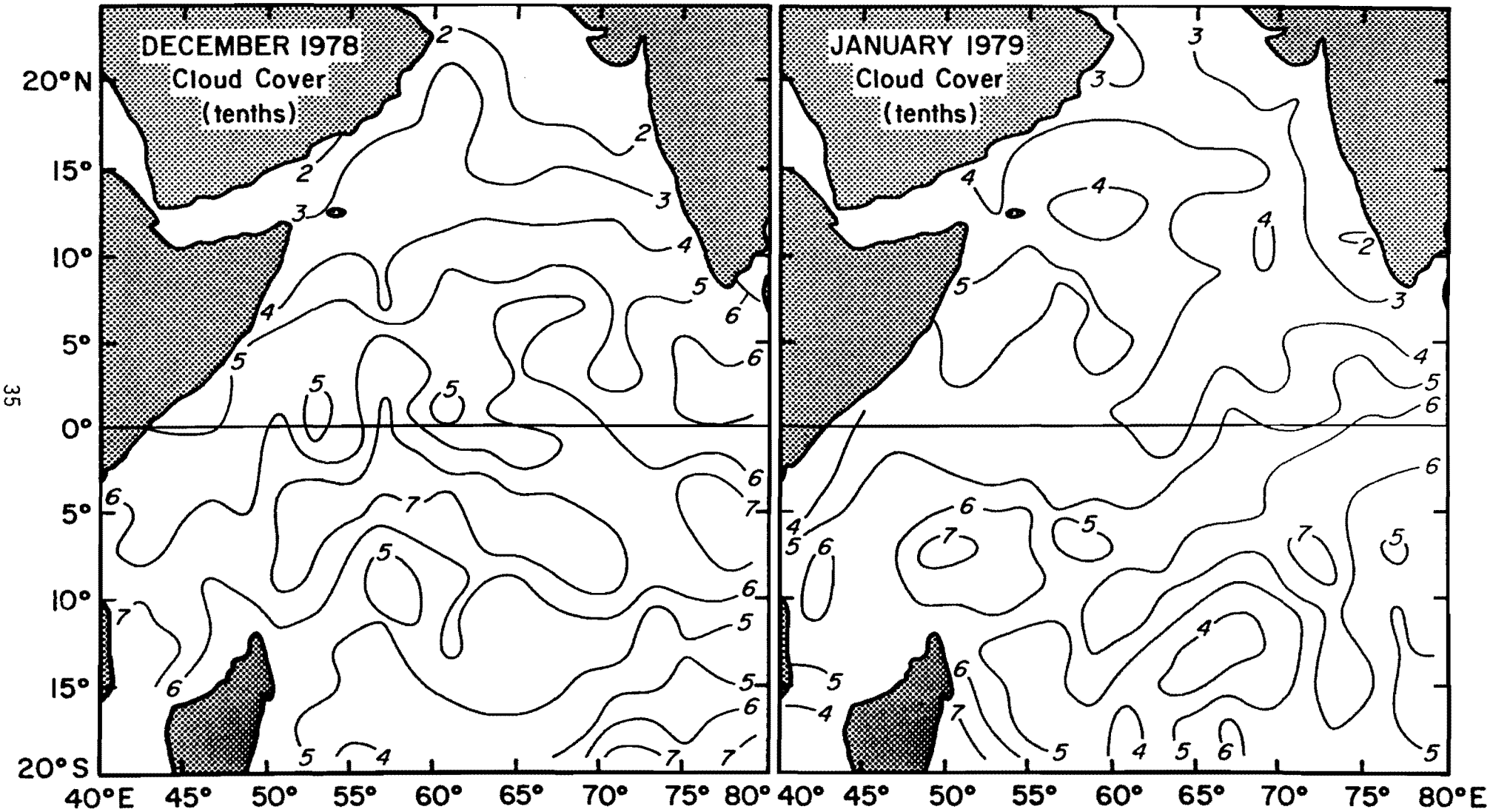

Figure 28. Monthly edited and smoothed cloud covers for December 1978 and January 1979, contoured every one-tenth.

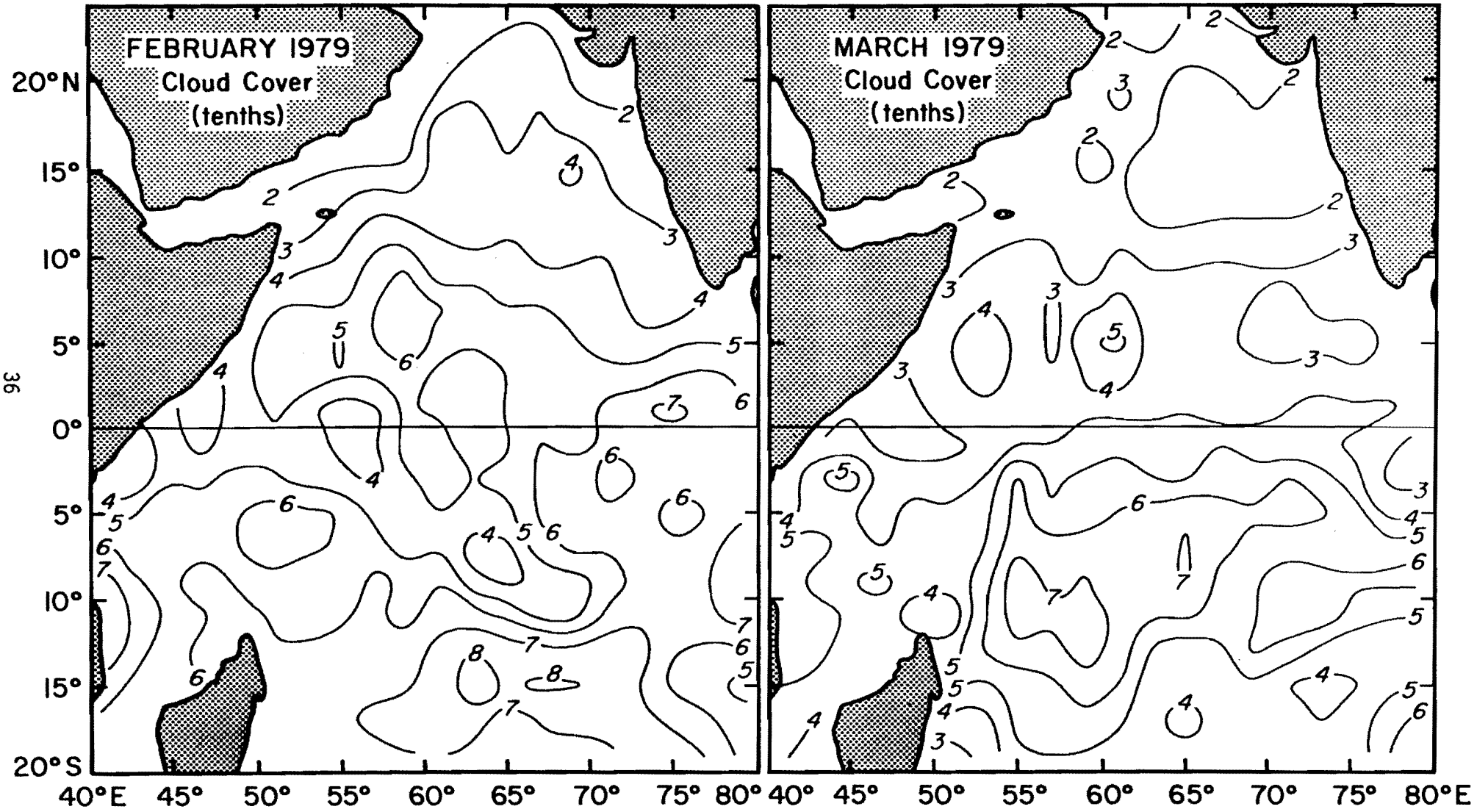

Figure 29. Cloud cover for February and March 1979 (as in Figure 28).

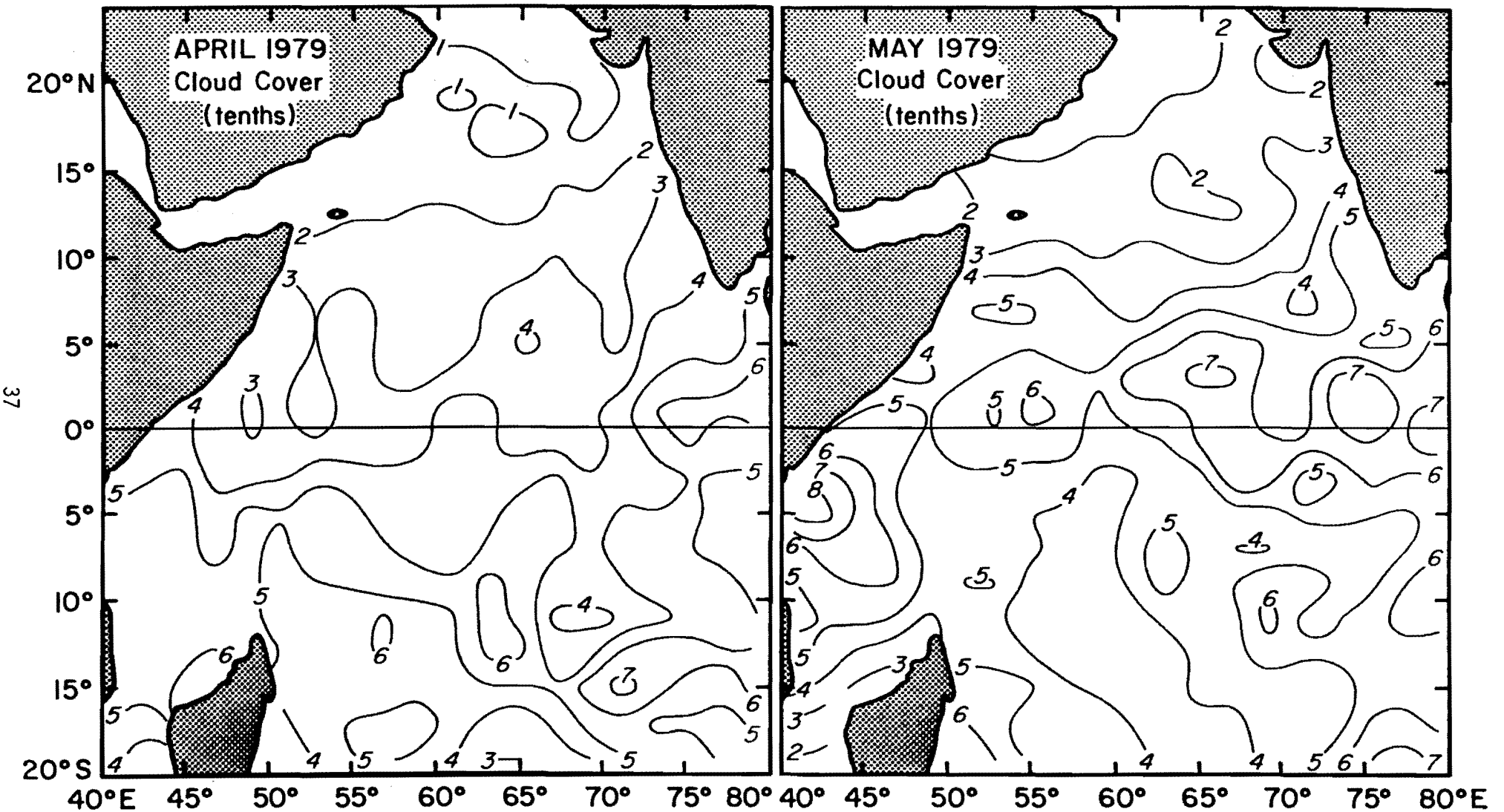

Figure 30. Cloud cover for April and May 1979 (as in Figure 28).

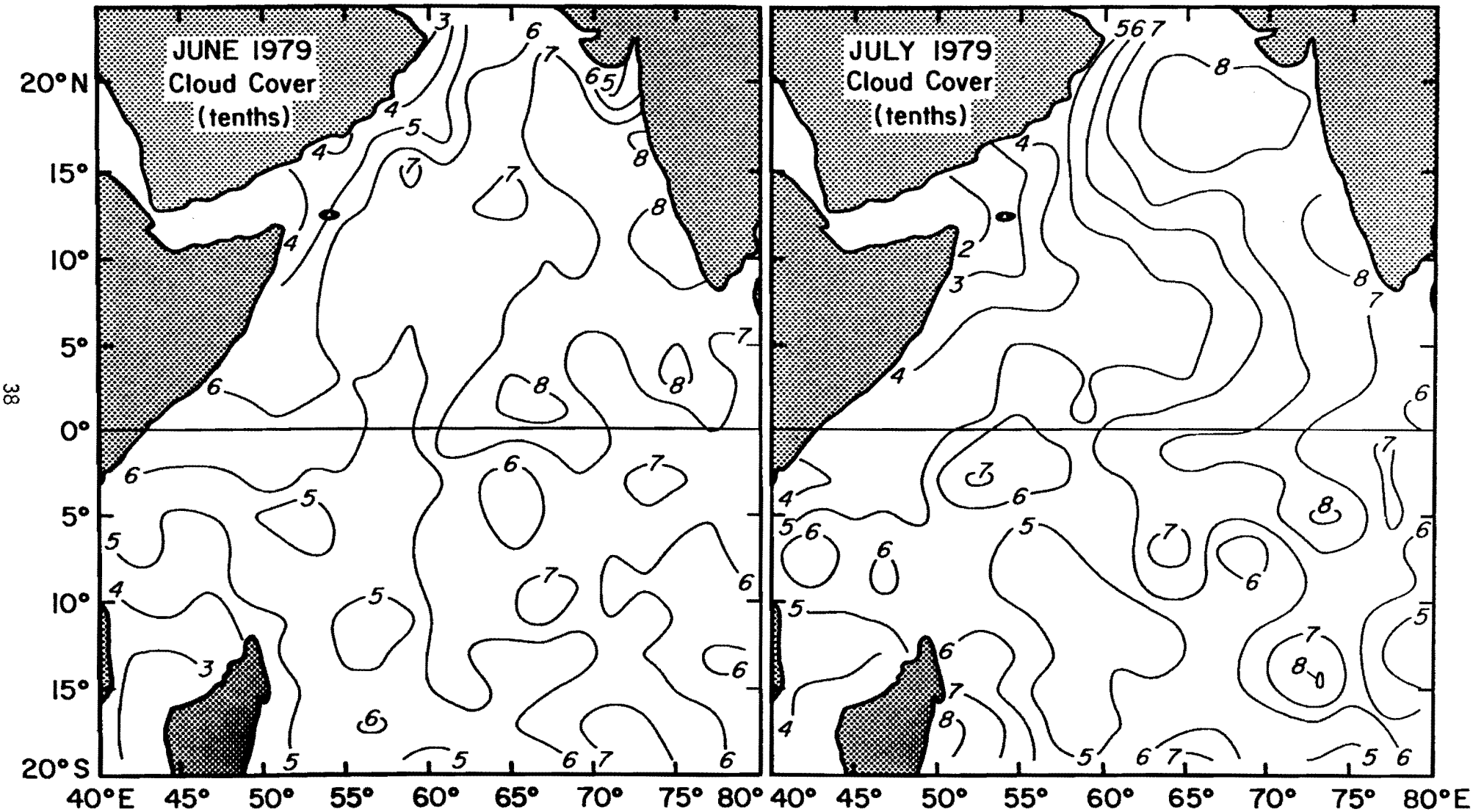

Figure 31. Cloud cover for June and July 1979 (as in Figure 28).

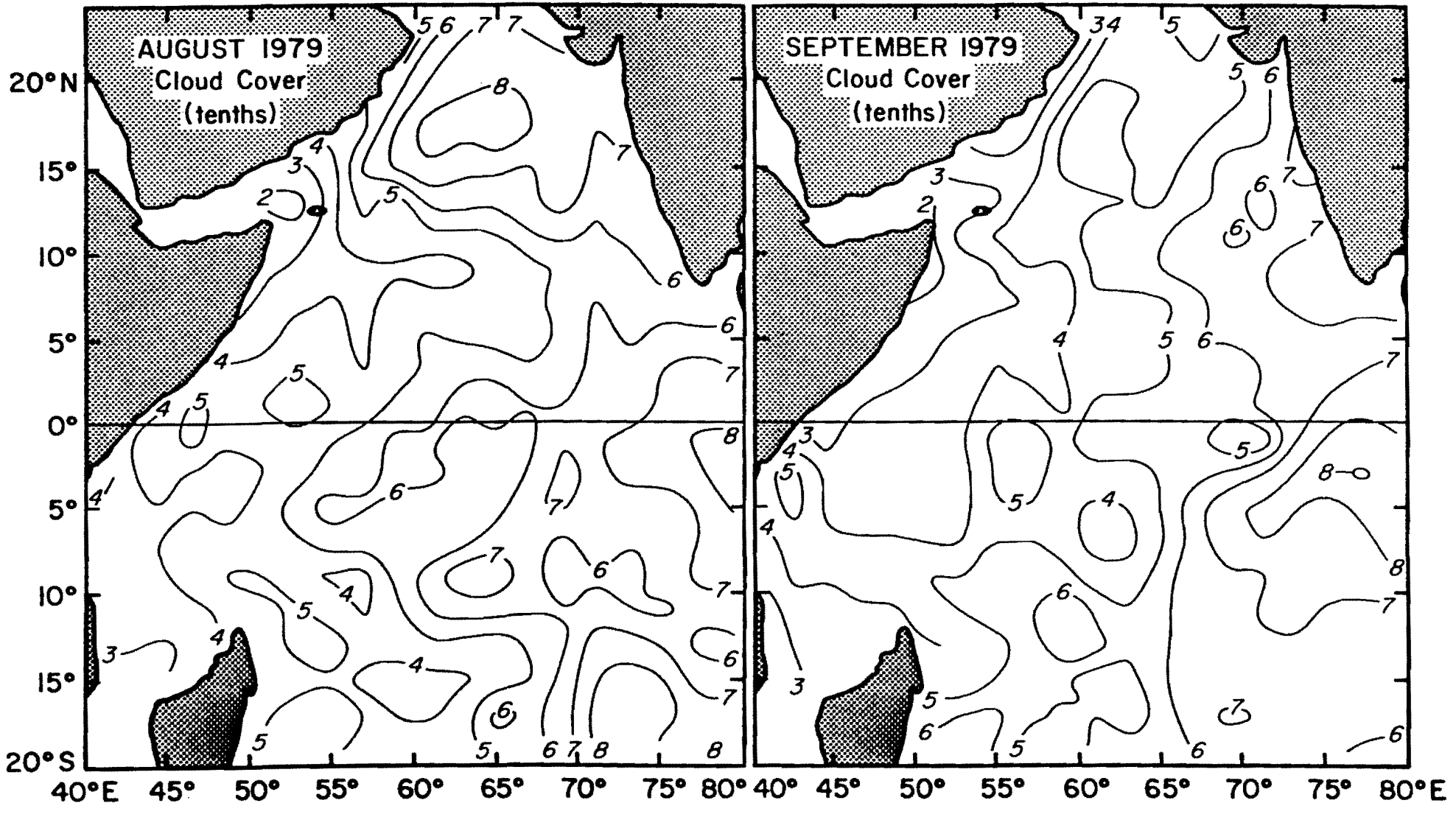

Figure 32. Cloud cover for August and September 1979 (as in Figure 28).

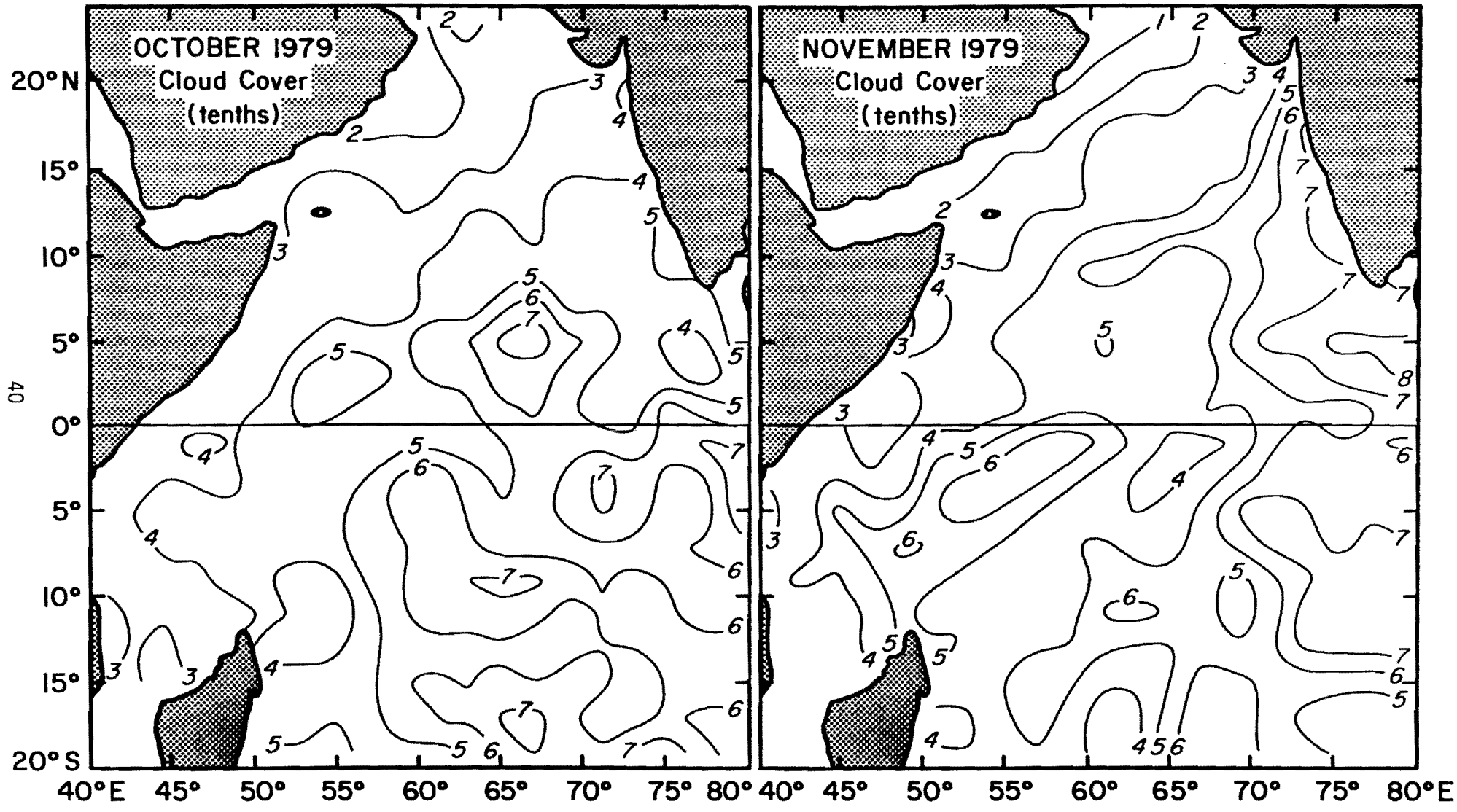

Figure 33. Cloud cover for October and November 1979 (as in Figure 28).

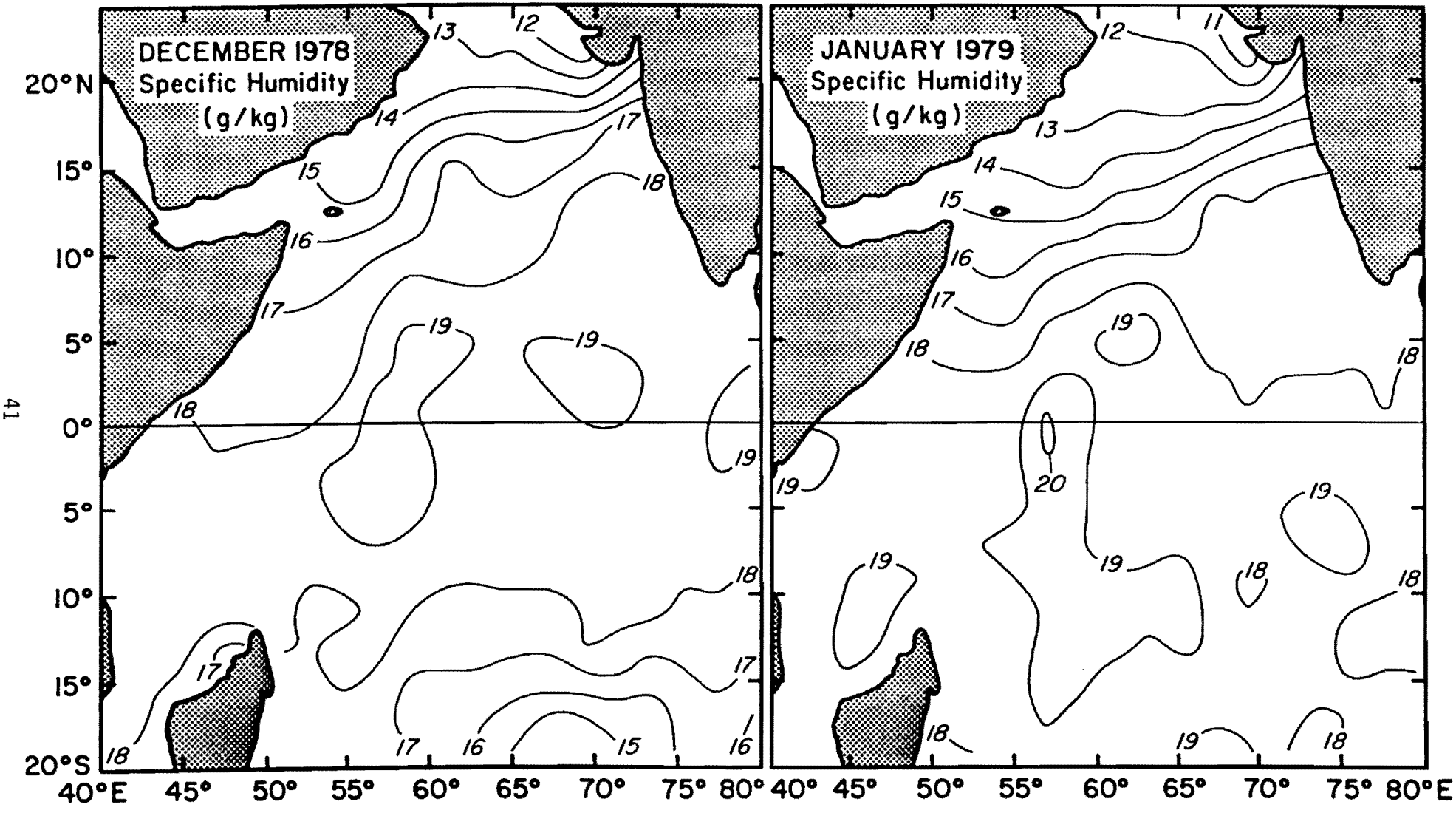

Figure 34. Monthly edited and smoothed specific humidity for December 1978 and January 1979, contoured every 1 g/kg.

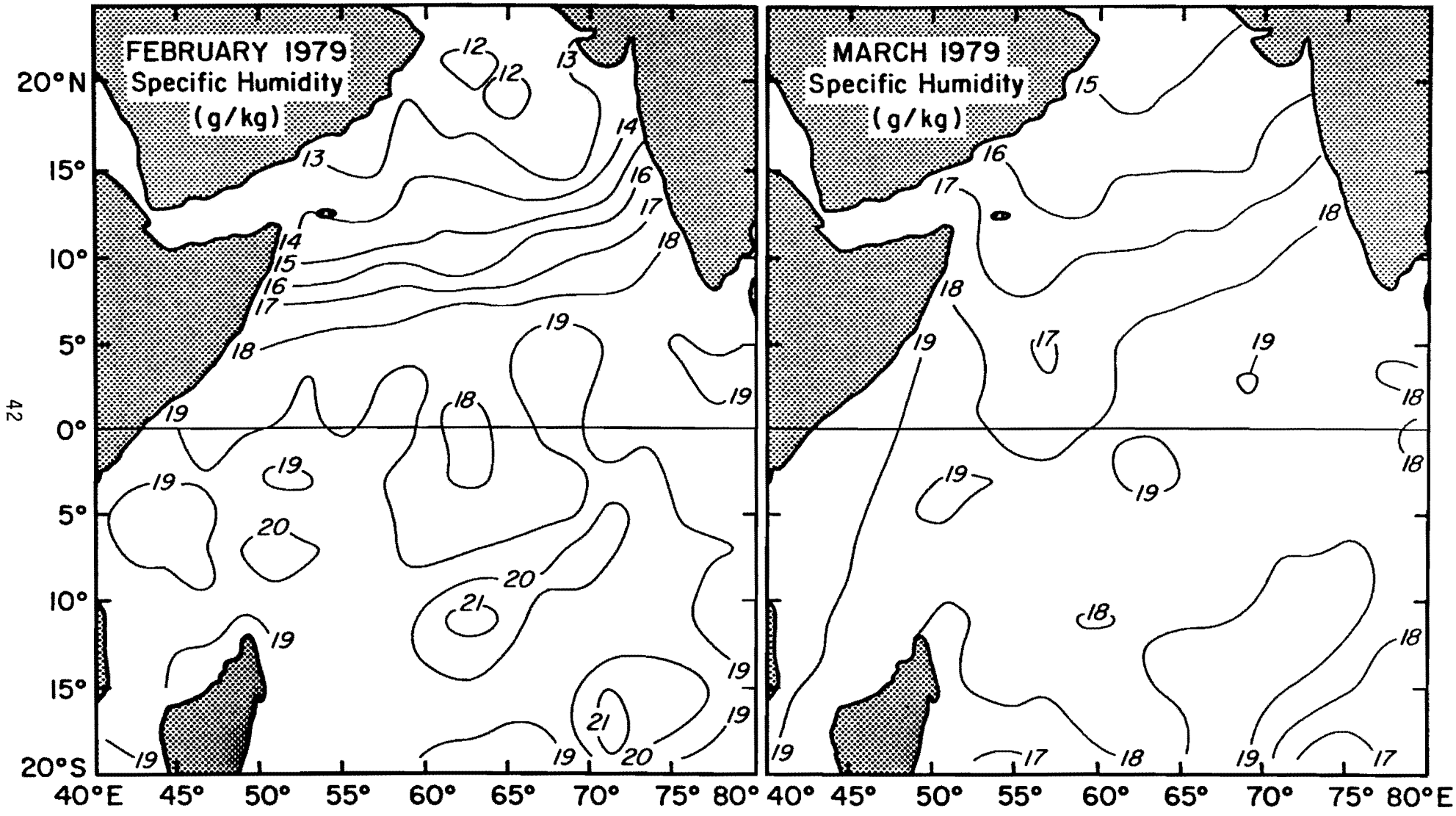

Figure 35. Specific humidity for February and March 1979 (as in Figure 34).

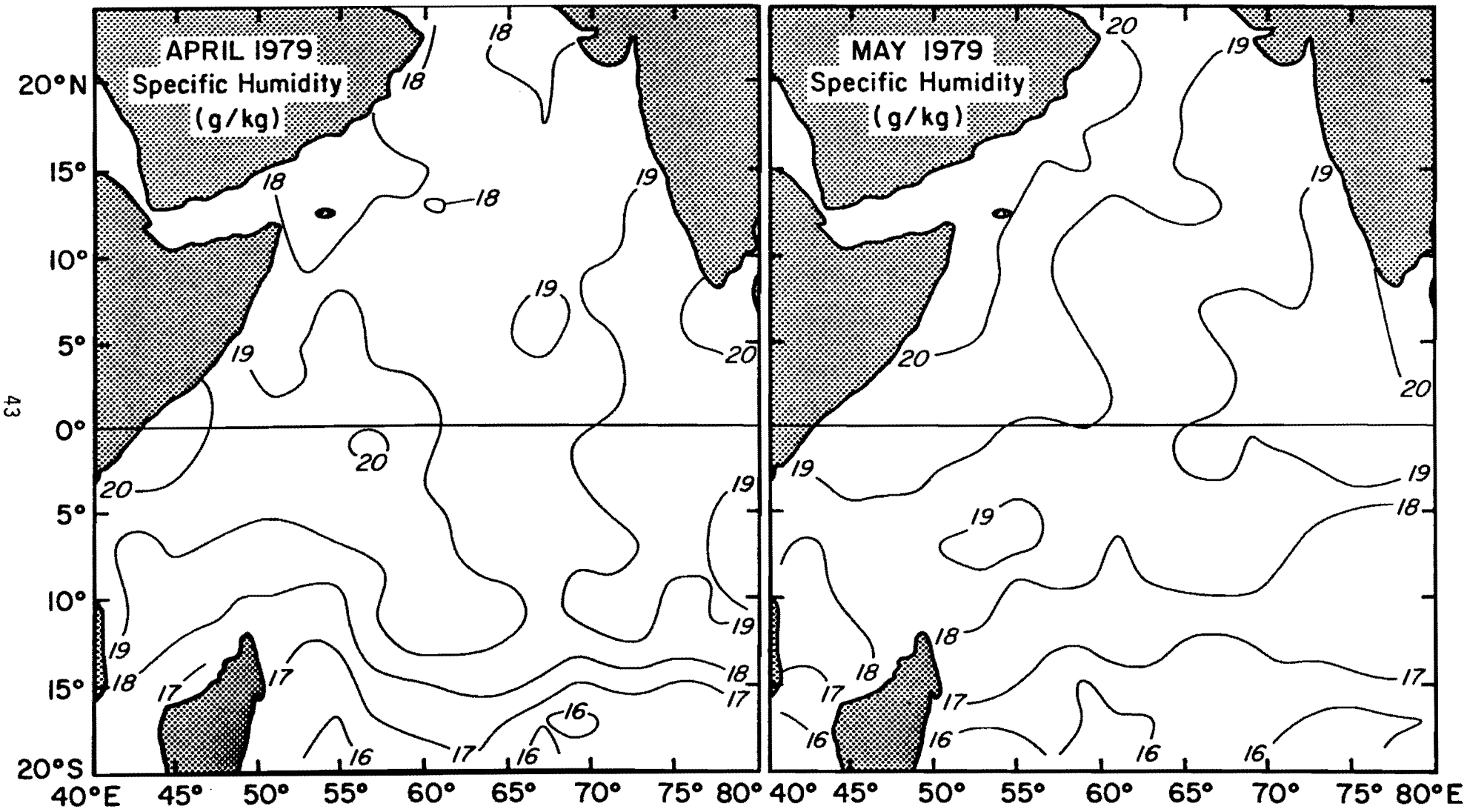

Figure 36. Specific humidity for April and May 1979 (as in Figure 34).

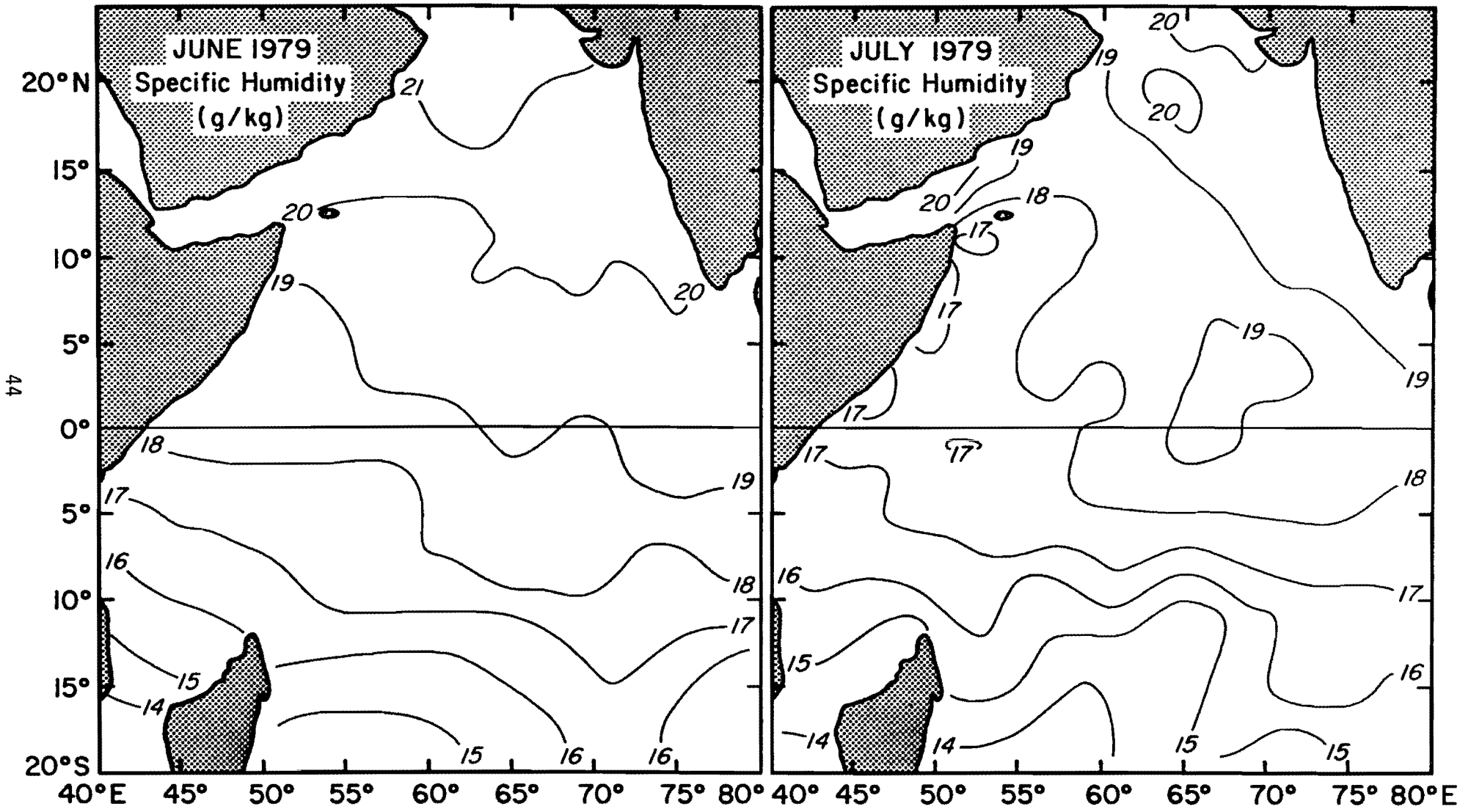

Figure 37. Specific humidity for June and July 1979 (as in Figure 34).

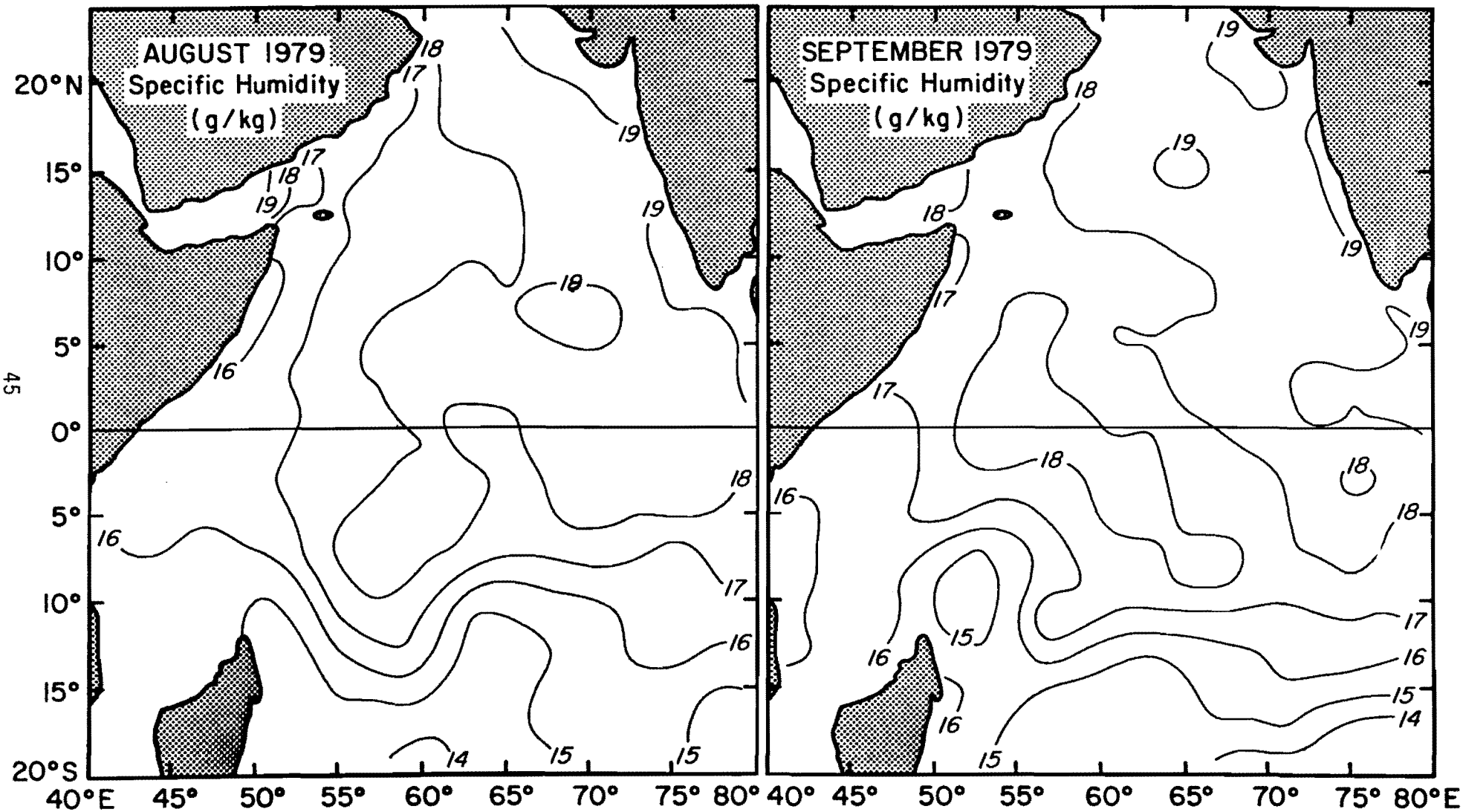

Figure 38. Specific humidity for August and September 1979 (as in Figure 34).

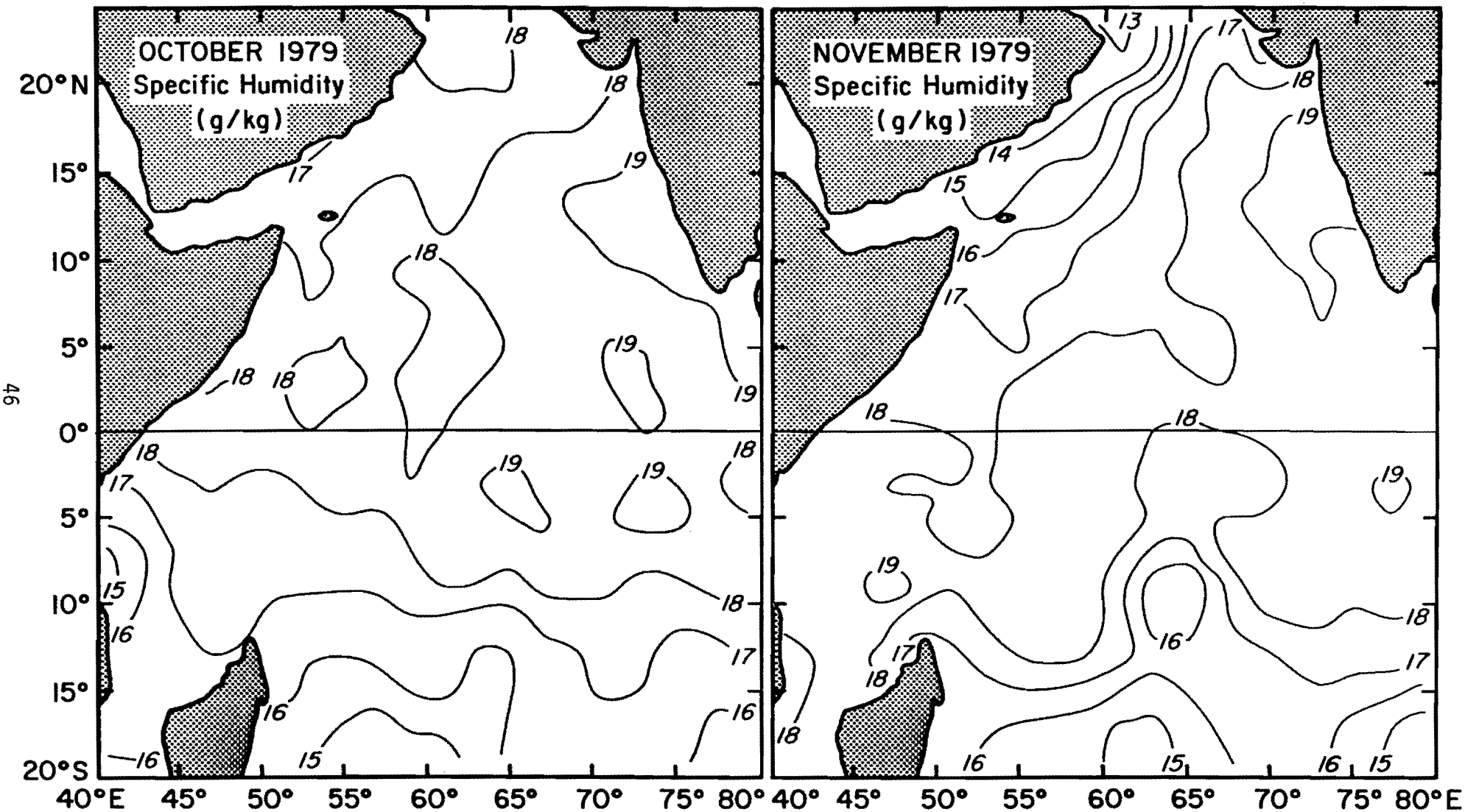

Figure 39. Specific humidity for October and November 1979 (as in Figure 34).

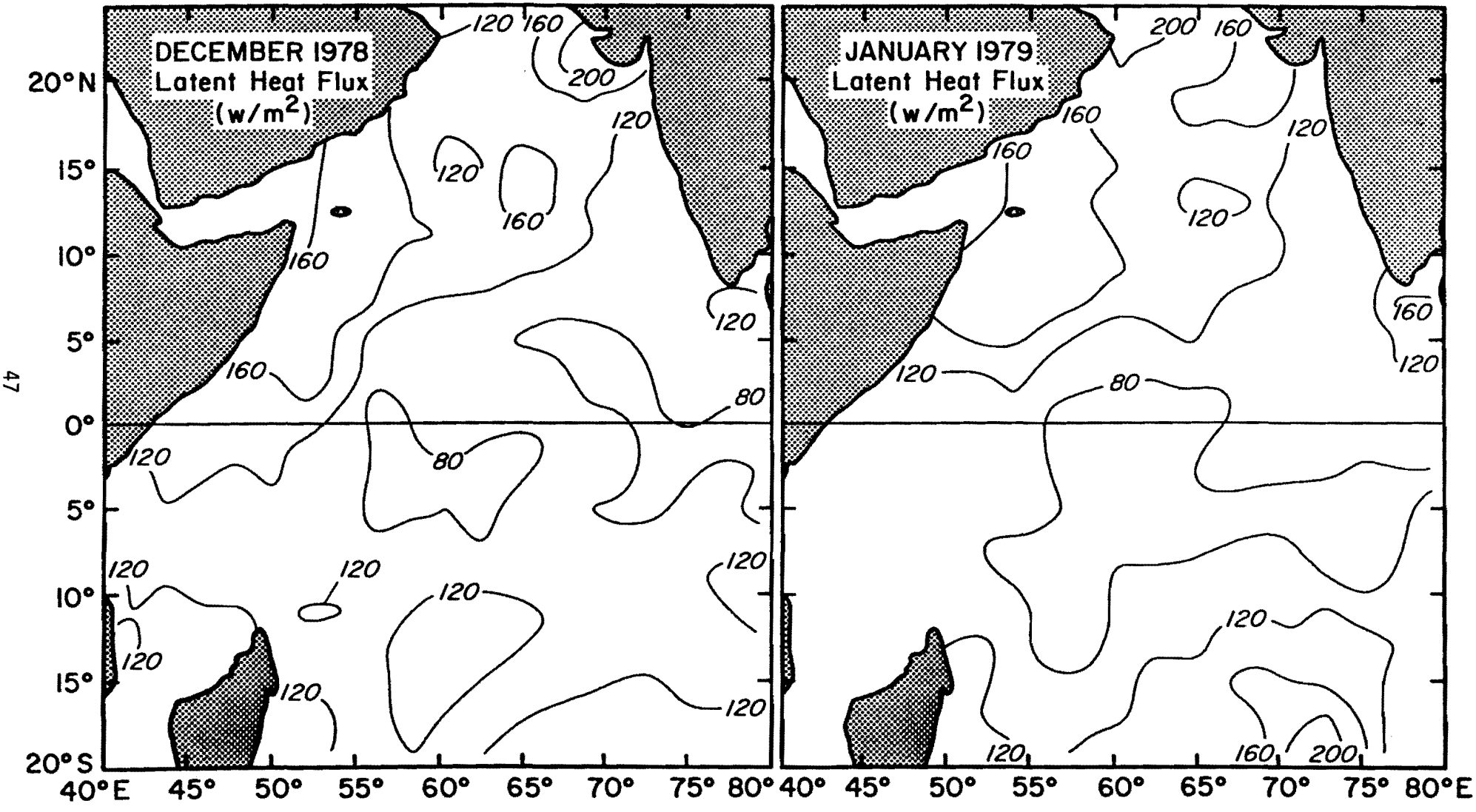

Figure 40. Monthly latent heat flux for December 1978 and January 1979 (computed from edited and smoothed observations), contoured every 40 W/m^2.

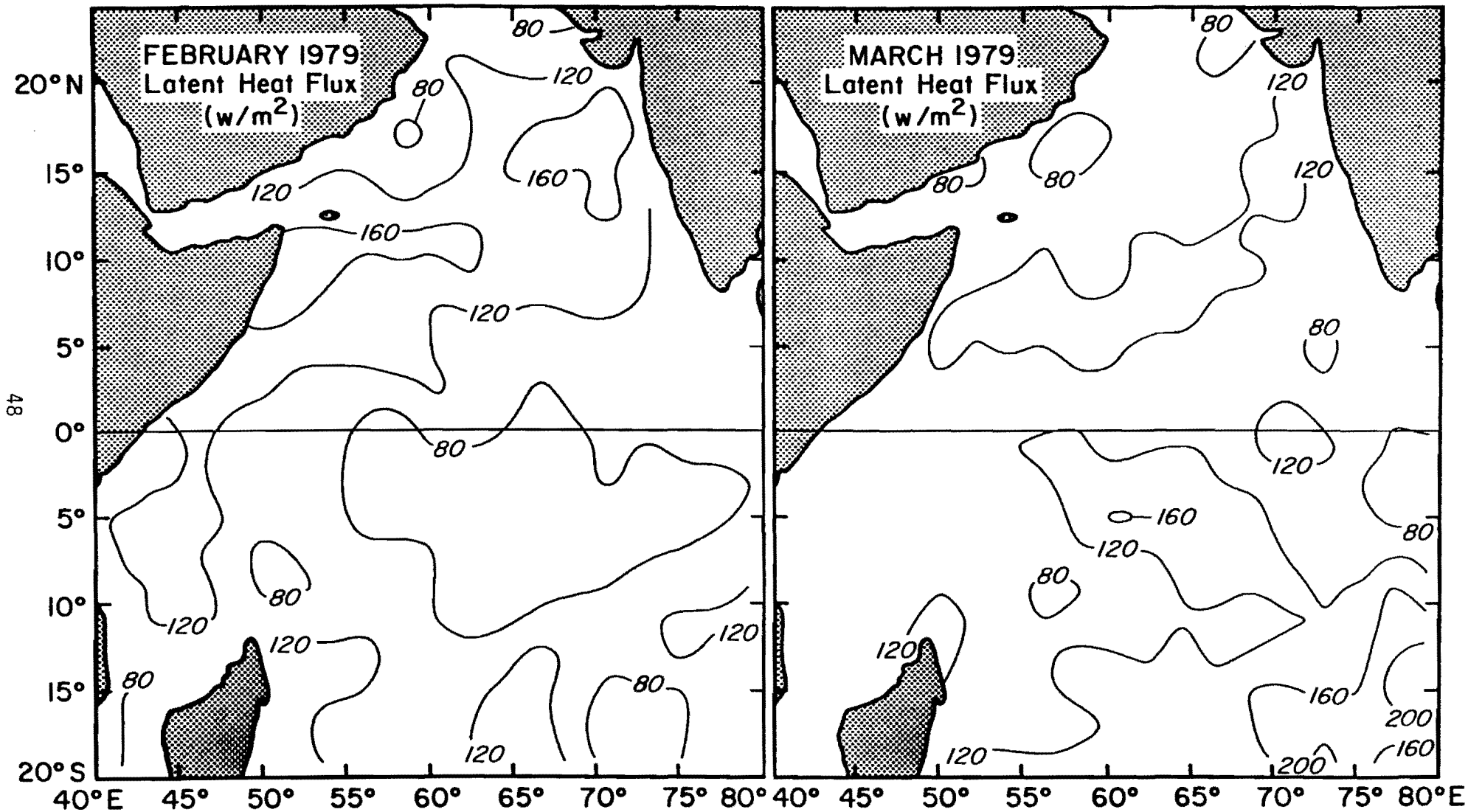

Figure 41. Latent heat flux for February and March 1979 (as in Figure 40).

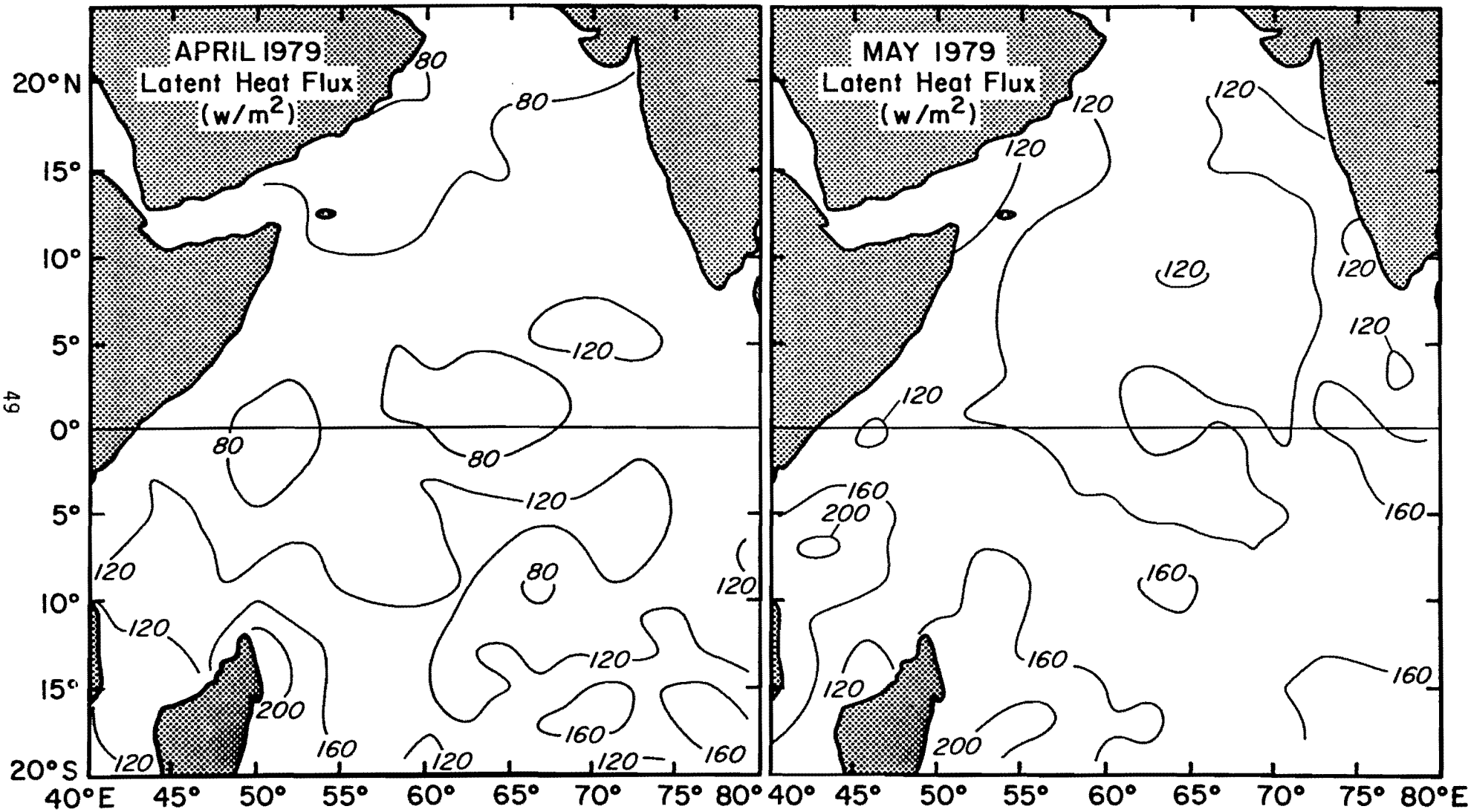

Figure 42. Latent heat flux for April and May 1979 (as in Figure 40).

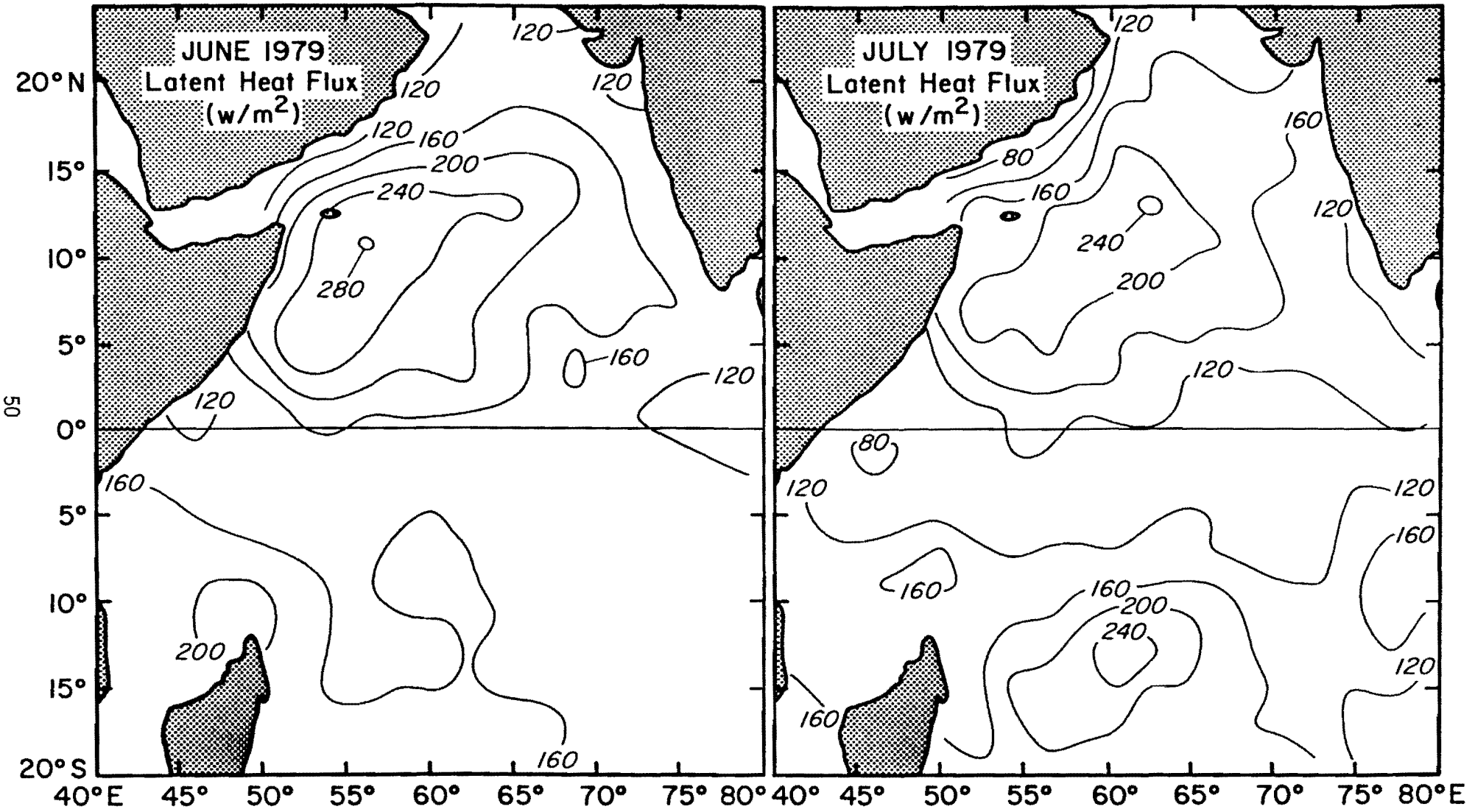

Figure 43. Latent heat flux for June and July 1979 (as in Figure 40).

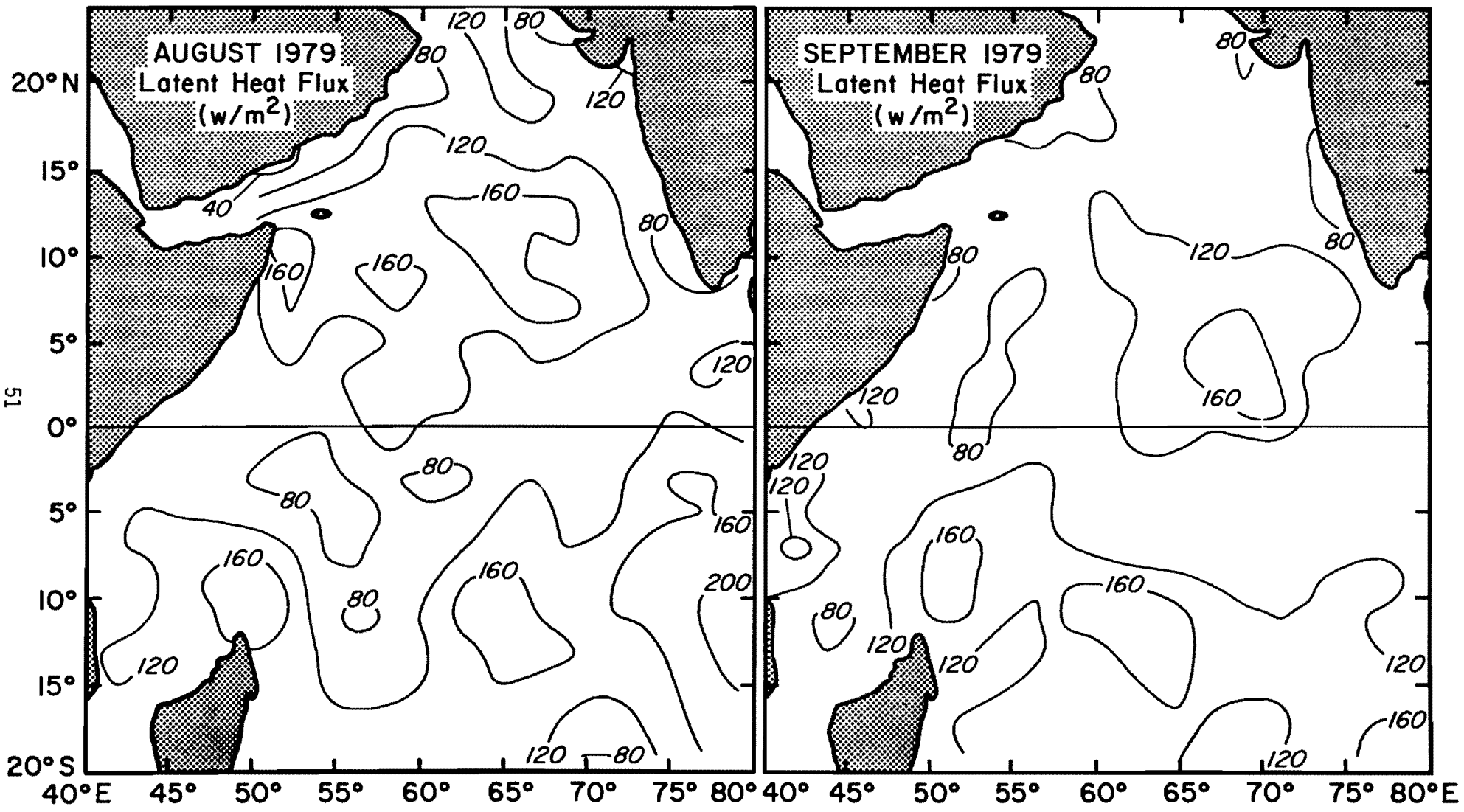

Figure 44. Latent heat flux for August and September 1979 (as in Figure 40).

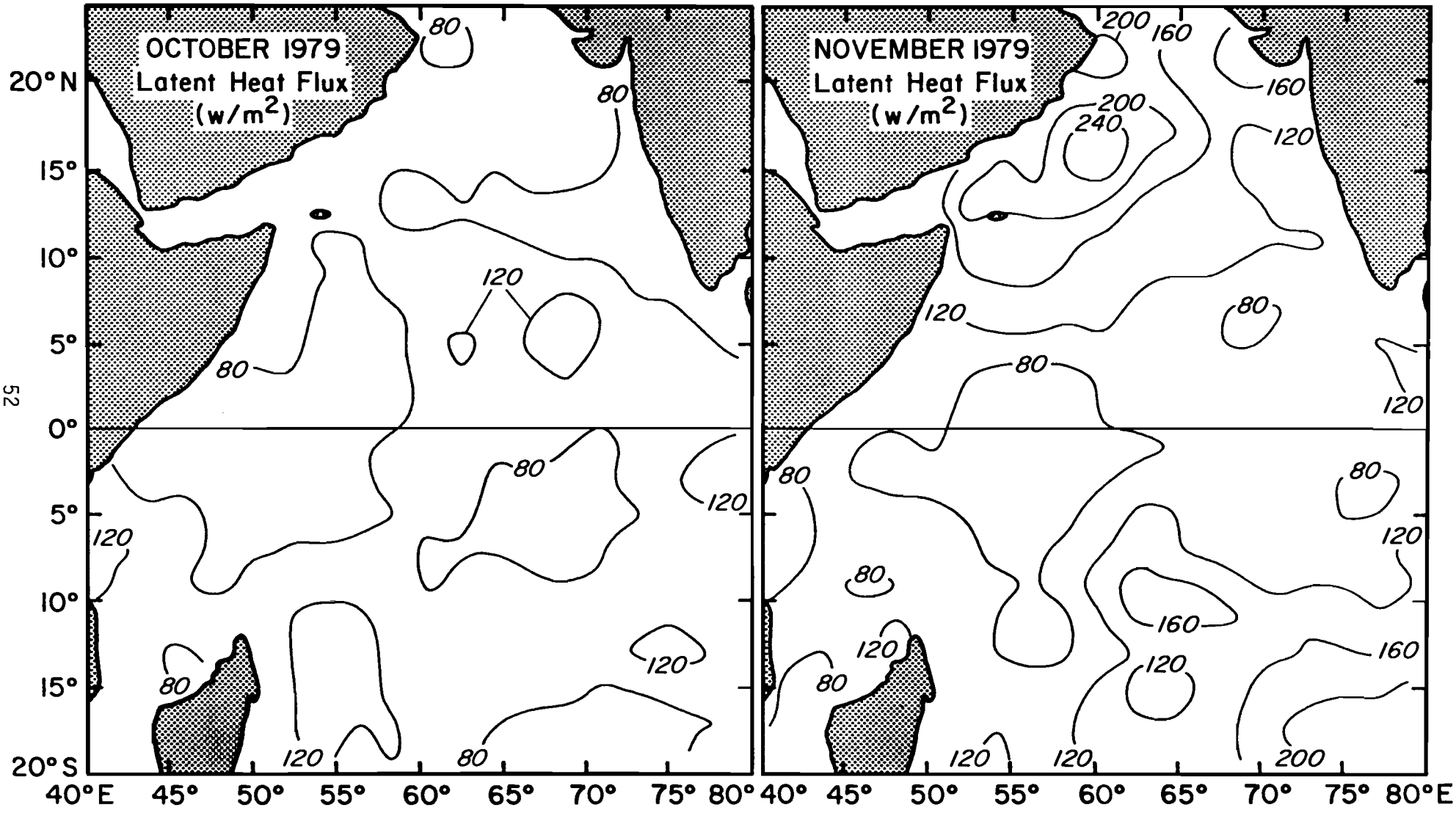

Figure 45. Latent heat flux for October and November 1979 (as in Figure 40).

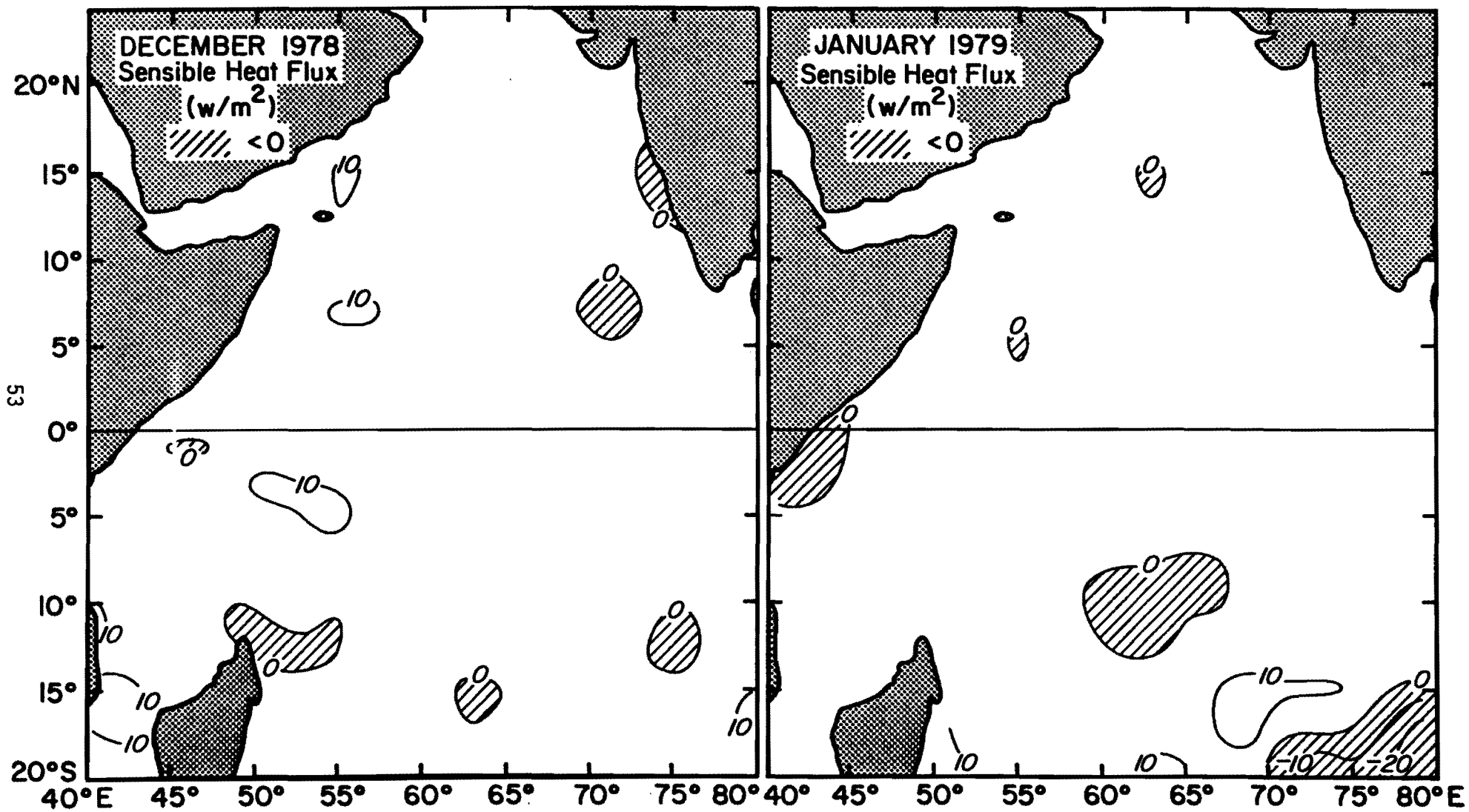

Figure 46. Monthly sensible heat flux for December 1978 and January 1979 (computed from edited and smoothed observations), contoured every 10 W/m^2. Shaded areas denote regions of heat loss.

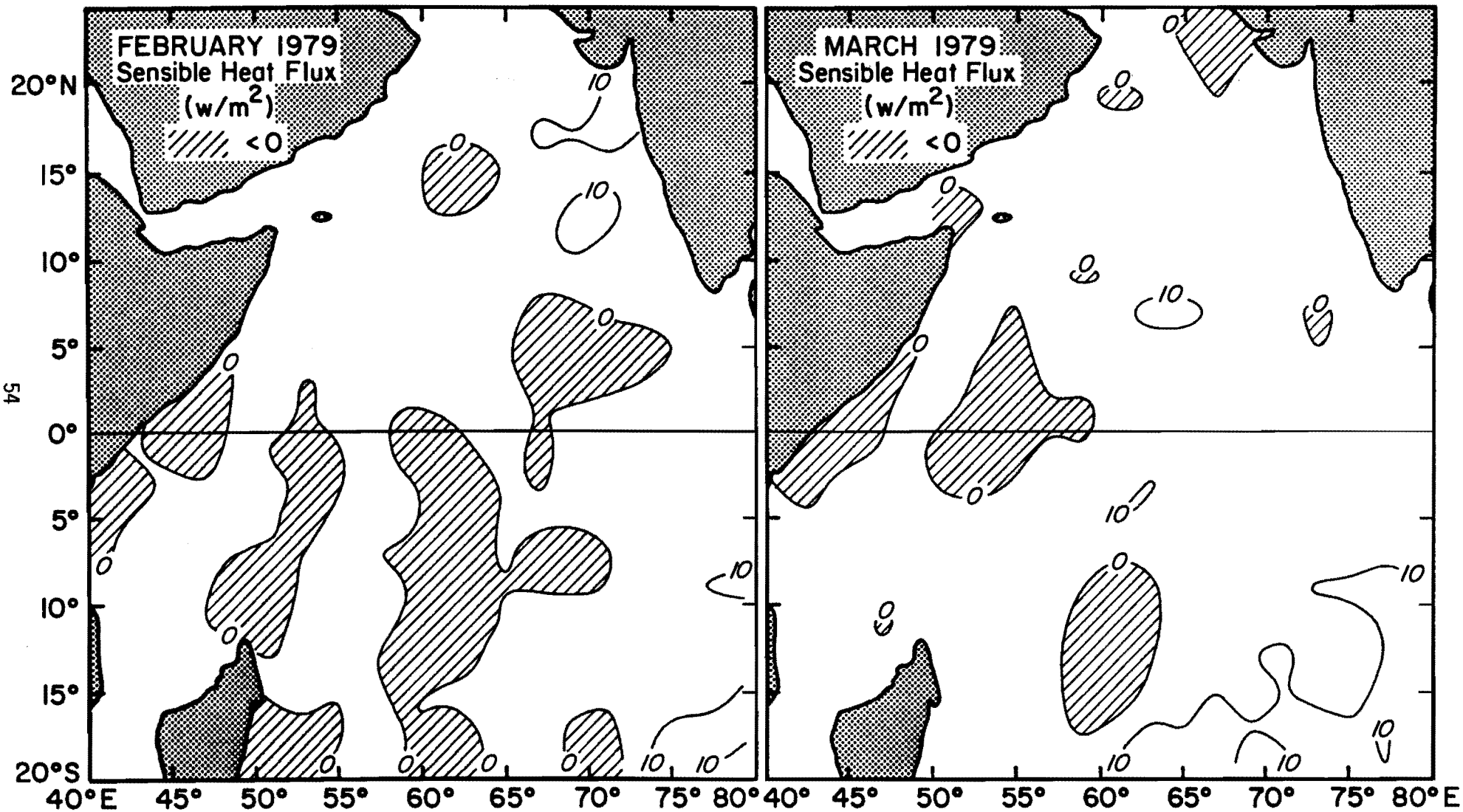

Figure 47. Sensible heat flux for February and March 1979 (as in Figure 46).

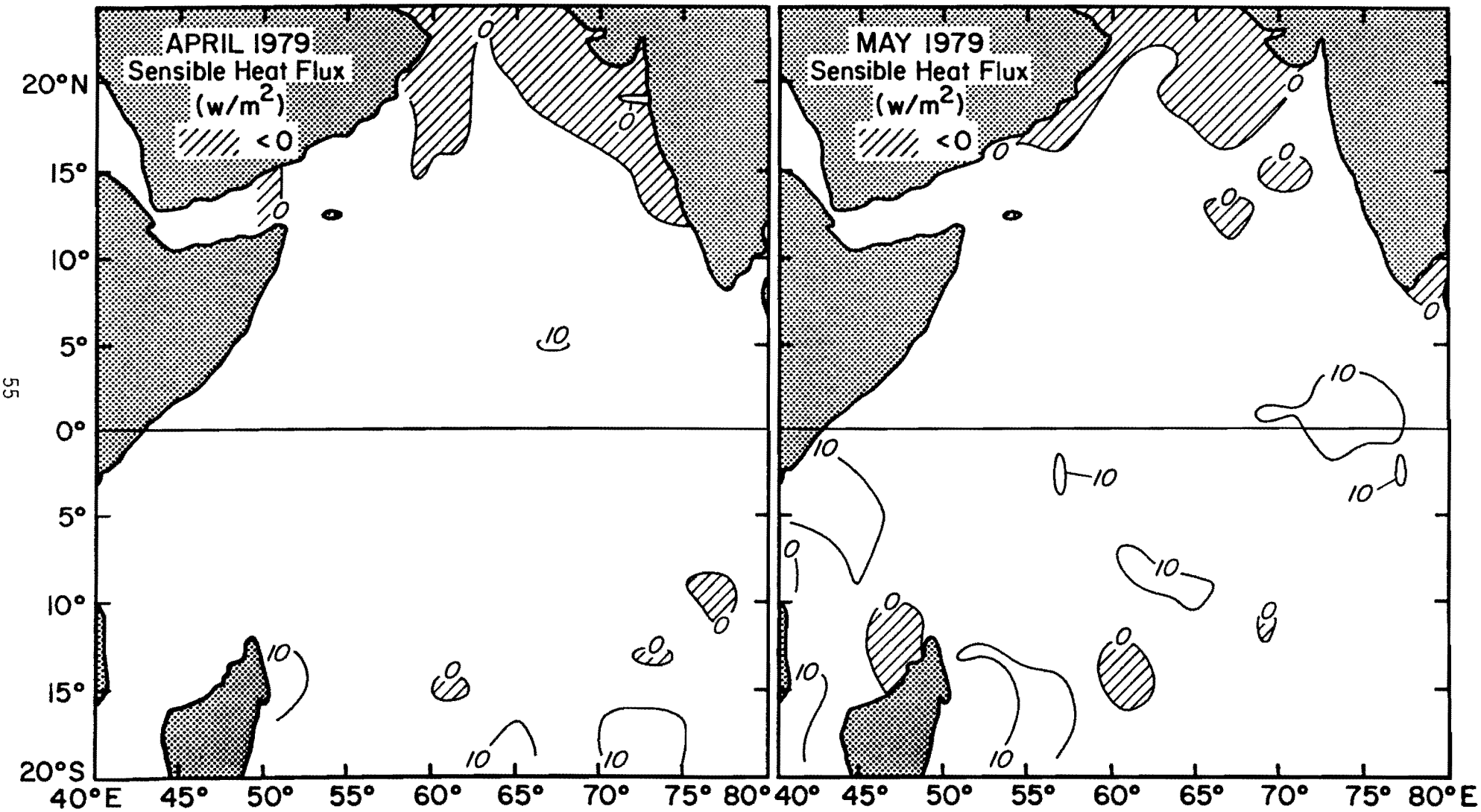

Figure 48. Sensible heat flux for April and May 1979 (as in Figure 46).

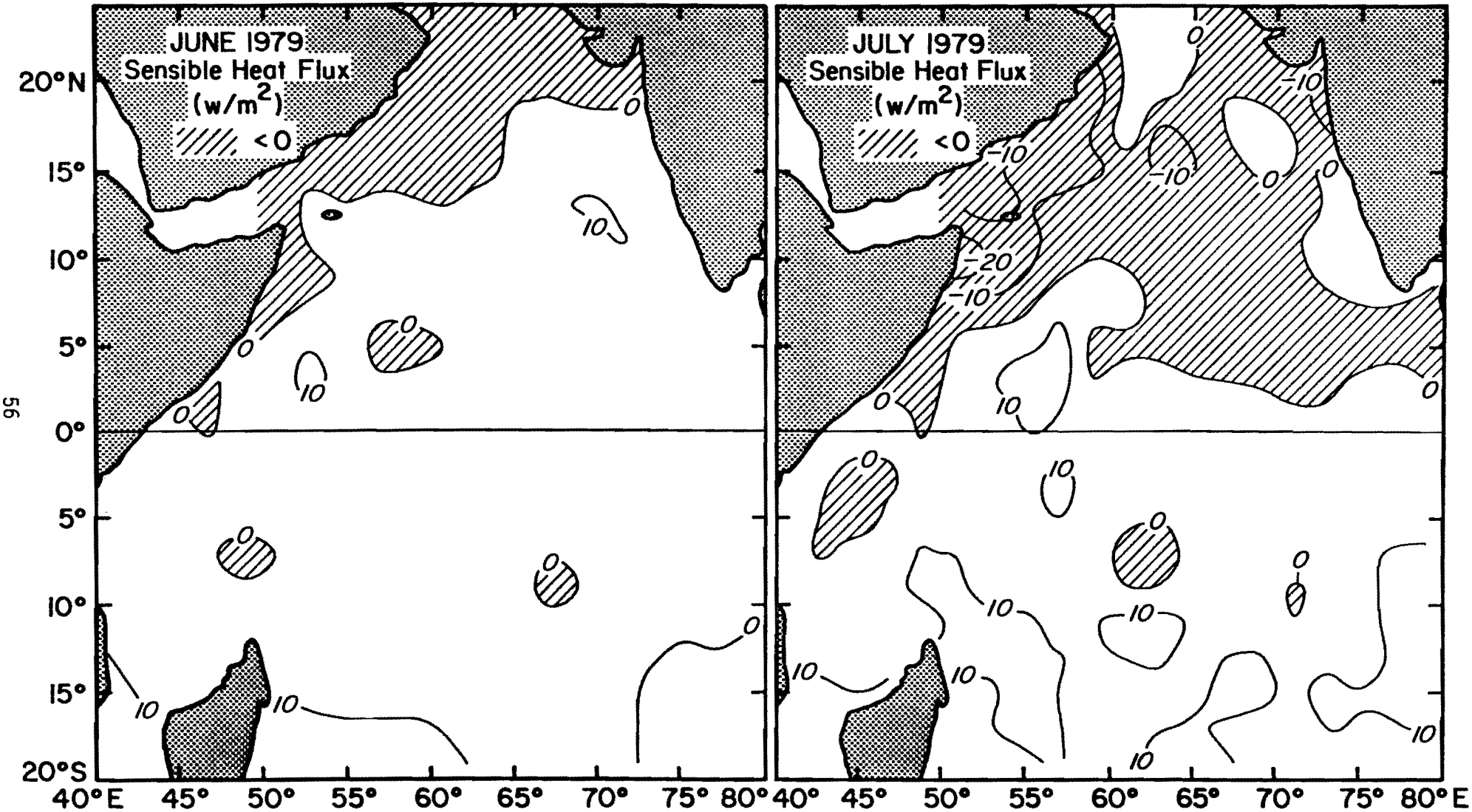

Figure 49. Sensible heat flux for June and July 1979 (as in Figure 46).

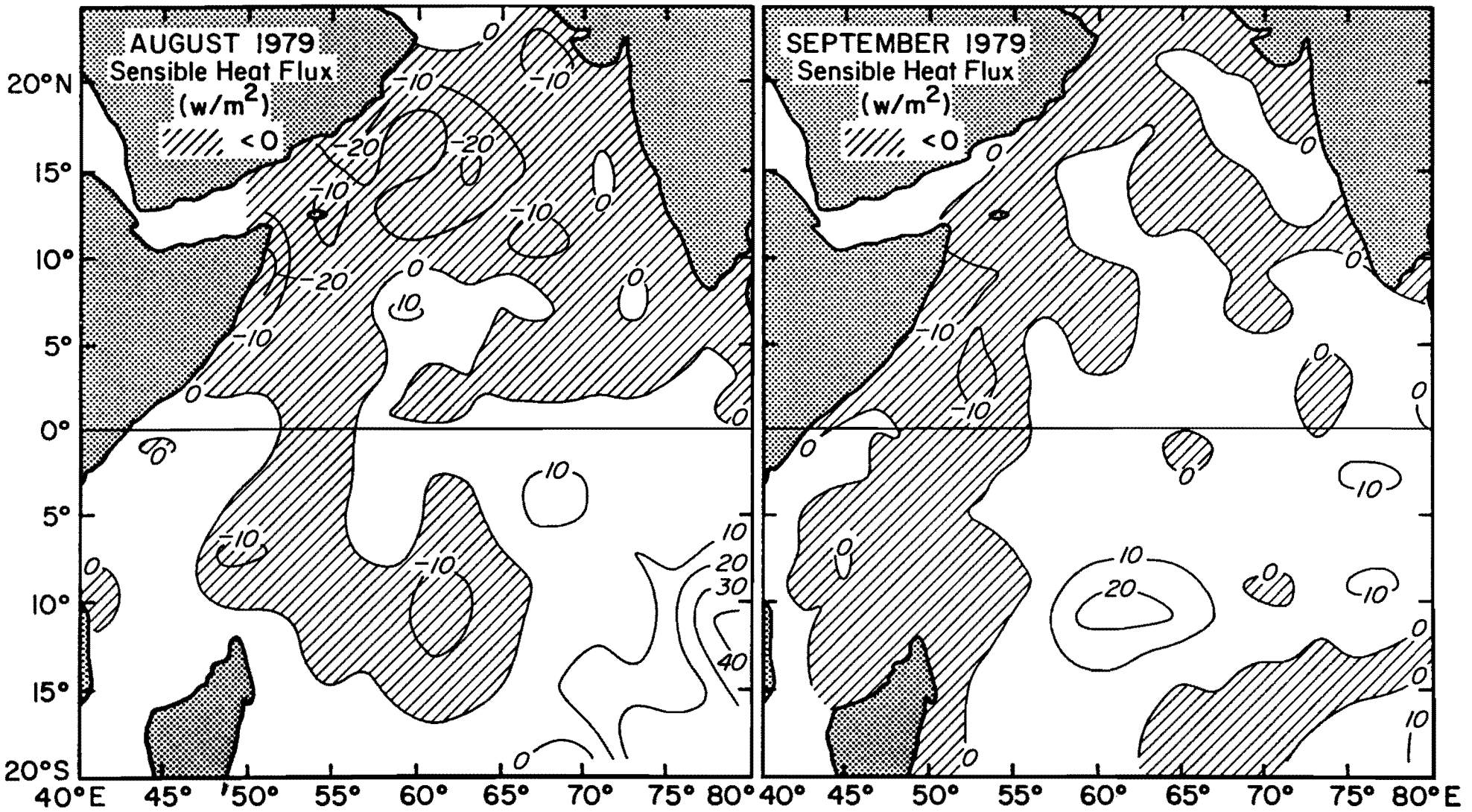

Figure 50. Sensible heat flux for August and September 1979 (as in Figure 46).

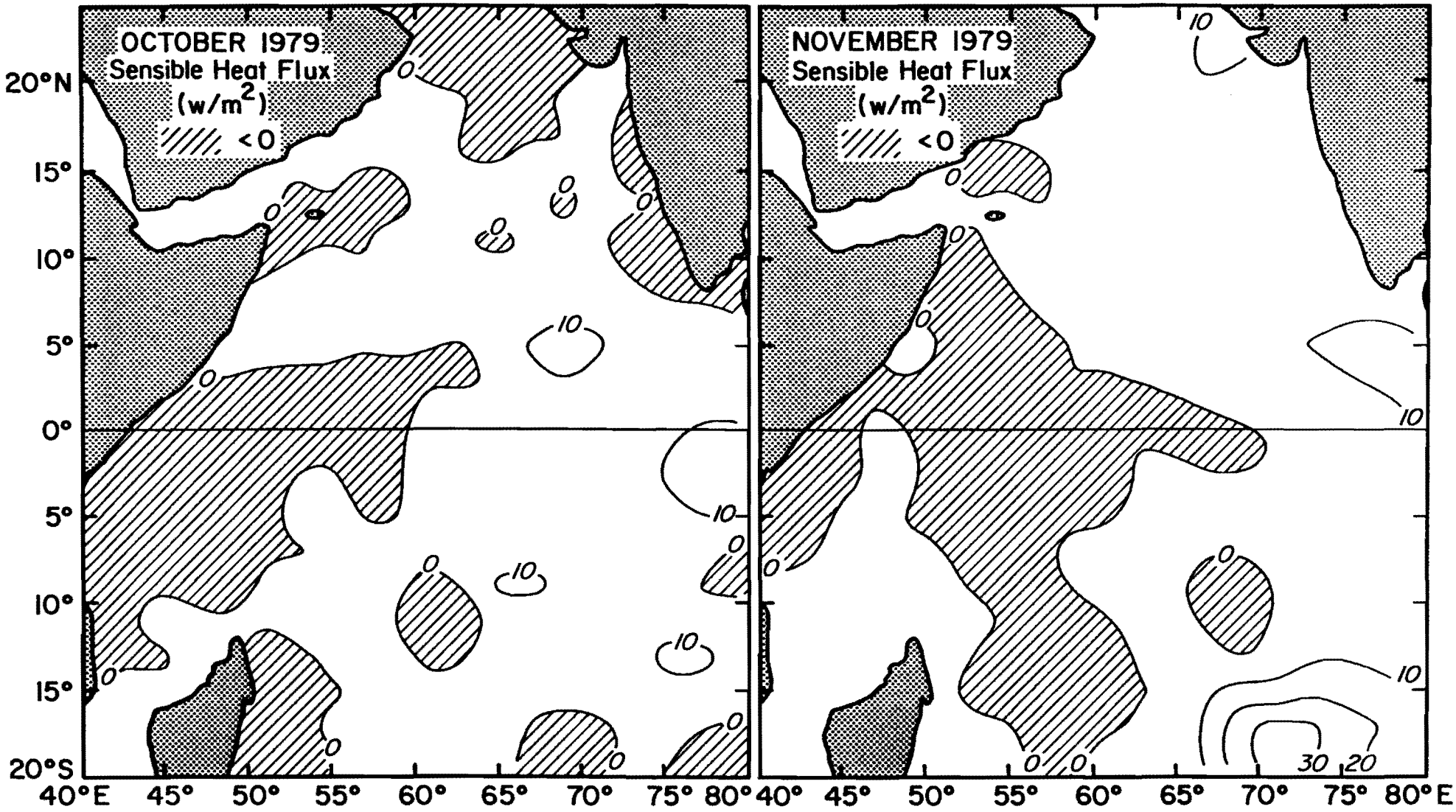

Figure 51. Sensible heat flux for October and November 1979 (as in Figure 46).

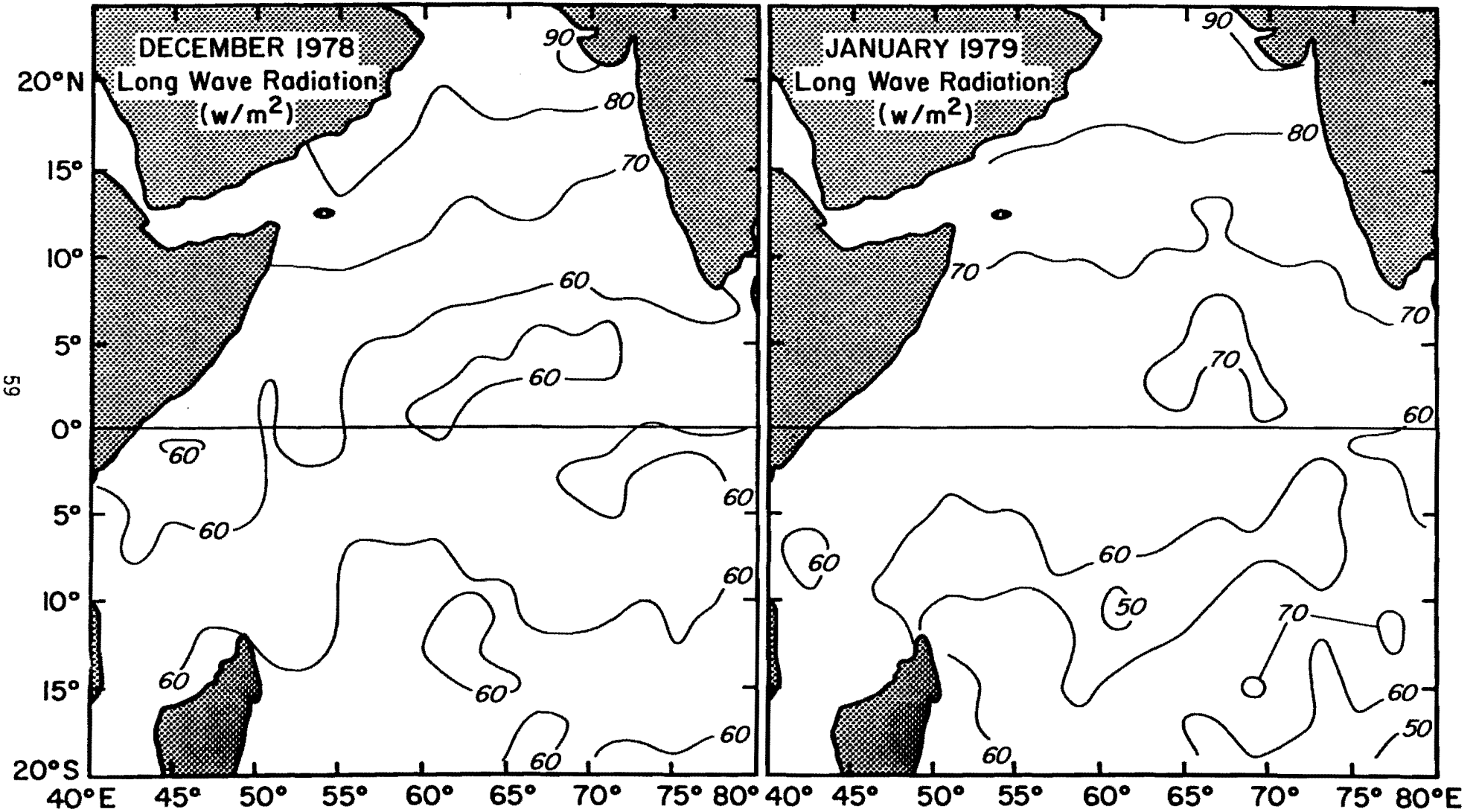

Figure 52. Monthly long-wave radiation for December 1978 and January 1979 (computed from edited and smoothed observations), contoured every 10 W/m^2.

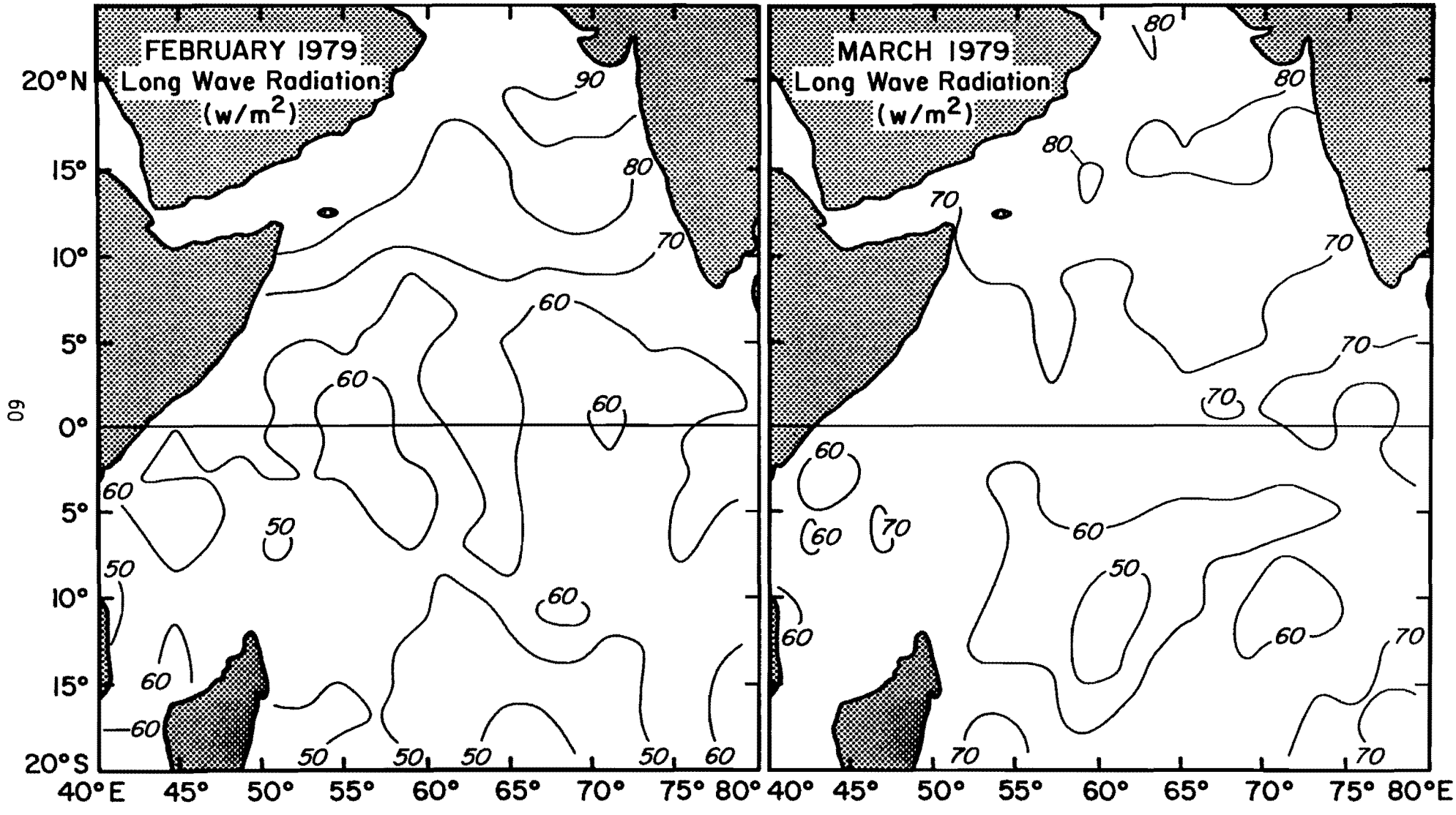

Figure 53. Long-wave radiation for February and March 1979 (as in Figure 52).

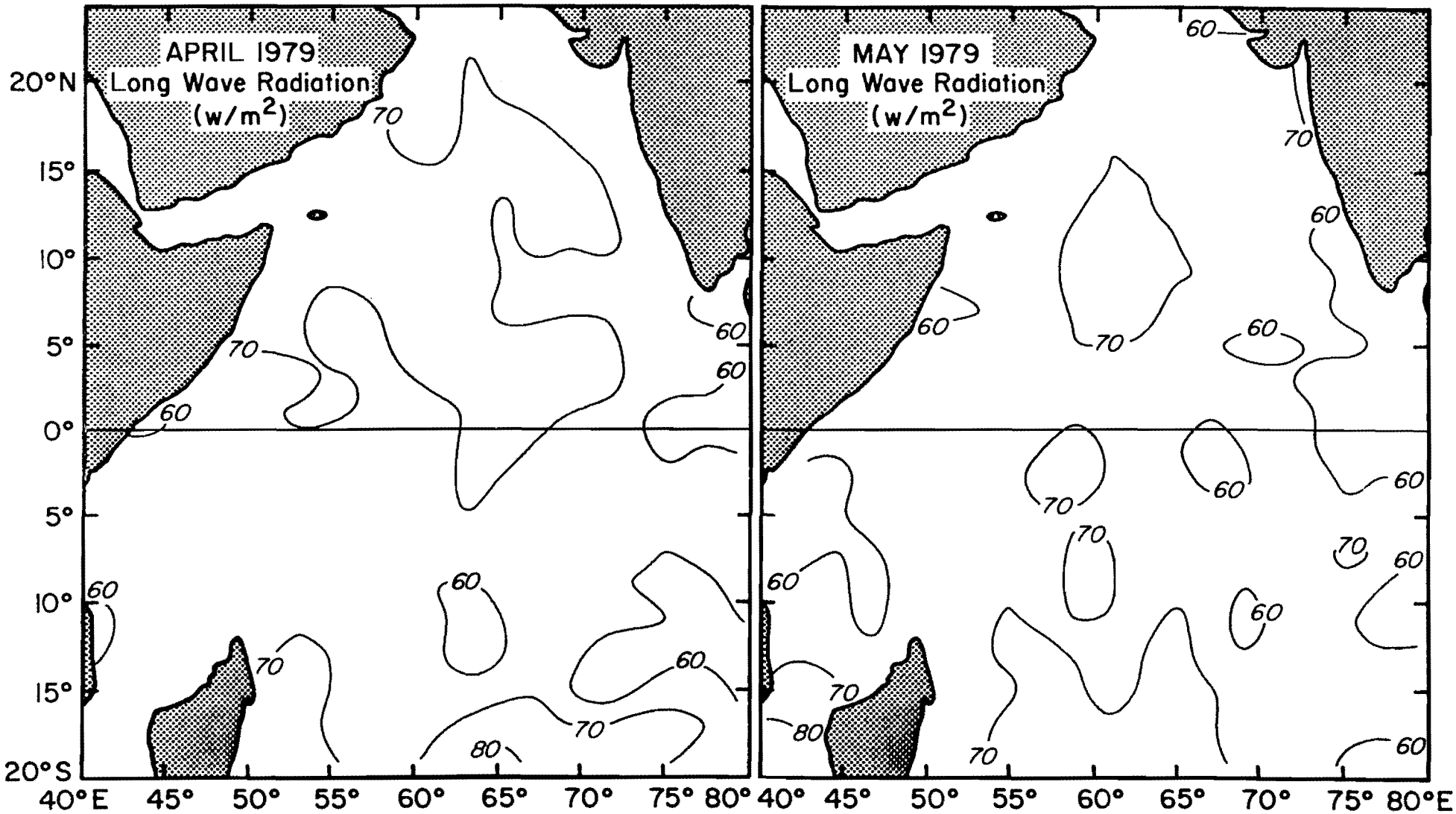

Figure 54. Long-wave radiation for April and May 1979 (as in Figure 52).

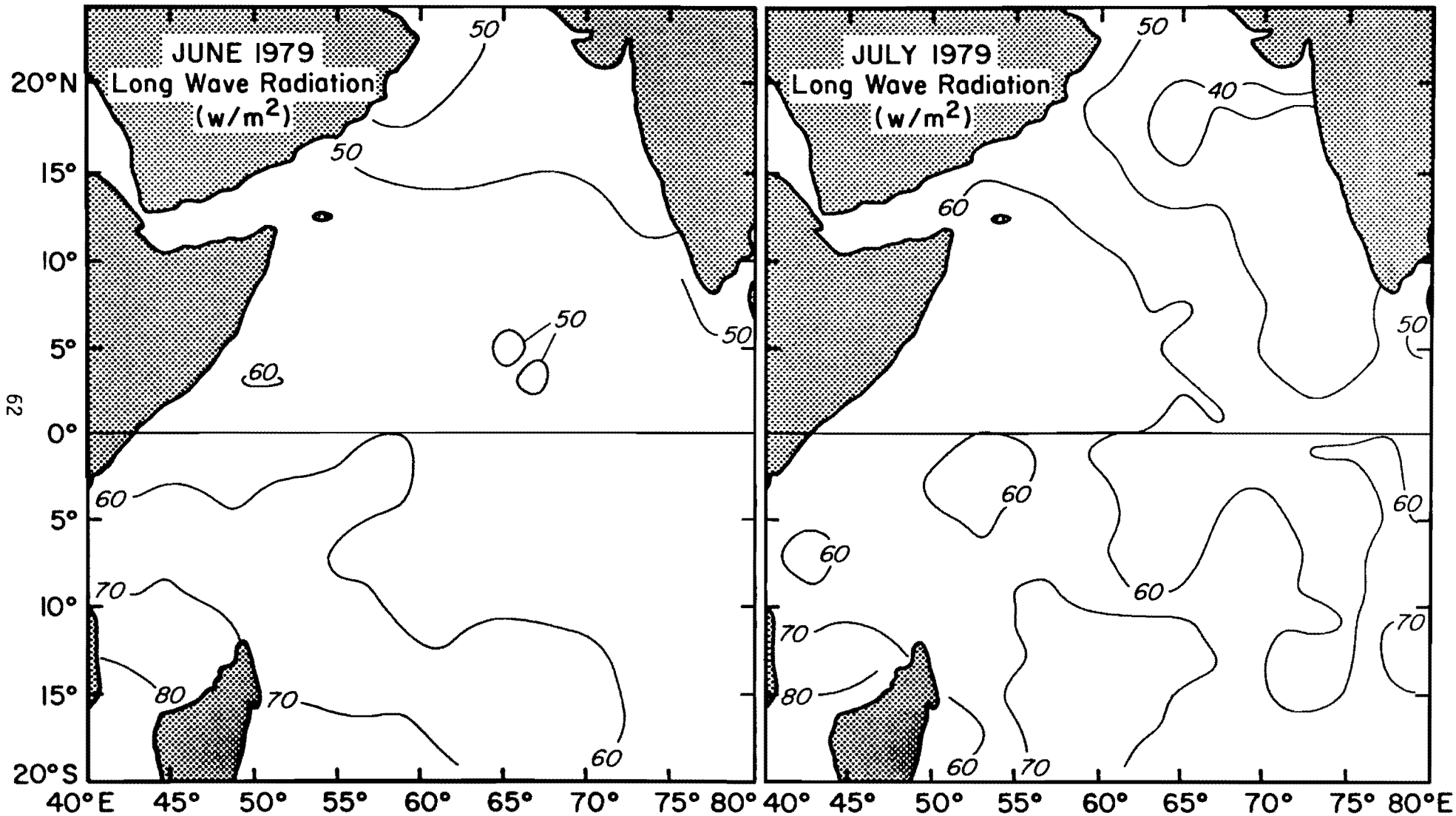

Figure 55. Long-wave radiation for June and July 1979 (as in Figure 52).

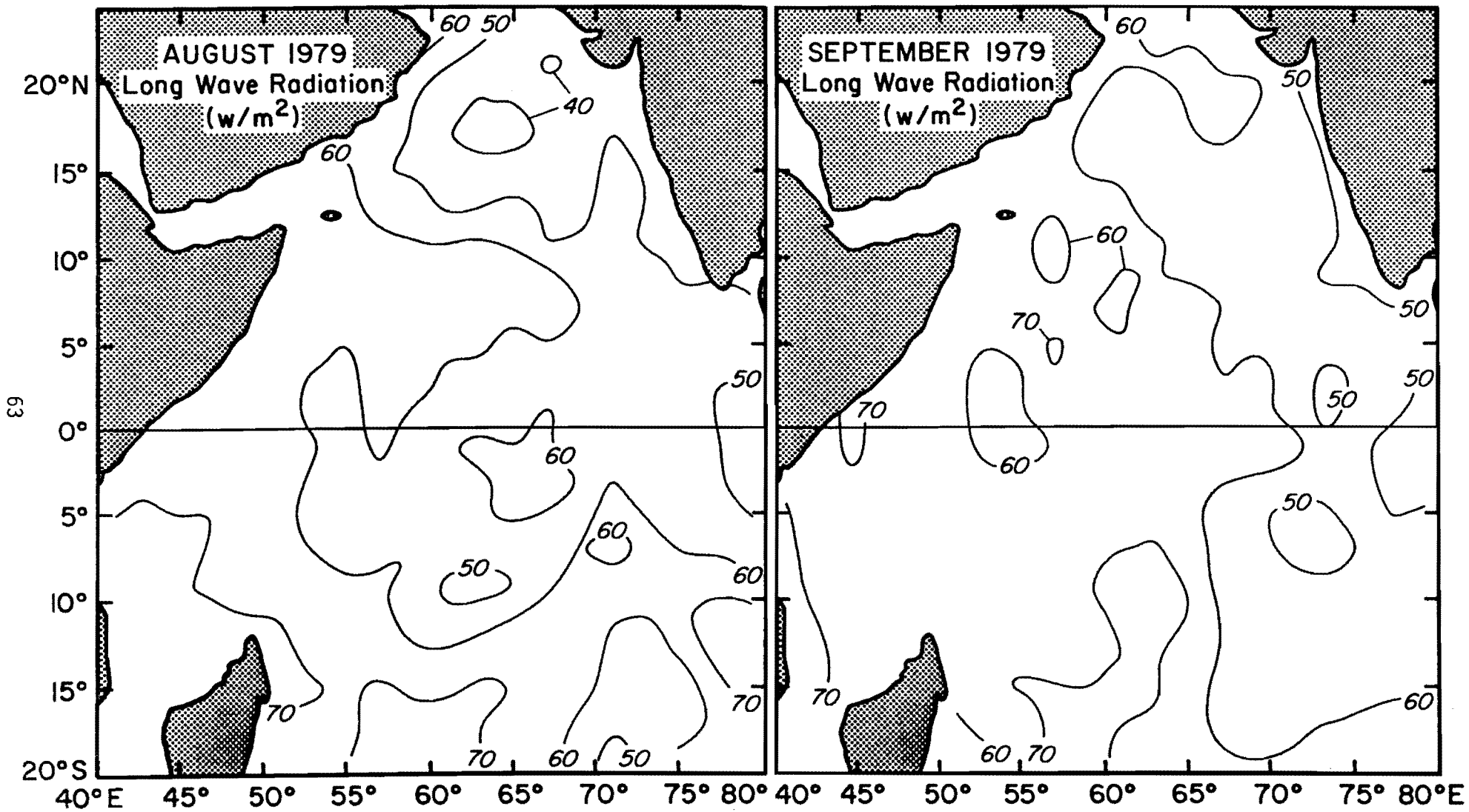

Figure 56. Long-wave radiation for August and September 1979 (as in Figure 52).

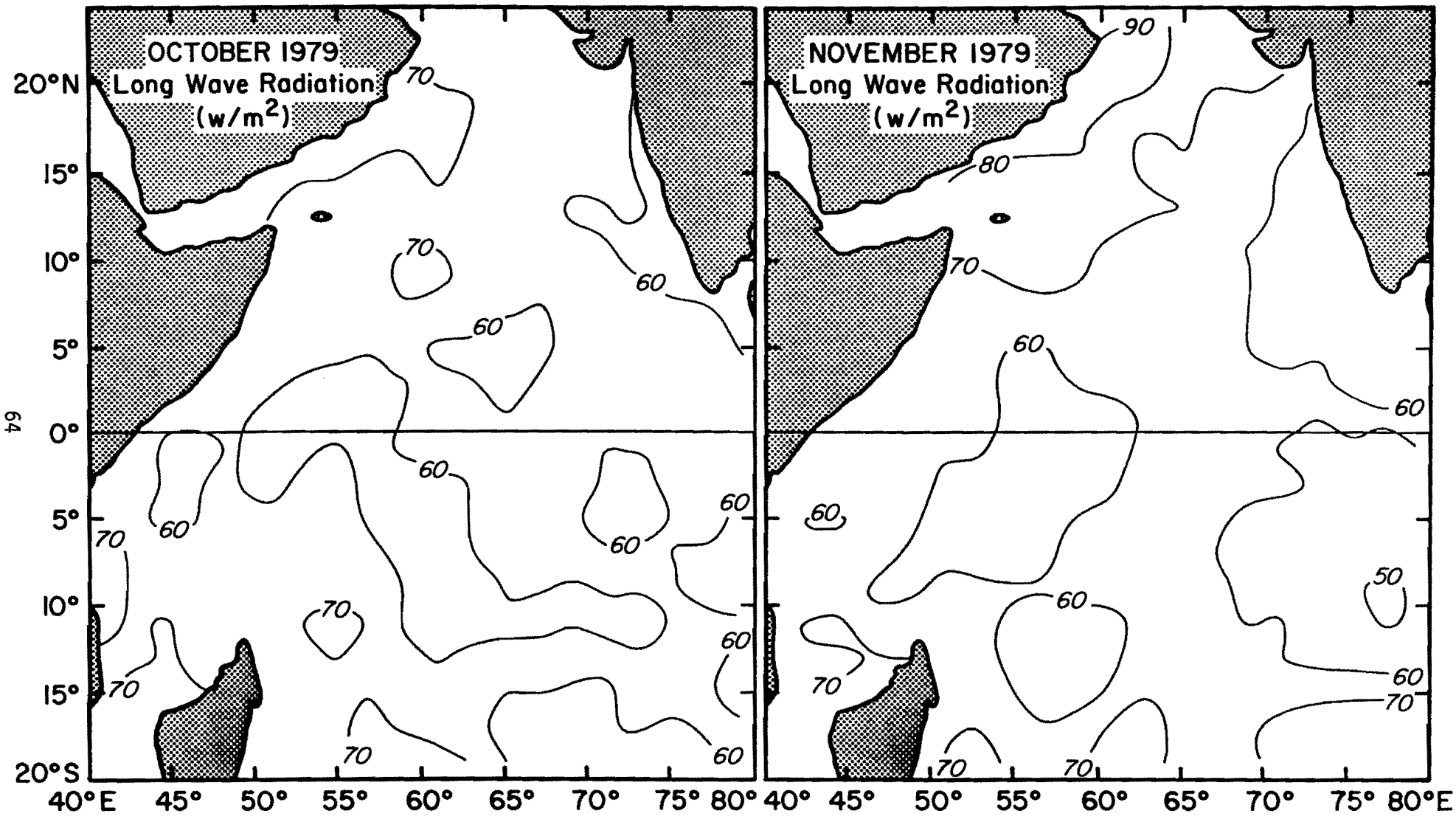

Figure 57. Long-wave radiation for October and November 1979 (as in Figure 52).

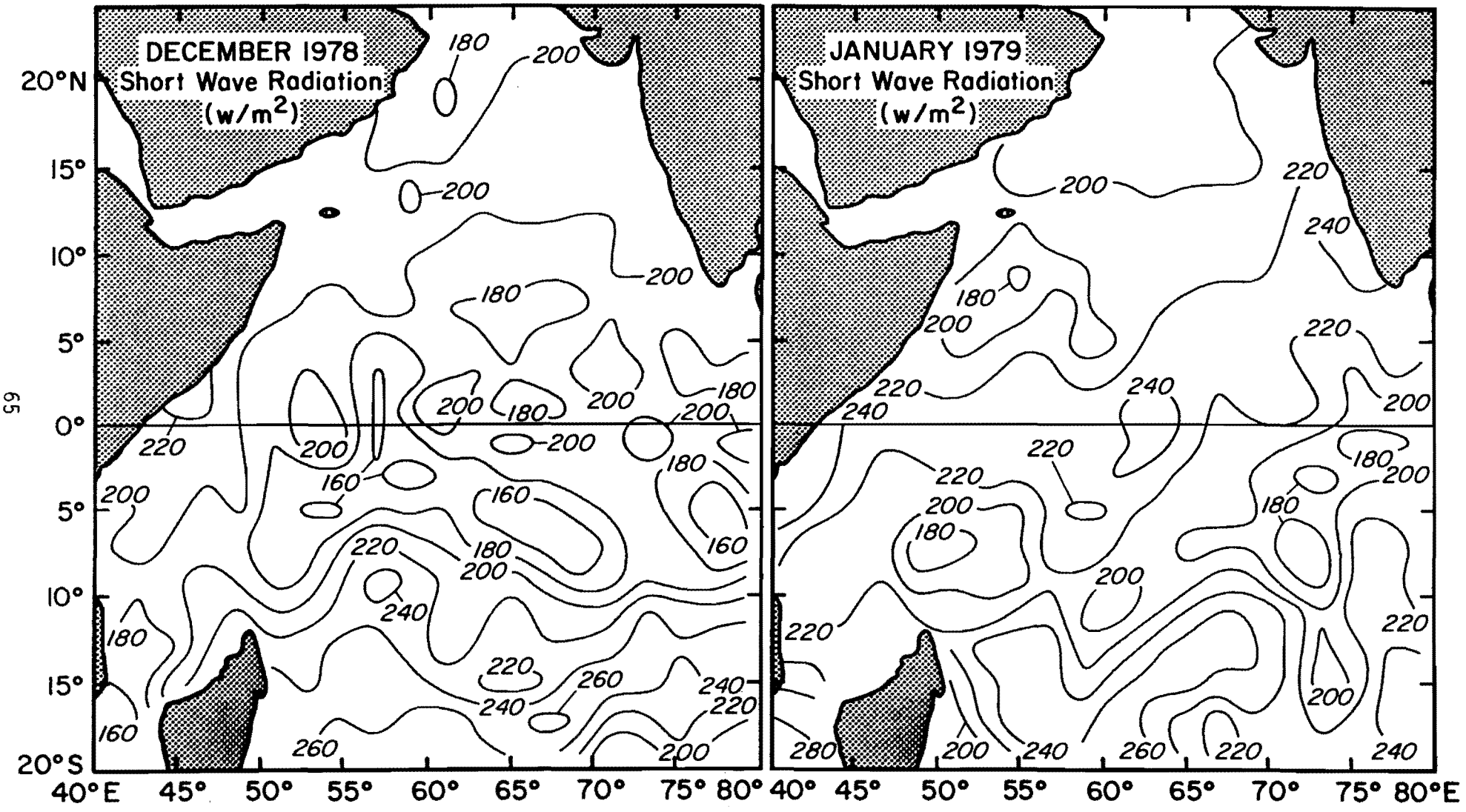

Figure 58. Monthly short-wave radiation for December 1978 and January 1979 (computed from edited and smoothed observations), contoured every 20 W/m^2.

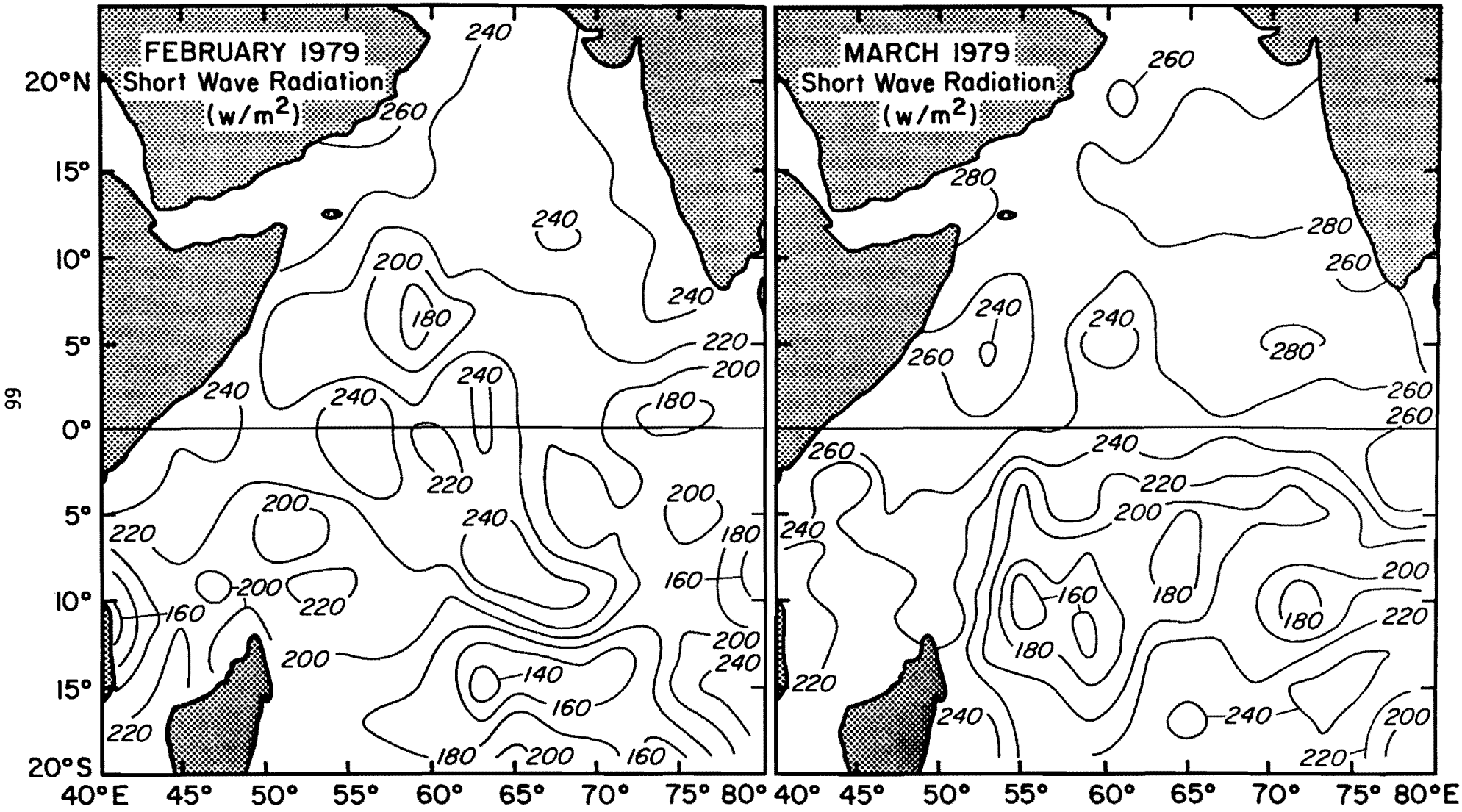

Figure 59. Short-wave radiation for February and March 1979 (as in Figure 58).

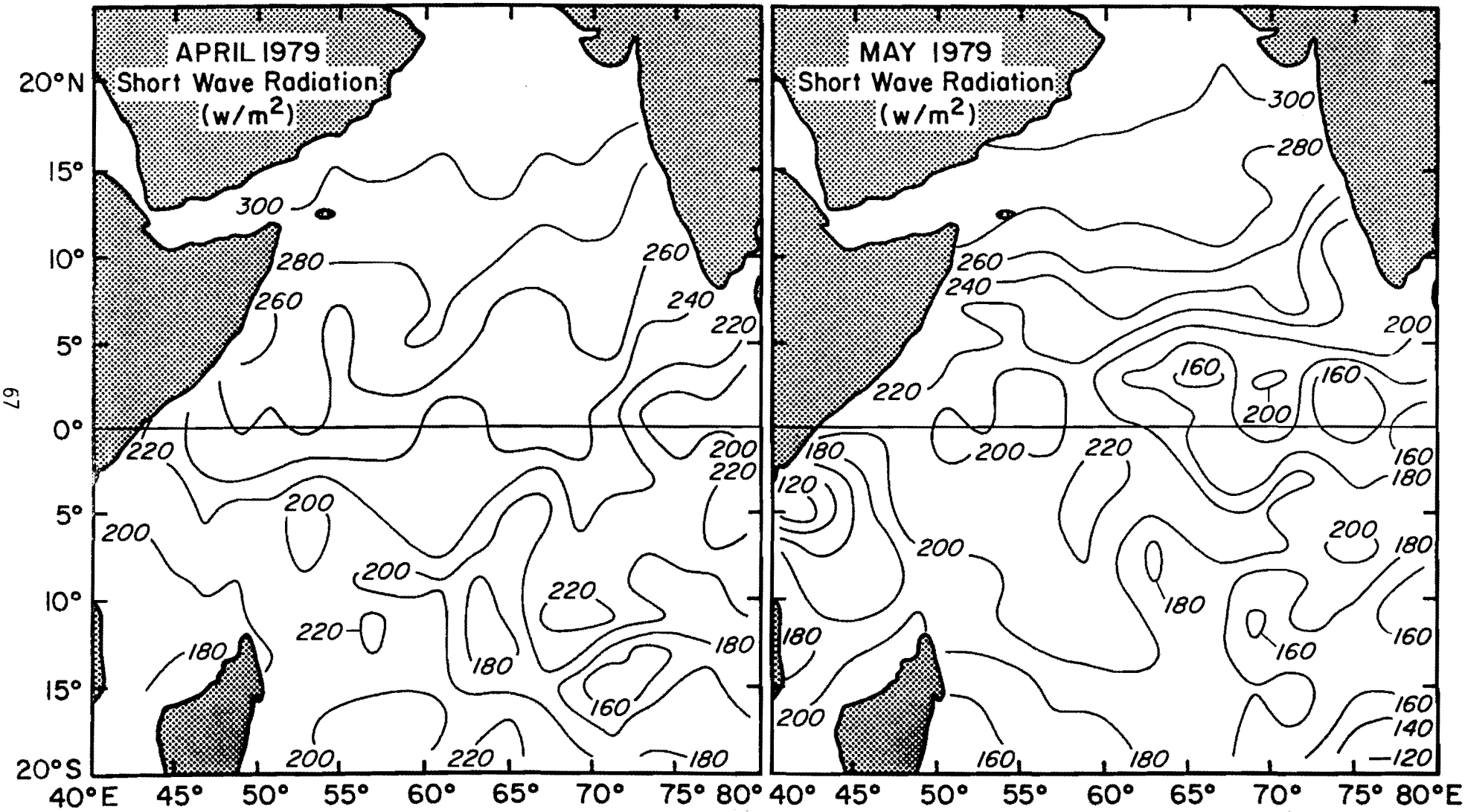

Figure 60. Short-wave radiation for April and May 1979 (as in Figure 58).

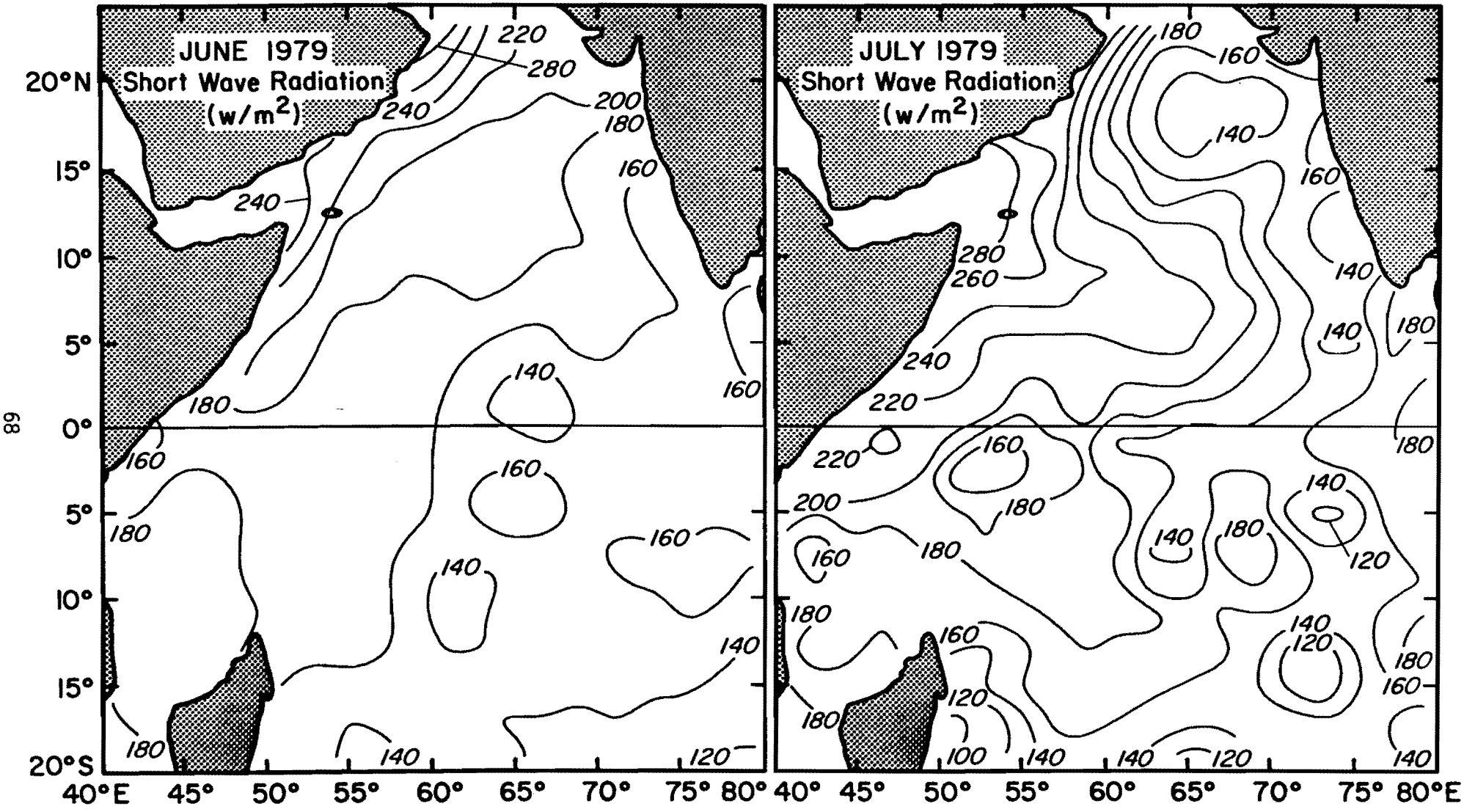

Figure 61. Short-wave radiation for June and July 1979 (as in Figure 58).

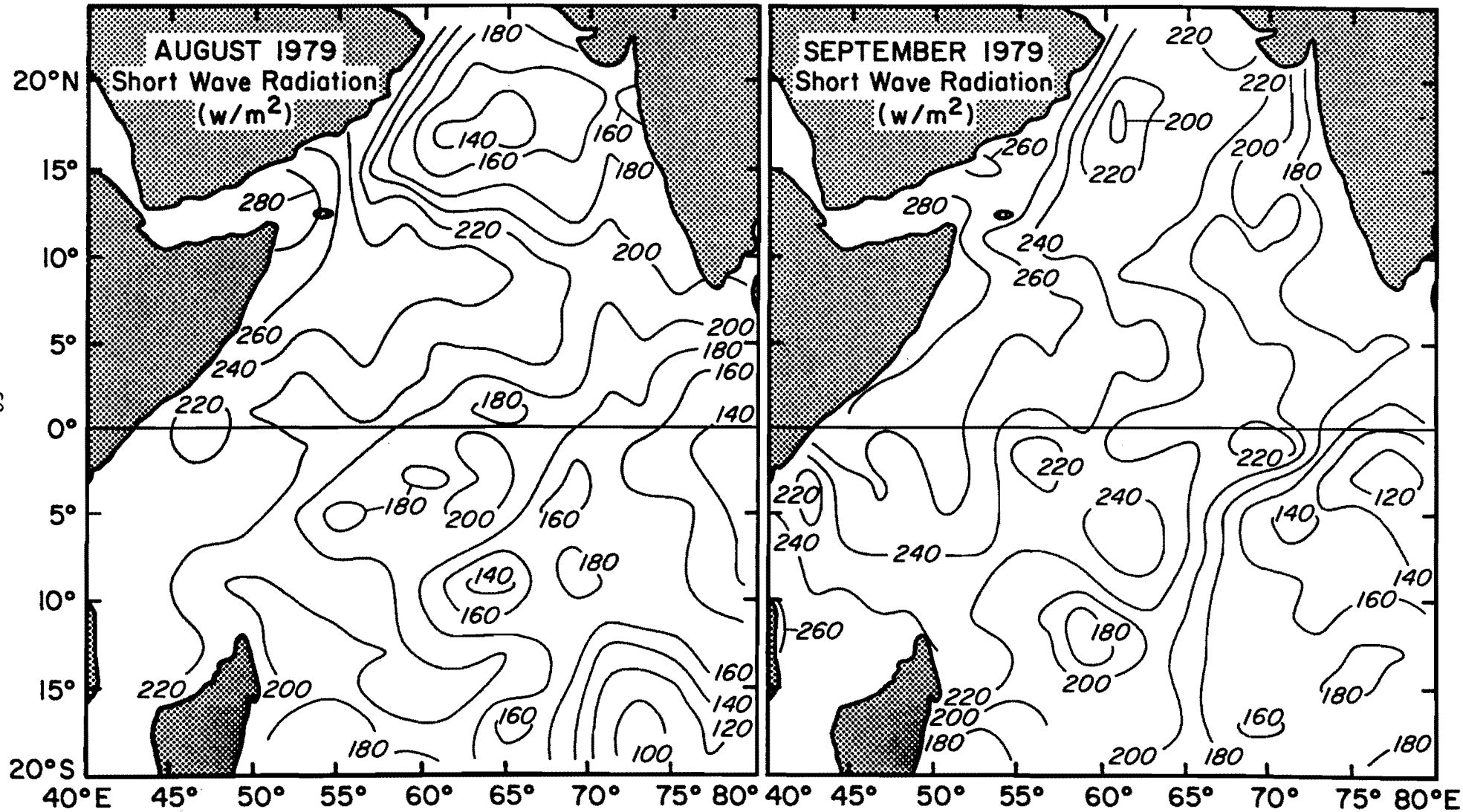

Figure 62. Short-wave radiation for August and September 1979 (as in Figure 58).

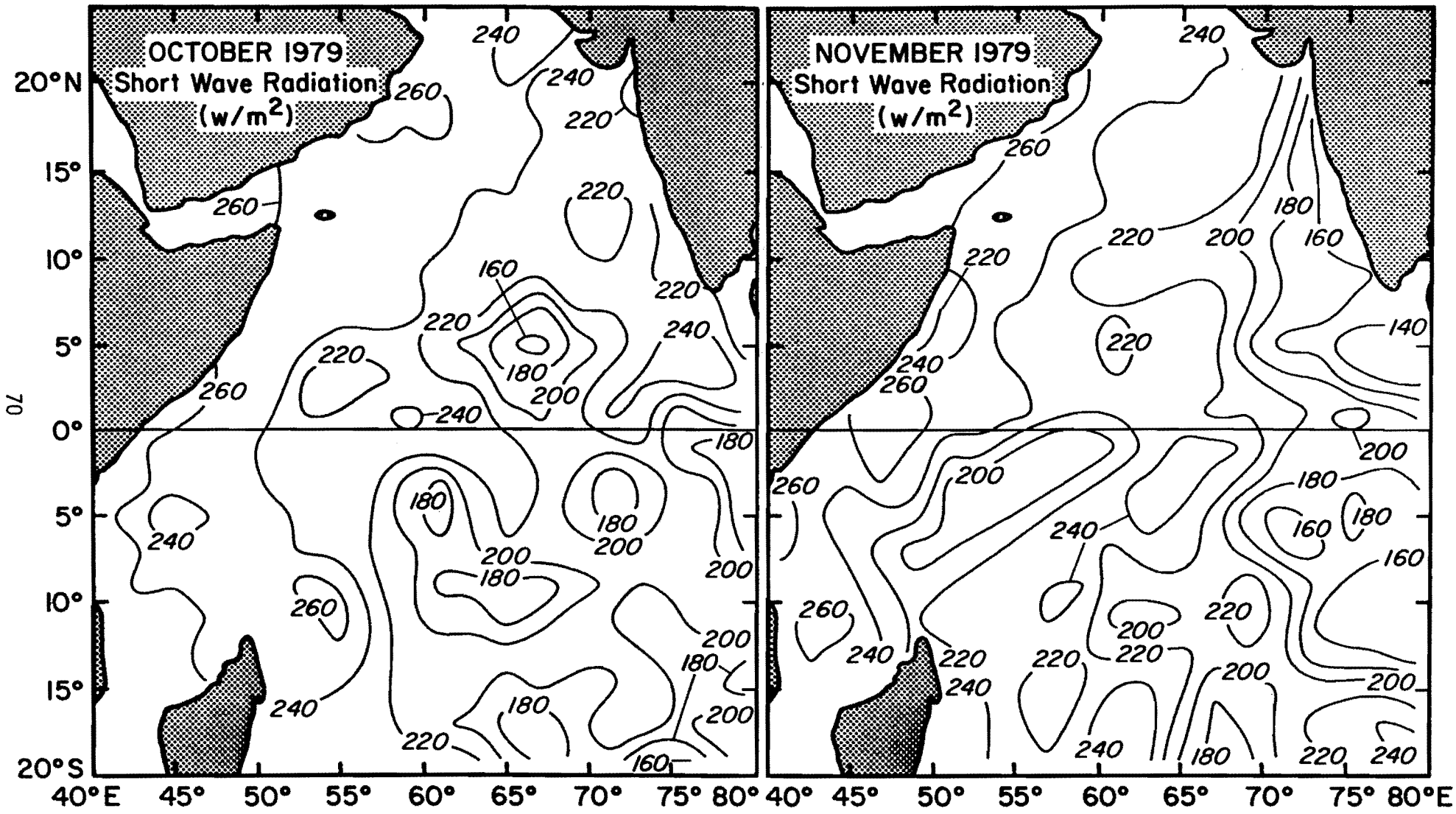

Figure 63. Short-wave radiation for October and November 1979 (as in Figure 58).

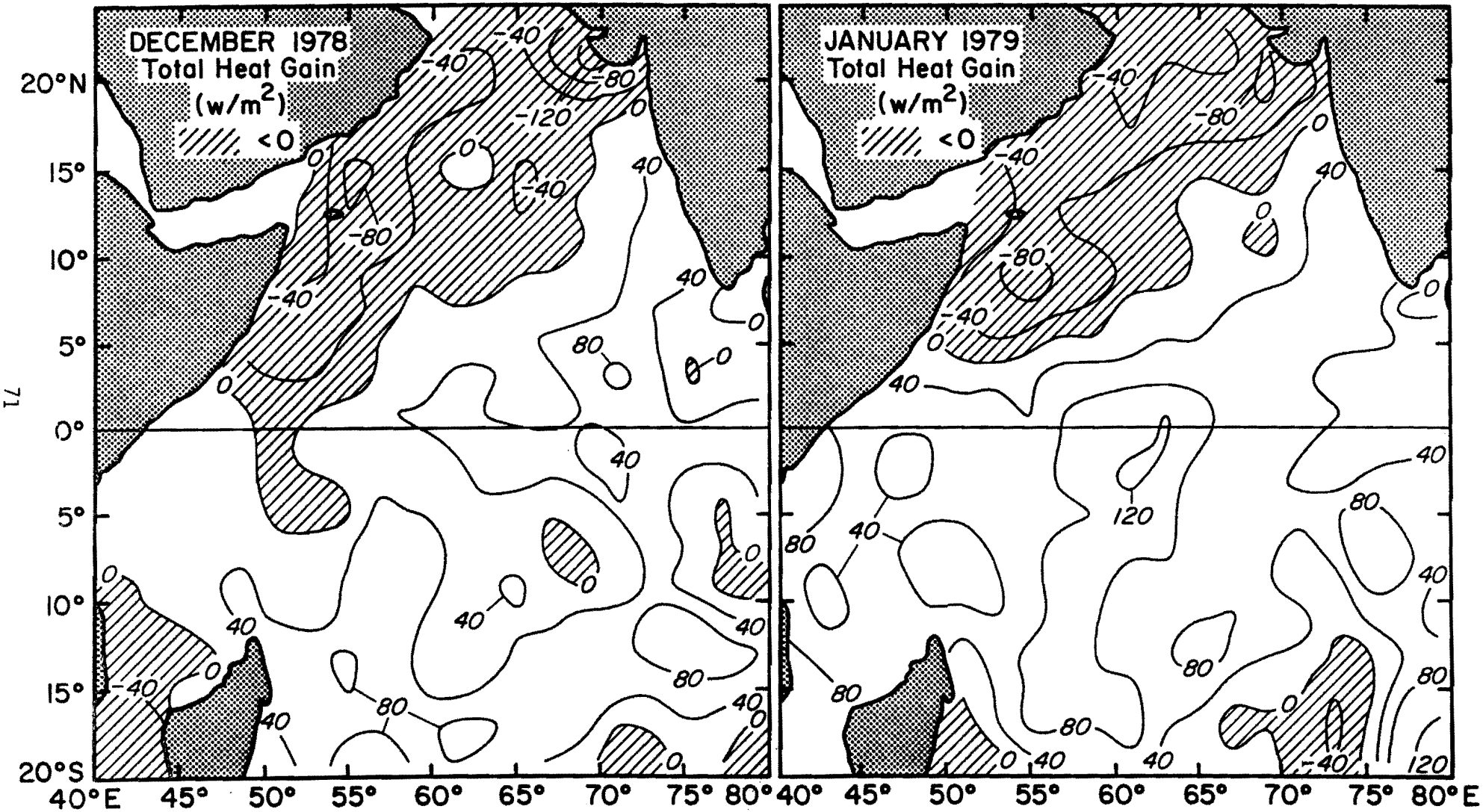

Figure 64. Monthly total heat gain for December 1978 and January 1979, contoured every 40 W/m^2. Shaded areas denote regions of heat loss.

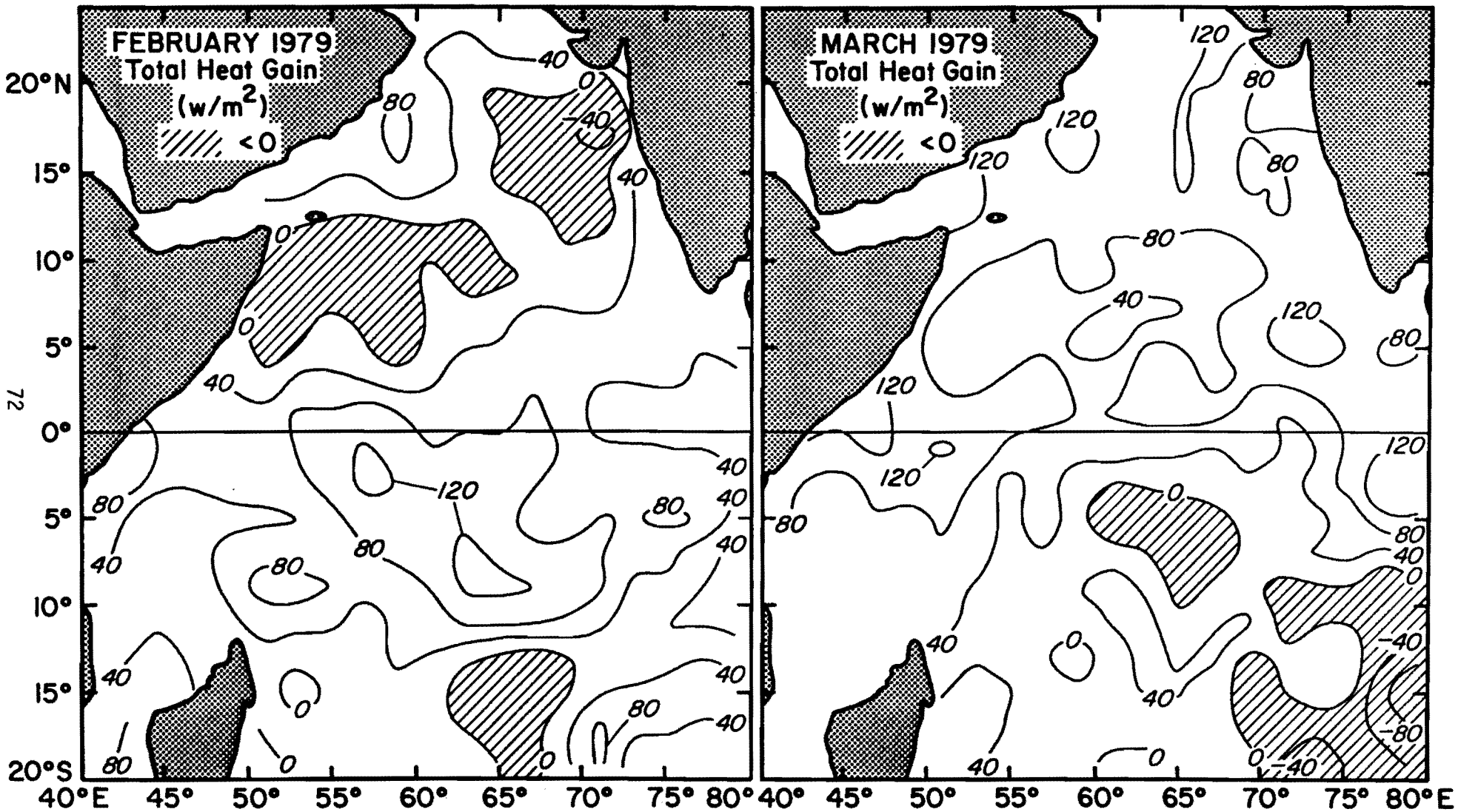

Figure 65. Total heat gain for February and March 1979 (as in Figure 64).

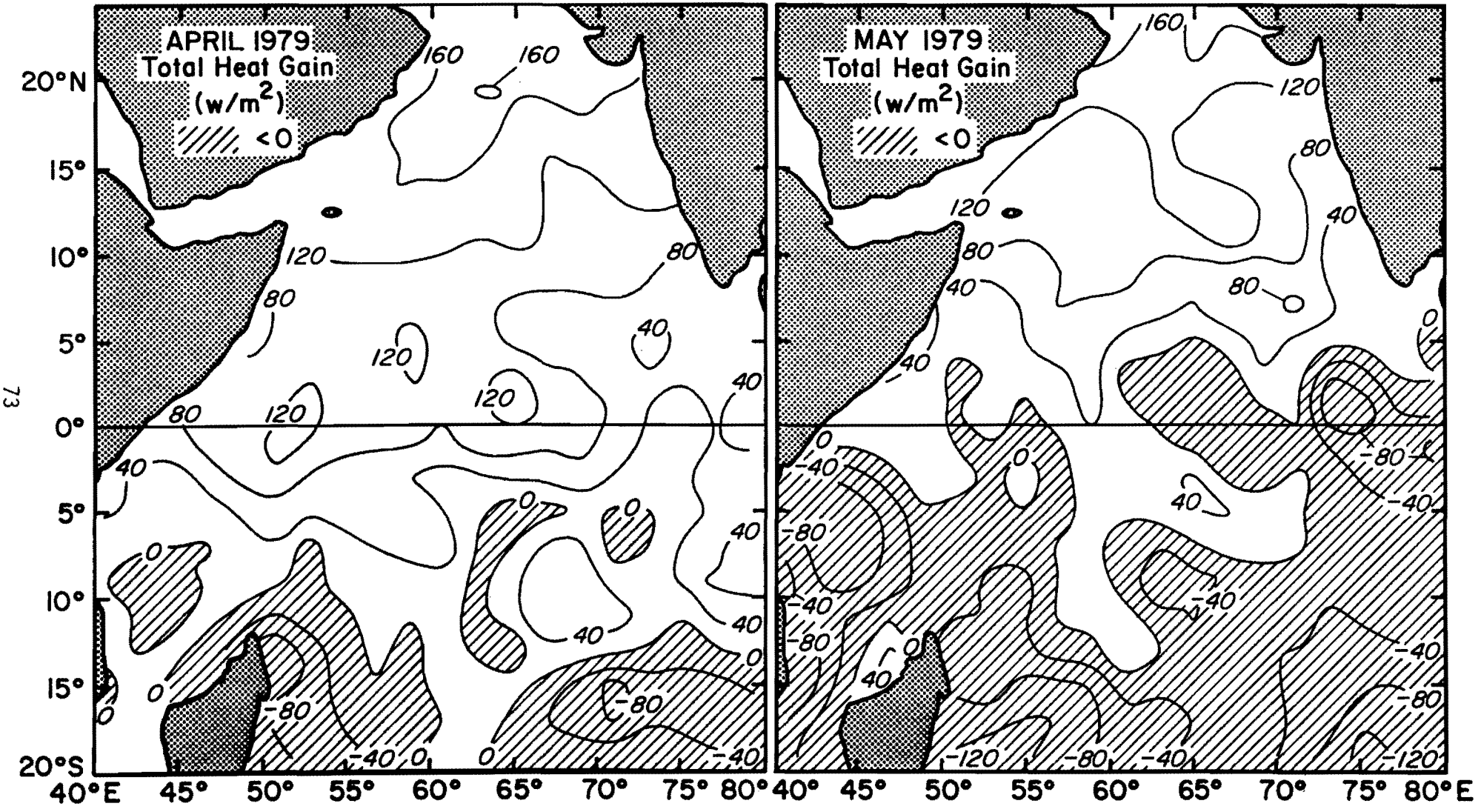

Figure 66. Total heat gain for April and May 1979 (as in Figure 64).

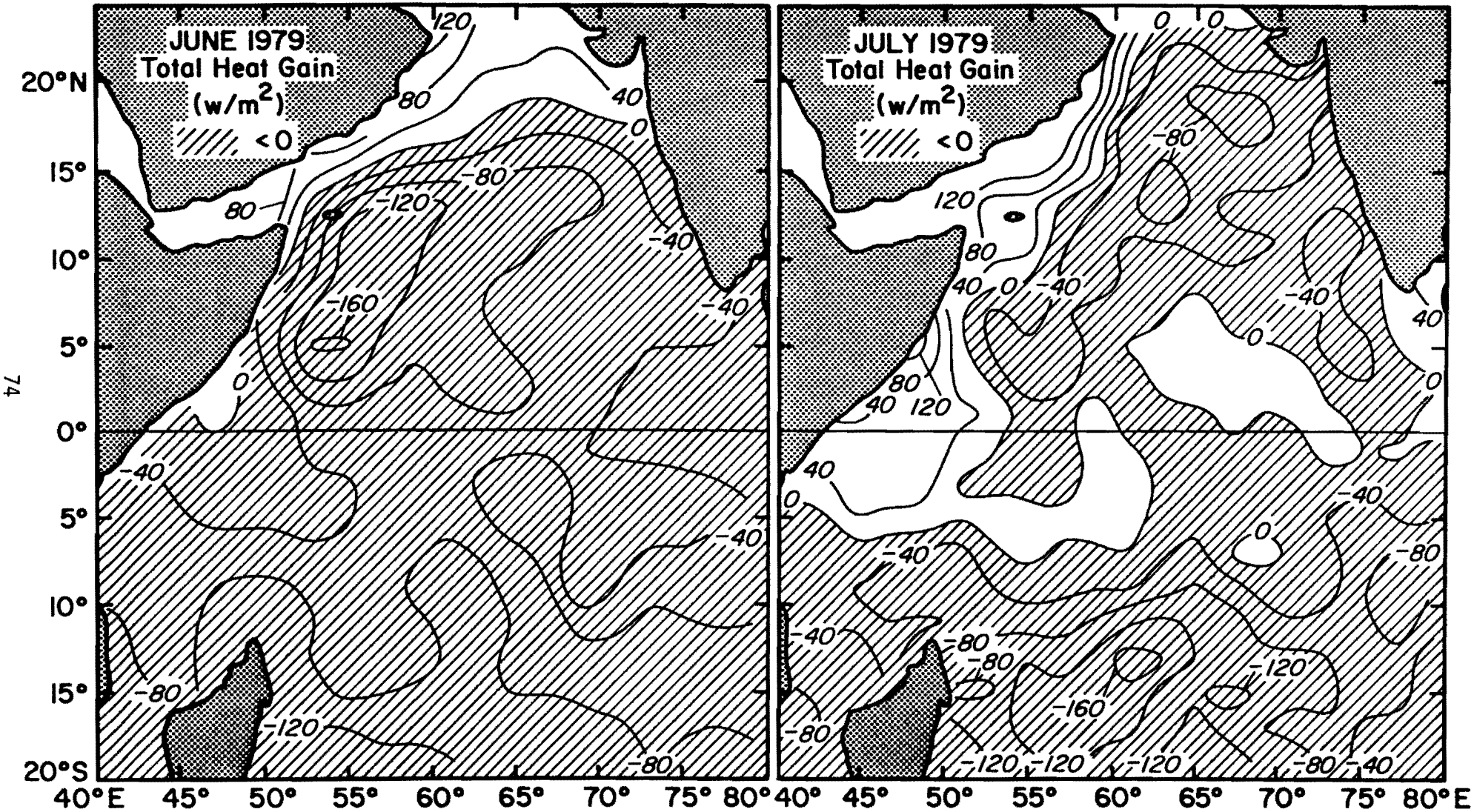

Figure 67. Total heat gain for June and July 1979 (as in Figure 64).

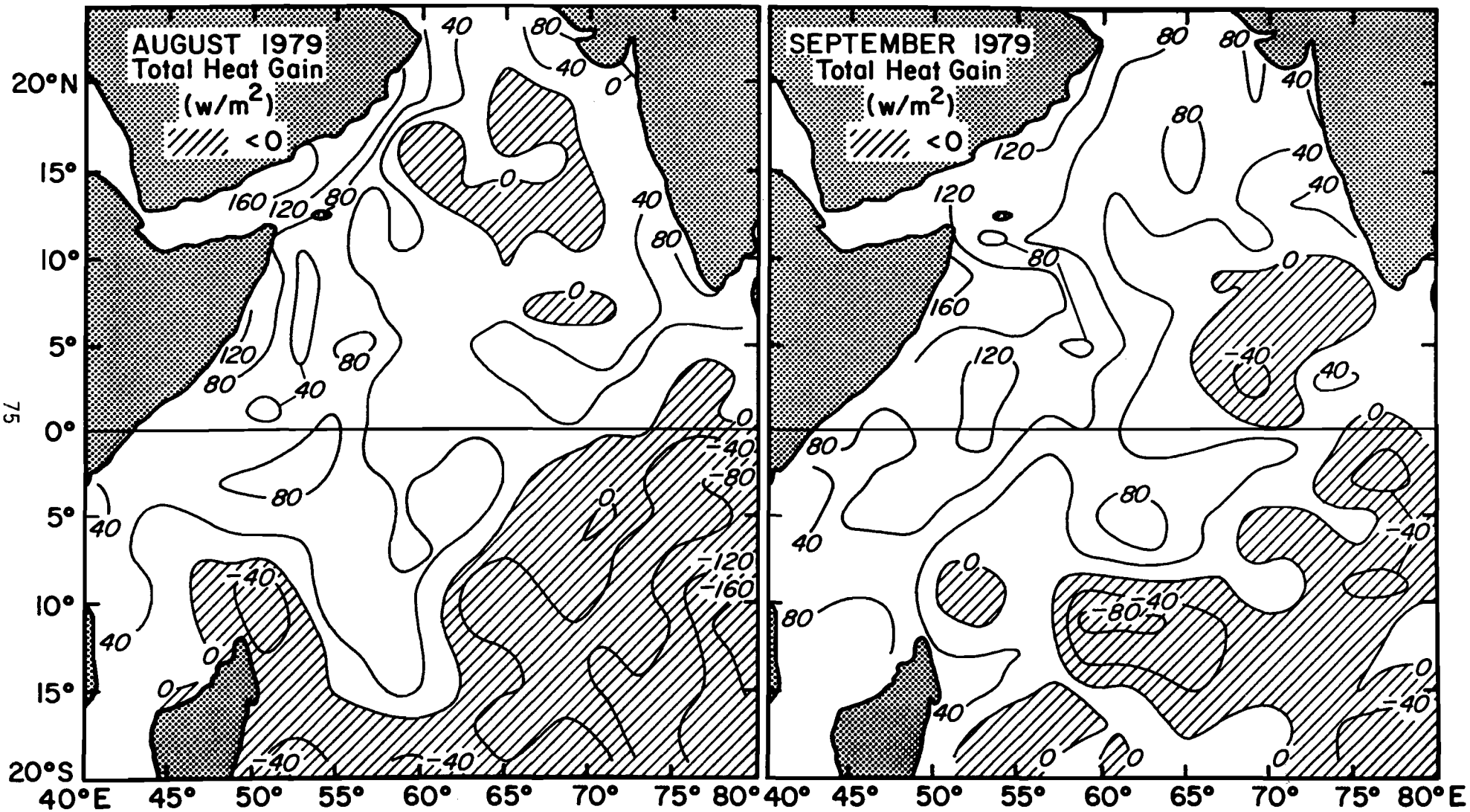

Figure 68. Total heat gain for August and September 1979 (as in Figure 64).

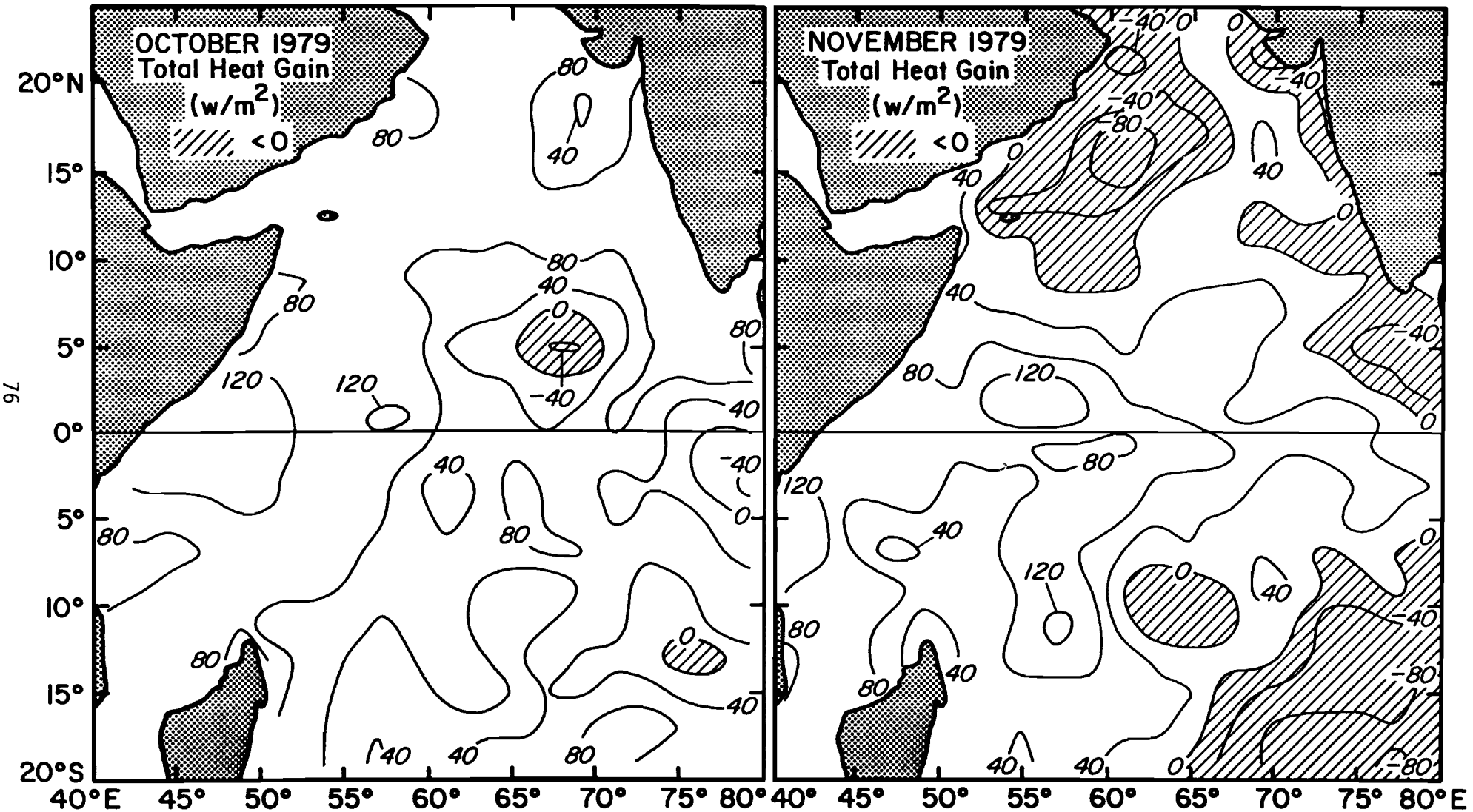

Figure 69. Total heat gain for October and November 1979 (as in Figure 64).